Fabrication & Characterization of Carbon Nanocomposite Photopolymers via Projection Stereolithography

Earl Andrew Campaigne III

Thesis submitted to the faculty of the Virginia Polytechnic Institute and State University in partial fulfillment of the requirements for the degree of

Master of Science
In
Mechanical Engineering

Christopher B. Williams (Chair)
Thomas A. Campbell
John P. Bird

June 13, 2014
Blacksburg, Virginia

Keywords: Additive Manufacturing, Microstereolithography, Vat Polymerization, Nanocomposite Polymer, Carbon Nanotubes

Fabrication & Characterization of Carbon Nanocomposite Photopolymers via Projection Stereolithography

Earl Andrew Campaigne III

ABSTRACT

Projection Stereolithography (PSL) is an Additive Manufacturing process that digitally patterns light to selectively expose and layer photopolymer into three dimensional objects. Nanomaterials within the photopolymer are therefore embedded inside fabricated objects. Adding varying concentrations of multi-walled carbon nanotubes (MWCNT) to the photopolymer may allow for the engineering of an object's tensile strength and electric conductivity. This research has two goals (i) the fabrication of three-dimensional structures using PSL and (ii) the material characterization of nanocomposite photopolymers. A morphological matrix design tool was developed and used to categorically analyze published PSL systems. These results were used to justifying design tradeoffs during the design and fabricate of a new PSL system. The developed system has 300µm resolution, 45mm x 25mm fabrication area, 0.23mW/cm^2 intensity, and 76.2mm (3") per hour vertical build rate. Nanocomposite materials were created by mixing Objet VeroClear FullCure 810 photopolymer with 0.1, 0.2, and 0.5 weight percent MWCNT using non-localized bath sonication. The curing properties of these nanocomposite mixtures were characterized; adding 0.1 weight-percent MWCNT increases the critical exposure by 10.7% and decreases the depth of penetration by 40.1%. The material strength of these nanocomposites were quantified through tensile testing; adding 0.1 weight-percent MWCNT decreases the tensile stress by 45.89%, the tensile strain by 33.33%, and the elastic modulus by 28.01%. Higher concentrations always had exaggerated effects. Electrical conductivity is only measurable for the 0.5 weight-percent nanocomposite with a 5kΩ resistance. The 0.1 weight-percent nanocomposite was used in the PSL system to fabricate a three-dimensional nanocomposite structure.

Acknowledgements

First, I would like to thank my father for inspiring me in my youth to become an engineer. He is a constant source of motivation and encouragement; providing support and direction whenever I need it the most.

I would also like to thank Dr. Thomas Campbell and Dr. John Bird for their guidance as participating members of my committee. Research funding is attributed to The Center for Innovative Technology's (CIT) Commonwealth Research Commercialization Fund (CRCF), whose goal is to advance science and technology-based research, development, and commercialization in Virginia to drive economic growth.

Many people helped me with the work presented in this thesis and I would like to acknowledge them with my sincere appreciation: Dr. Tim Long and Allison Schultz for assisting me in obtaining tensile test results; Dr. Benn Knap and Deba Saha for measuring electrical conductivity; Stephen McCartney and Christopher Winkler at the Nanoscale Characterization and Fabrication Laboratory (NCFL) for capturing the TEM sample images.

The companionship my friends and peers in the DREAMS lab have provided throughout the trials and tribulations of earning a graduate level degree was invaluable. They are an exceptional group of people who I am thankful for having the pleasure of knowing. I would also like to thank Phillip Lambert in particular for his constant camaraderie during our scientific endeavors and life experiences. He provided reassurance, motivation, friendship, and hardy laughs during the most stressful and challenging times.

I began my career at Virginia Tech as an undergraduate shortly after Dr. Williams began his career at Virginia Tech. Many years after sitting in his lecture my freshmen year, I was fortunate enough to leave a lasting impression that resulted in the research position from which this thesis was written. Dr. Williams' support, criticism, guidance, and graciousness have not only made my graduate career possible but a successful endeavor. His dedication to his students has created a lasting impression of true leadership, and I can only hope to have left an equally valuable impression on Dr. Williams and my lab mates.

Table of Contents

List of Figures

List of Tables

1. Background and Motivation

Unlike traditional subtractive manufacturing processes that selectively remove material from a billet, an Additive Manufacturing (AM) process is any fabrication process that fabricates three dimensional objects by selectively adding and patterning material. Most commonly, material is patterned in two dimensional layers, each representing a thin cross section of an object, that are stacked throughout the process to manufacture the object. Because AM processes selectively places material only where it's required, they are more material efficient than subtractive manufacturing processes which often discard more material than is used for the part. AM is also able to create complex geometries and shapes because of its layer by layer approach, breaking the design conventions established for manufacturing with subtractive techniques. These two key advantages make AM processes ideal for the material efficient fabrication of geometrically complex parts. Throughout its brief history additive manufacturing has been popularized under the terms rapid prototyping, rapid tooling, direct digital fabrication, and 3D printing. However these terms are not all inclusive and are often incorrectly used to describe additive manufacturing processes.

Stereolithogrpahy (SL) is a well-established additive manufacturing process that fabricates three dimensional objects by crosslinking layers of photopolymer resin with a scanning ultraviolet (UV) laser beam. Projection Stereolithography (PSL) is a stereolithography process that replaces the scanning UV laser with a UV light source and dynamic pattern generator (of dynamic mask) to digitally pattern light and expose an entire cross-sectional layer at once. Unlike traditional SL processes, PSL is not limited by the laser beam radius or its scan speed, and thus enables the creation of features sizes smaller than 10um while also reducing build times by an order of magnitude.

In 1995 Arnaud Bertsch presented the first PSL system, which he then called integral stereolithography [1]–[3]. The general PSL process flow is illustrated in Figure 1-1 below. Light is first created by a source - commonly a light emitting diode (LED), lamp, or laser. This light is often conditioned by a series of optics that may include collimating lenses, wavelength filters, and homogenizing rods. The dynamic pattern generator digitally patterns and projects this incident light as a two dimensional image. An optical lens, or series of lenses, resizes and focuses the projected image onto the surface of contained liquid photopolymer. The projected image initiates the crosslinking of monomers within the photopolymer resin, changing it from a liquid to a solid in a process called photopolymerization. Subsequent layers are cured onto the previous layer by repositioning the build platform to coat the previous layer with liquid photopolymer. Images of sequential cross-sectional layers are repeatedly projected to photopolymerize liquid polymer until the final cross-section is fabricated. The completed part is then removed and post-processed.

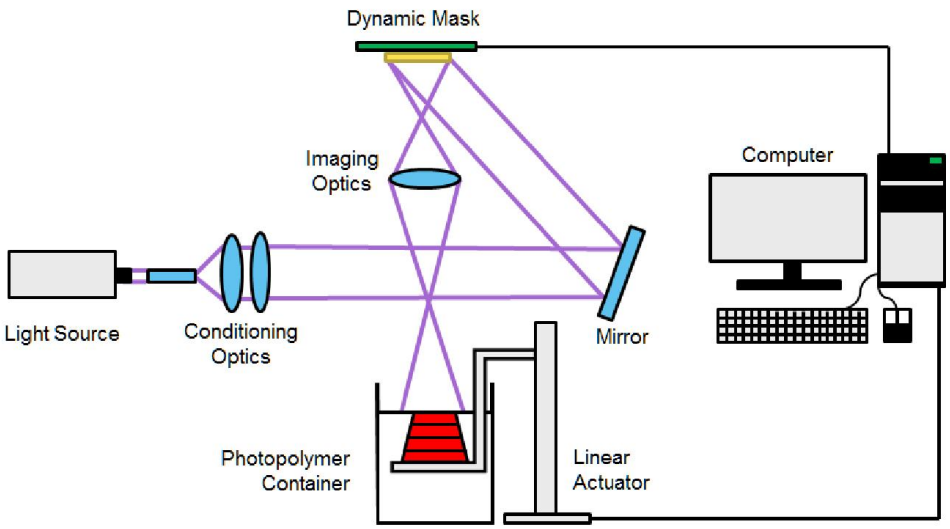

Figure 1-1. Diagram of a typical PSL system. Purple lines highlight the travel of light.

Because PSL uses liquid photopolymer as its raw material, any nanoparticle that can be suspended in the photopolymer can be cured within a parts final geometry. The addition of nanocomposite materials into photopolymer may allow for the fabrication of three dimensional objects with enhanced material properties, providing new opportunities for creating functional end-use devices. The PSL process is therefore ideal for manufacturing objects from custom nanocomposite photopolymers.

There exists prior literature on the incorporation of nanomaterials within AM processes [4]. Specifically for the stereolithography process, work has been published exploring the advantages of carbon nanotubes [5] and semiconductor/ceramic nanoparticles [6]. Carbon nanotubes (CNT) are of specific interest for their low density, exceptionally high aspect ratio (~1000:1), high tensile strength (~100 GPa), high stiffness (~1000 GPa), and their electrical conductivity (~0.5μΩm) [7]. Sandoval and Wicker have demonstrated a 17% increase in the ultimate tensile stress, a 37% increase in the fracture stress, a ~16 increase in the hardness, and a ~30% decrease in fracture strain for photopolymers loaded with 0.05 weight percent multi-walled carbon nanotubes (MWCNT) [5]. Their research shows that small quantities of carbon nanotubes may have significant effects on the physical properties of photopolymerized resins; and by varying the concentration of the nanocomposite, the material properties of existing photopolymers may be engineered for specific applications with demanding material properties [9].

The photopolymerization of nanocomposites within AM goes unstudied beyond these efforts, however Virginia Tech is well suited to explore this knowledge gap with our expertise in AM, nanomaterials, and polymer science. As Virginia Tech does not have a PSL system, the first research objective is to design and develop a PSL system specifically for fabricating objects from these novel materials. The second research objective is the synthesis and characterization of photopolymer nanocomposites containing carbon nanotubes. Characterization includes modeling how these nanocomposites photopolymerize as well as how the addition of carbon nanotubes affects the strength and conductivity of the photopolymer material.

1.1 Research Questions and Thesis Roadmap

Before undertaking the entire design process, the research and developmental questions that guide this research must be explicitly defined. Corresponding research tasks must also be developed to create a framework for the design process to follow and build upon. Table 1-1 below shows the key questions asked by this work. Table 1-2 below shows the roadmap followed to solve these research questions and provide an organizational layout of this thesis.

The overall research goal is to (i) use the PSL process to fabricate three dimensional parts made from novel nanocomposite materials and (ii) gain an understanding about how CNT affect the PSL process and its resultant parts. The few commercially available PSL systems are prohibitively expensive, so a PSL system must first be designed and developed for processing the novel photopolymers (Developmental Question #1 and #2). The second research objective is the material characterization of these novel nanocomposites, illustrating the practicality of their application in AM. This work is novel and contributes to state of the art by filling a current knowledge gap in how carbon nanotubes affect the PSL process and printed photopolymer structures (Research Questions #1 and #2).

Table 1-1. A summary of the research and developmental questions asked by this project.

Research Questions	Development Questions	Research Tasks
1. How does the addition of multi-walled carbon nanotubes by weight percent change the curing characteristics of the photopolymer? 2. How do the multi-walled carbon nanotubes affect the material properties (tensile strength and electrical conductivity) of the photopolymer?	1. What features and components does a PSL system designed to process nanocomposites possess and what is their embodiment? 2. What is the resolution, accuracy, precision, and vertical print speed of a PSL system designed to process nanocomposites	1.1. Design and fabricate a PSL system based upon a set of performance parameters 1.2. Design and fabricate test parts to measure system performance. 1.3. Quantify the final system performance in regards to those parameters. 2.1 Characterize the depth of penetration and critical exposure for nanocomposites made from commercially available photopolymer and multi-walled carbon nanotubes. 2.2 Characterize the material strength and electrical conductivity of these nanocomposites.

Table 1-2. Overview of the following chapters and their role in the overall design process.

Design Step	Chapter No.	Description and Scientific Contribution
PSL Literature Review	2	Presents the history and state of the art for PSL systems in literature, while offering design guidelines for the future development of such systems. This section also categorizes many PSL systems and quantifies their performance.
Design of the PSL System	3	Identifies the problem, research needs, and system specifications for designing this PSL system (3.1). Shows the conceptual design of the sub systems (3.2). Presents the final system embodiment and the detailed system design (3.3).
PSL System Validation	4	Quantifies the accuracy, precision, print speed, and resolution of the PSL system using fabricated test pieces. The overall success of the design is also measured using the target performance parameters established in Chapter 3.
Curing Characterization of Nanocomposite Photopolymer	5	Presents the photocuring characterization of nanocomposite mixtures created from VeroClear photopolymer and multi-walled carbon nanotubes. Models for critical exposure and depth of penetration were created from experimental data and qualitatively justified.
Material Property Characterization of Nanocomposite Photopolymer	6	Presents the characterization of tensile strength and electrical conductivity for the nanocomposite photopolymers. These trends are discussed qualitatively and quantitatively.
Conclusions and Future Work	7	Restates the purpose of this work, provides a list of research contributions, and makes suggestions for future work regarding the study of nanocomposite photopolymers in PSL.

1.2 A Note on Terminology

Throughout prior literature, various acronyms and terms have been used to identify stereolithography processes that utilize a dynamic mask. Mask Image Projection Stereolithography (MIPSL or MPSL), Mask Projection Micro-Stereolithography (MPuSL), and integral stereolithography are terms many people familiarly associate with dynamic mask based stereolithography processes. I propose that the correct and most accurate term is simply projection stereolithography (PSL) for the following reasons:

1. In MEMS fabrication, a lithography process similar to stereolithography uses static masks made from quartz to selectively expose and pattern photoresists. Mask-less lithography machines use the same digital pattern generators used in PSL to avoid the use of static physical masks. For consistency with the MEMS community, PSL systems are best not described as masked since they uses the same mask-less digital pattern generators.
2. The prefix micro is often associated with PSL systems to emphasize their ability to create micron-scale features. However, the general application of this term would exclude systems that are not capable of fabricating micron-scale features. Does adjusting the magnification to create milli and centi-scaled features turn a µSL machine into a mSL or cSL machine?
3. Image, projection, and integral are words often used to describe PSL machines. The word projection is most intuitive when describing any stereolithography processes using a dynamic pattern generator because it functions by projecting an image onto a surface. This terminology also alludes to the origins of the dynamic pattern generator in Digital Light Patterning (DLP) projectors, which are often used in PSL machines.

For these reasons the term PSL will be used exclusively to describe all stereolithography systems using a digital pattern generator regardless of when the system was developed. It is also my suggestion that this term be used in discussion and literature to describe future systems of this nature.

2. PSL Literature Review

PSL systems have been developed to meet the requirements for a wide variety of applications; however, these systems all possess the same fundamental system functionalities. This literature review analyzes published PSL systems and abstracts the inherent system tradeoffs to create a guide for designing PSL systems, including the system presented later in Chapter 3. Section 2.1 describes the PSL process in terms of functional components and design considerations. Following the AM classification approach suggested by Williams, Rosen and Mistree [10], a morphological matrix design tool for the categorization of PSL design solutions is also presented for this purpose. Section 2.2 identifies the performance tradeoffs between the various PSL components that reoccur throughout published PSL systems. The performance metrics used to quantify these tradeoffs are the systems' (i) achievable layer thickness, (ii) minimum feature size, (iii) build volume, and (iv) vertical build time. Within the organizational context of the presented morphological matrix, this paper then categorizes many PSL systems in Section 2.3, while drawing conclusions about their performance metrics from their design decisions. The results and conclusions of this review are presented in Section 2.4. The work presented in this chapter was performed in collaboration with Phillip Lambert and published as part of the Solid Freeform Fabrication (SFF) Conference proceedings in 2013.

2.1 PSL Functional Analysis

This section describes the PSL process as a set of subfunctions and performance parameters, which are shown through a functional decomposition and a morphological matrix.

2.1.1 PSL System Subfunctions

The PSL process can be discretized into a set of functional subsystems, each with their own set of unique design considerations. The final performance of a PSL system is dependent on the sum of these functional parts. They are as follows:

- *Light source* produces the luminous energy that is projected to selectively cure photopolymer.
- *Conditioning optics* change properties of the projected light for PSL applications.
- *Dynamic mask* digitally patterns and projects incident light to selectively cure photopolymer.
- *Projection orientation* is the position of the dynamic mask relative to the polymer container.
- *Imaging optics* expand or reduce the projected image to achieve the desired image resolution.
- *Recoat method* supplies liquid photopolymer over previous layers for the creation of new layers.
- *Build platform* supports the object being made.
- *Vertical actuator* repositions the build platform for the creation of new layers.
- *System controls* programmatically alter system properties during the fabrication process.
- *Photopolymer container* holds the reservoir of photopolymer and contains the build platform.
- *Photopolymer* is the raw material used in PSL to fabricate three dimensional objects.

These subfunctions, and their respective design considerations, are presented as a functional decomposition in Figure 2-1**.** This list includes the core system functionalities of PSL systems; however, it is not necessarily comprehensive. Some applications may require application-specific considerations, such

as humidity control or gas metering within an enclosed build volume to reduce the influence of environmental inconsistencies [11].

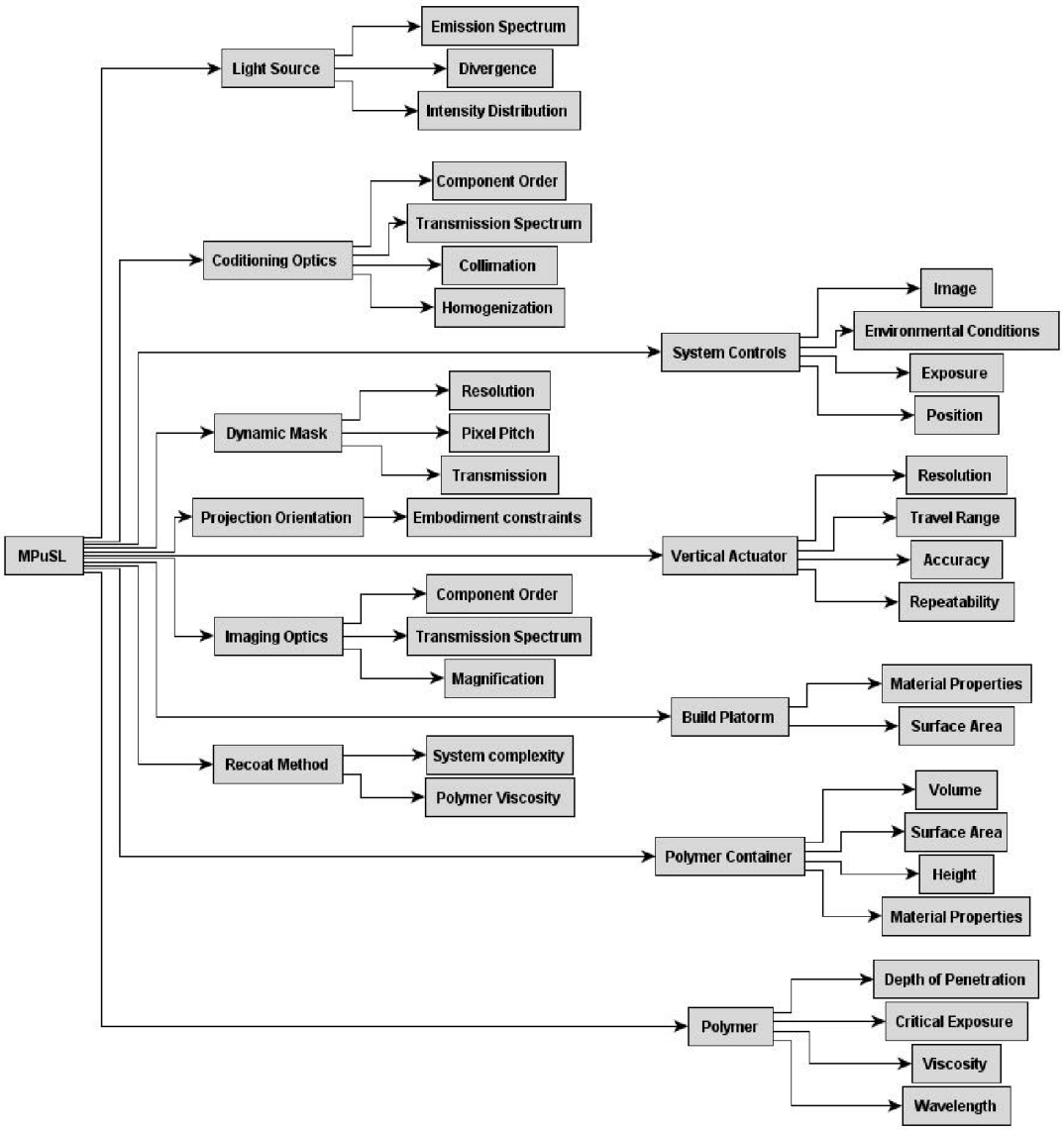

Figure 2-1. Functional decomposition of the PSL process relating subfunctions to design considerations

This discretization of the PSL process into a set of necessary functional subsystems enables the categorization and comparison of PSL systems. A morphological matrix – a design tool that presents system subfunctions and their respective potential design solutions – is provided for the PSL process in Figure 2-2**.** Using this tool, a designer is able to create different PSL embodiments by implementing unique combinations of subfunctions. In addition, this tool can be used as a framework for categorizing and comparing existing PSL systems on a functional basis.

It is important to note that the presented matrix features only those subfunctions that have the most direct effect on overall system performance. The remaining subfunctions (build platform, vertical

actuator, system controls, and photopolymer) are not detailed in this work as they either have only indirect effects on system performance, are common engineering components, and/or are not within the scope of this paper (e.g., controls and material issues).

Sub-functions	***Solutions***			
Light Source	Lamp	Light Emitting Diode (LED)	Laser	
Conditioning Optics	Homogenization	Collimation	Filtering	Beam Expansion
Pattern Light	Liquid Crystal Display (LCD)	Digital Micromirror Device (DMD, DLP Projector)	Liquid Crystal on Silicone (LCoS)	
Projection Orientation	From Above	From Below		
Imaging Optics	Image Expansion	Image Reduction		
Recoat Method	By gravity	By spreading	By pumping	By dipping

Figure 2-2. Morphological matrix discretizing the PSL process into functional subsystems and solutions.

2.1.2 PSL Performance Parameters

As they share the same broad design goals, all PSL systems can be evaluated via a common set of design metrics, and thus provide a basis for comparison. The PSL performance parameters and relationships are as follows:

- *Layer thickness (µm)* is a metric for quantifying vertical (z-axis) resolution. The achievable layer thickness is largely determined by the employed recoating method, actuator resolution, polymer characteristics, and projection orientation.
- *Minimum feature size (µm)* defines the cross-sectional resolution and smallest obtainable features in the X-Y plane. The dynamic pattern generator, projection orientation, and imaging optics define the projected cross-sectional resolution, while the recoating method restricts the physical minimum feature size.
- *Build volume (mm^3)* is a metric for quantifying the dimensions of the largest printed part. The dynamic mask and imaging optics limit the size of the projected image in the X-Y plane and thus the maximum build volume.
- *Vertical build rate (mm/s)* is a metric that quantifies process throughput. Unfortunately, PSL build rates are often published using unclear terms. For example, many authors state throughput in units of seconds per layer, but do not specify whether this is the exposure time per layer or total build time per layer. This is compounded by the fact that each system uses different photopolymers, which

require different exposures. This often prevents the direct comparison of vertical build rates for previously published work.

A Process Planning matrix (from Quality Function Deployment methodology) is used to illustrate the interrelationships between subfunctions and performance metrics in Table 2-1. The strength of each relationship is indicated by assigned values where 1 represents a weak relationship, 3 a medium relationship, and 9 a strong relationship. For example: There is a strong relationship (9) between the minimum feature size (µm) and imaging optics of a PSL machine, because the imaging optics expand or reduce the projected features. In addition, build rate is primarily determined by projection orientation and recoating method.

Table 2-1. QFD Process Planning matrix illustrating the interrelationships between PSL functional subsystems and performance parameters.

	Minimum Feature Size (µm)	Layer Thickness (µm)	Build Volume (mm^3)	Vertical Build Time (mm/s)
Light Source			1	3
Conditioning Optics	1			3
Pattern Light	9		9	
Projection Orientation	9	1		9
Imaging Optics	9		9	9
Recoat Method	9	3		9

2.2 PSL System Components

This section discusses the potential solutions for the PSL subfunctions in Figure 2-2. These options are discussed in terms of general design considerations as well as their influence on the overall system's performance parameters.

2.2.1 Light Source

There are three performance criteria that are important for selecting a light source for PSL applications:

- The *emission spectrum* of the light source must include the wavelength required by the selected photopolymer to achieve photopolymerization.

- The *intensity of light* at that wavelength must be great enough to reach the photopolymer's critical exposure in a reasonable amount of time (e.g., < 60 seconds). This is a key factor in determining system build speed.
- The *divergence* and *intensity profile* of light determine the conditioning and imaging optics required to generate a focused image of homogenous intensity.

Lamp-based light sources reflect light emitted in all directions from a bulb into a light guide. These lamps output high intensity, broad-spectrum light often ranging between 350nm and 500nm. For this reason, lamp light sources are compatible with a wide variety of photopolymer resins of different wavelength sensitivities. Lamp-based light sources are the most commonly used light source for exposing photopolymers in PSL systems [11]–[25].

Light Emitting Diode (LED) sources are also used in PSL systems [26]. In general, LED sources have longer operating lives, lower cost, smaller package size, and lower heat generation than mercury lamps and lasers. LED sources generally output lower light intensities than lamps at one or more wavelengths, which may be chosen to match the photopolymer's polymerization wavelength. LED sources are therefore more energy efficient than mercury lamps and lasers, using energy more efficiently to photopolymerize the same volume of photopolymer [26].

Lasers have also been used in PSL systems [2], [3], [27]–[30]. Laser light sources may emit light at a single wavelength or across multiple wavelengths. Lasers are available in ultraviolet, visible, and infrared wavelengths, but often cost thousands of dollars more than the other two light source options.

2.2.2 Conditioning Optics

The system of optical components between the light source and dynamic mask generator is referred to as the conditioning optics (Figure 1-1). These optical components change the properties of the original light source before reaching the dynamic mask. Unfortunately, published PSL systems underreport the specifics of these optical components, so it is difficult to discuss them in great detail. However, commonly mentioned components include:

- *Homogenizing rods* that internally reflect light repeatedly to statistically create even intensity profiles. Light without a homogenous intensity profile fabricates inconsistent layer thicknesses along the projected image. These inconsistencies will compound and create dimensionally inaccurate parts [19], [21].
- *Collimating lenses* may be used to collimate a highly diverging source such as a lamp. Well collimated light diverges very little, preventing unwanted beam divergence and the resulting decrease in light density [11]–[13], [18], [20], [22]–[24], [31].
- *Filters* may be used to remove unwanted wavelengths, isolating the desired wavelength [11]–[13], [18], [20], [22]–[24], [31].
- *Beam expanding optics* may be used to expand already collimated light from an LED, laser, or collimating lenses [2], [3], [25], [27]–[30].

Different light sources produce different levels of collimation and homogeneity. Lasers produce the most collimated light with the most homogenous light intensity. Lamp light sources often possess a Gaussian intensity distribution and non-collimated, widely diverging light. It is the authors' experience that LED light sources are often less collimated than lasers and possess periodic drops in intensity distributions originating from their diodes. Using the optical components listed above, the collimation and homogeneity of lamp and LED light sources can be improved; however, it is difficult to achieve the same level of performance as a laser.

2.2.3 Pattern Light

A dynamic pattern generator digitally patterns and projects the conditioned light. Dynamic masks all operate by discretizing light over a 2D array of pixels, each individually controlling the light's path. Important design considerations of the dynamic mask include its resolution, pixel pitch, and transmission. Dynamic masks are used primarily in the digital display industry and come in standard resolutions (e.g., 800x600, 1024x768, and 1920x1080). The pixel pitch represents the size of each pixel and the space between pixels. Because optical magnification must be uniform, the resolution and pixel pitch determine the ratio between the projected image area and the minimum feature size. This limitation can only be overcome by moving the mask in relation to the build platform, such that images are stitched together in the photopolymer [20]. Digital Micromirror Device (DMD), Liquid Crystal Display (LCD), and Liquid Crystal on Silicon (LCoS) technologies have been used as dynamic masks throughout PSL.

2.2.3.1 Liquid Crystal Display (LCD)

Early PSL systems were implemented using LCD devices as the dynamic mask [2], [3], [25], [27]–[30]. LCD chips digitally pattern light by switching pixels between opaque and transparent states, achieved by controlling the orientation of the liquid crystal molecules comprising the pixel. However, the original LCD devices were not designed for use with UV light, and only transmit about 12.5% of UV light [21].

2.2.3.2 Digital Micromirror Device (DMD)

Given LCD's limited UV transmission, the DMD was used almost exclusively in PSL systems after 1999 [11]–[16], [18]–[24], [28], [31], [32]. DMD's discretize light over a 2D array of aluminum micromirrors that are individually actuated between on and off orientations ($\pm$12 degrees) by electrostatic forces applied at their hinges. The DMD offers many advantages when compared to other available dynamic masks:

- The DMD has small pixel sizes and narrow gaps between pixels. Because of this, DMDs are designed with greater pixel density and can reflect incident light with a more uniform intensity (less light is lost in the gaps). Therefore DMDs have a higher filling ratio (reflective area/total area) compared to LCDs: 91% versus 57% [21].
- The modulation speed between states for individual pixels is also much less for DMDs as compared with LCDs: 20µs versus 20ms. This allows for greater control of exposure time and an increased ability to modulate individual pixels as to achieve gradient, grayscale projection and digitally modulate the intensity of reflected light [21].
- The mirrors of the DMD are surfaced with aluminum that reflects approximately 88% of the incident light, while LCDs typically transmit only 12.5% of incident light. DMDs are therefore more

efficient at patterning light and require less powerful light sources, reducing system cost and complexity [21].

2.2.3.3 Liquid Crystal on Silicone (LCoS)

Liquid Crystal on Silicone (LCoS) devices are a reflective version of LCD technologies. LCoS chips possess a 2D array of liquid crystals between one transparent thin-film transistor (TFT) and one silicon semiconductor. The transparency of each pixel is controlled by applying voltage just like with LCD technology. The opaque pixels pass light to the underlying reflective coating which acts like a DMD mirror. However, unlike a DMD, the reflective surface is static while the liquid crystals determine the pixel pattern instead of mirror orientation. [26].

LCoS devices possess many of the same advantages over LCD devices as DMD devices. LCoS devices generally have higher fill rates and smoother reflective surfaces than the DMD. Unfortunately LCoS chips have poor contrast ratios and do not produce deep blacks. In PSLA, projected images will have a base level of intensity even in areas that are meant to be absent of light. This may unintentionally cure photopolymer and may even encourage the development of artifacts or otherwise restrict dimensional accuracy within the cross section. Furthermore, LCoS chips are difficult and expensive to manufacture making their availability and cost to performance ratio less than that of DMDs [33].

2.2.4 Imaging Optics

The optical components that modify the projected image are regarded as the imaging optics. This series of lenses is typically designed with the intention of capturing the light projection transmitting from the pattern generator and focusing it on the build surface. By choosing lenses with specific focal lengths and numerical apertures, a desirable reduction ratio can be achieved.

The reduction ratio is what determines the achievable resolution and working area, but there is a tradeoff between the two characteristics. A higher reduction ratio (lower magnification) means that higher resolutions are achievable, but this reduces the overall projection area and results in smaller part sizes. System magnification can be calculated using lens equations. For example, Choi explains for a system with a magnification of 0.434, one pixel on the DMD (pitch of 13.68 µm) would reduce to approximately 5.9 µm on the resin surface [12]. This constitutes the physical limit of the X-Y resolution of a system, provided other components do not inhibit achievable feature sizes.

2.2.5 Recoat

There are several methods for reapplying resin to the build surface. The methods include recoating by gravity, by gravity, by pumping and by spreading (Figure 2-2).

2.2.5.1 Recoat by dipping

Recoat by dipping is the most commonly used method for recoating in PSL. In this method, the build platform is dipped below the resin surface to exactly one layer thickness depth. That layer is cured, and the stage descends into the vat of photopolymer, which allows for fresh uncured resin to flow over the previously created layer. The stage then returns to a location where the previously cured layer is exactly one layer thickness below the resin surface [11]–[15], [20]–[23].

2.2.5.2 Recoat by Gravity

Recoat by gravity is used exclusively in bottom-up projection systems (explained further in section 3.6). Unlike the dipping process when projecting from above, the build platform is raised by the z-axis actuator to create a gap between the platform and the resin container for the next layer. If the photopolymer has a low viscosity, it will flow into the created gap. If the photopolymer has a high viscosity, the platform needs to be raised to an exaggerated height such that the photopolymer can fill the gap. The z-axis actuator than moves the platform down until the desired layer thickness gap is achieved, while extra photopolymer is forced to the sides [32]. Hypothetically, pumping the resin into the created gap could assist the recoat process when the viscosity is too high.

2.2.5.3 Recoat by Pumping

Recoat by pumping is used rarely and does not refer specifically to a recoat practice. Systems that utilize pumping in the recoat process typically are paired with a dipping process. One instance of pumping identified in literature is a syringe pump that purges uncured resin from the build surface with a high density "filler" material to prepare for the next layer [16]. In a multi-material system developed by Choi, a "deep dip" process is imitated through precise and extensive pumping [31].

2.2.5.4 Recoat by Spreading

Wiping or spreading uncured resin for recoating is a method common in stereolithography practices [34], and some PSL systems utilize a squeegee or wiping system to recoat or level the resin surface [17].

2.2.6 Projection Orientation

When deciding upon a base design for a PSL system, besides the dynamic mask, one of the most critical considerations is the orientation in which the system will be projecting light on the build surface. Typically, there are two orientation options as shown in Figure 2-3: a top-down approach where the path of light is projected from above onto the resin surface (also referred to as "from above" projection orientation) and a bottom-up approach where light is projected through the bottom surface of vat through a transparent window (also referred to as "from below" projection orientation).

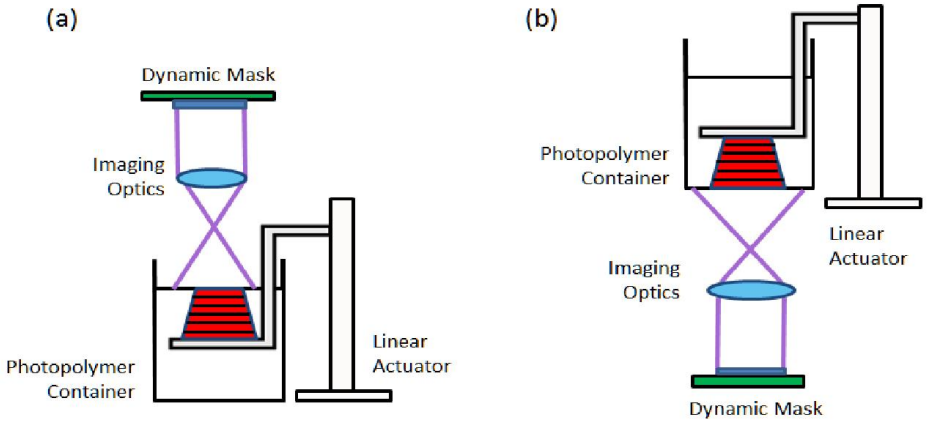

Figure 2-3. Illustration of different projection orientations: (a) image projection from above and (b) image projection from below.

2.2.6.1 Projecting from Above

Typically the slower and more common of the two possible system orientations, projecting from above generally utilizes the dipping method to recoat the part. This approach demands that a designer account for resin characteristics, such as surface tension, viscosity, and wetting, to tune the process and achieve the desired layer thickness. In addition, these characteristics affect polymer settling time, which along with actuator speed, directly influences the process throughput.

In an effort to reduce recoat times, vibration assisted leveling has been experimented with to encourage quicker leveling time of the photopolymer and to obtain thin layers [15], [35]. Also, as mentioned in Section 2.2.5, Takahashi provides one instance in which a squeegee mechanism is used for adjustment of the resin surface in PSL [17]. However, as high resolution is generally in the scope of the top-down design, this type of recoat is avoided as sweeping motions may be enough to agitate the resin or catch the part, destroying the print entirely.

2.2.6.2 Projecting from Beneath (Constrained Surface PSL)

Projecting images through the bottom of the photopolymer container offers several advantages over projecting images from above the container.

- Less photopolymer is required in the reservoir. Because the build part is not submerged in photopolymer as when projecting from above, the reservoir container is independent of part height and can be shallower. Less photopolymer can save time and/or reduce cost.
- System complexity decreases while the overall vertical print speed increases. When projecting from below, gravity is used to more quickly move and settle the photopolymer. Therefore it is unnecessary to implement recoating mechanisms like squeegees or long waiting periods for photopolymer to settle.
- Thinner layers are theoretically possible. Achievable layer thickness in this orientation is determined by the gap between the previously printed layer and the floor of the container, which is directly limited and controlled by the resolution of the vertical actuator of the build platform.
- Photopolymer can polymerize faster because it is removed from ambient oxygen that would otherwise inhibit crosslinking.

As photopolymer cures between the floor of the resin container and the previous layer, it adheres strongly to both. Forces upwards of 50N must be applied to overcome this adhesion and move the build platform, destroying smaller features in the process [32]. Therefore, there is an inherent tradeoff between printing speed and printing resolution for PSLA machines.

Researchers have developed a peeling process that is used when projecting underneath to alleviate feature destruction caused by separation. In this process either the build tray or resin vat is separated from the other by applying a gradual peeling force (like tape from a table). This process reduces the separation force greatly, preserving features smaller than using the same system without peeling. Unfortunately, the peeling process may prolong total build time and negate the inherent speed advantage. Chen's research group, however, has developed a fast mask projection stereolithography process that bypasses this design tradeoff by applying a flexible silicone membrane to the floor of the

resin container [32]. This SYLGARD silicone gel maintains a thin oxidation layer directly on its surface, inhibiting photopolymerization so that a substantially smaller adhesion force is developed. The membrane is also flexible so that the polymer container can slide easily under the build part, to another fresh section of photopolymer (in the same container) for the next layer to cure. This process emulates a peeling step but with much smaller displacements and applied forces, making the impact on overall print speed negligible.

2.3 Categorization and Analysis of PSL Systems

The morphological matrix introduced in Figure 2-2 provides a basis on which existing PSL systems can be analyzed. The existing systems are presented in this section via a categorization based on the critical architectural components of each system. Each morphological matrix is accompanied by a corresponding table that specifies the systems' respective performance parameters. Together, this data provides a basis for determining the effect of system design decisions on critical performance parameters.

2.3.1 First Generation – LCD PSL Systems

Bertsch, Chatwin, and Monneret published the first PSL systems. These systems all use beam expansion for their conditioning optics, LCD masks to pattern light, project images from above the photopolymer, reduce the projected image in size, and recoat photopolymer by dipping. This design architecture is illustrated in Figure 2-4 using the morphological matrix (Figure 2-2). The performance parameters of multiple systems using this architecture are compared in Table 2-2.

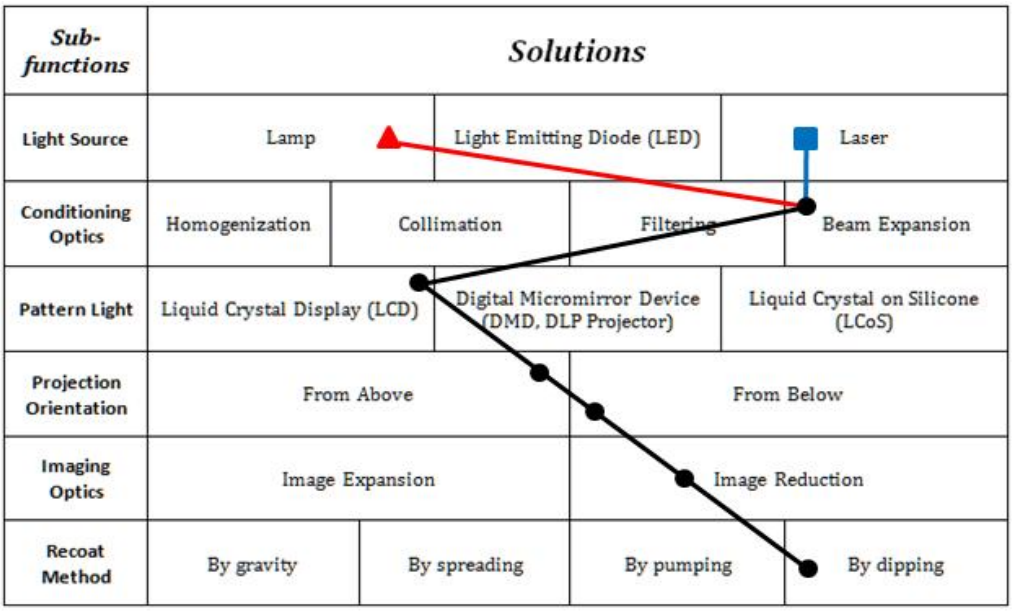

Figure 2-4. Morphological matrix categorizing PSL machines that use a LCD device to project images.

All of these machines are capable of producing 5 µm minimum feature sizes with layer thicknesses ranging from 5 to 10µm. The machines published by Bertsch and Monneret are particularly noteworthy because they use visible light to cure photopolymer. Future PSL research moved away from visible photopolymers

in favor of curing with UV light. Exposure times for these machines varied, but were roughly 60 seconds per layer on average. The following section introduces second generation PSL systems.

Table 2-2. Performance parameters for the PSL systems categorised in Figure 2-4.

	Ref	Research Group	Year	Special Features	Min. Feature Size	Min. Layer Thickness	Maximum Part Size	Vertical Build Rate
■	[2], [3]	Bertsch	1997	LCD,Laser, 515 nm	5 µm	5 µm	1.3 x 1.3 x 10 mm^3	110 layers in 90 minutes
■	[27]–[30]	Chatwin	1998	LCD,Laser, 351.1 nm	5 µm	Not reported	50 x 50 x 50 mm^3	60 second exposure per layer
▲	[25]	Monneret	1999	LCD,Lamp, 530nm	5 µm	10 µm	3.2 x 2.4 x 1.3 mm^3	60 layers per hour

2.3.2 Second Generation – DMD PSL Systems

The systems categorized in this section use a DMD to dynamically shape the projected image. These systems were grouped together in order to identify the paradigm shift in design decisions with the advent of the DMD. As outlined in Section 3.3.2, the transition from LCD to DMD was a result of better performance characteristics such as smaller pixel sizes, narrower gaps between pixels, higher modulation speeds, and high reflectivity. The morphological matrix presented in Figure 2-5 represents systems that utilize a lamp, DMD dynamic mask, from-above projection, image reducing optics, recoat by dipping, but employ unique conditioning optics.

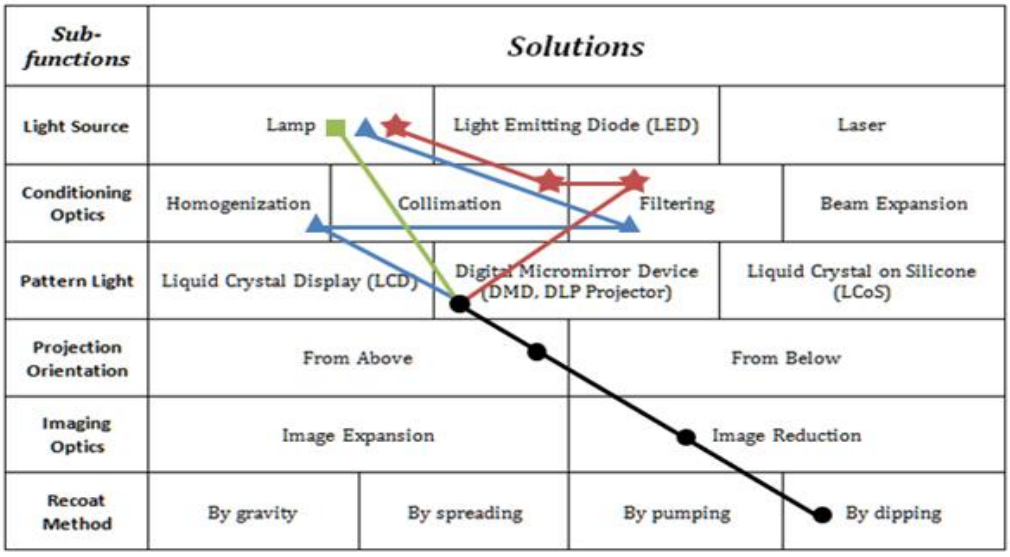

Figure 2-5. Morphological matrix categorizing PSL machines that use a DMD device to project images.

As seen in Table 2-3, the reported achievable feature size of the DMD projection from above systems utilizing the dipping recoat method ranges from 0.6 to 30 µm. While smaller feature sizes were achieved with DMD based systems, the average achievable feature size is not significantly smaller than LCD systems. Unfortunately, the vertical build rate metric for many of these systems are not comparable as many publications use different speed metrics (as discussed in Section 2.1.2). Regardless, all systems in Figure 2-4 and Figure 2-5 use the dipping recoat method, and their build times seem comparable. However, as LCD masks transmit only 12.5% of UV light (as mentioned in Section 2.2.3.1), build time can increase by a factor of 7 when compared to systems using a DMD with the same light source.

Table 2-3. Performance parameters for the PSL systems categorised in Figure 2-5.

	Ref	Research Group	Year	Special Feature	Min. Feature Size	Min. Layer Thickness	Part Size	Vertical Build Rate
★	[22]	Rosen	2007	DMD, 365 nm	6 µm	400 µm	2 x 2 x 1 mm^3	90s per layer
★	[11]	Rosen	2007	DMD, 365, 435, 647 nm	5 µm	5 µm	not reported	60s per layer
★	[12]	Wicker	2009	DMD, 365 nm	30 µm	4 µm	1.95 x 1.95 x 2.4 mm^3	<1s per layer
★	[20]	Lee	2008	DMD, 365nm, XY translation	2 µm	5 µm	10 x 10 x 2.68 mm^3	100s per layer
★	[23], [24]	Bertsch	1999	DMD, visible	5 µm	5 µm	6 x 8 x 15 mm^3	700 layers in 2.5 hours
★	[13], [18]	Bertsch	2000	DMD, UV	10 µm	10 µm	10.24 x 7.68 x 20 mm^3	200 layers in 1 hour
▲	[21]	Zhang	2005	DMD, 364 nm, fly-eye lens	0.6 µm	5 µm	not reported	not reported
■	[14]	Roy	2006	DMD, 355 nm	20 µm	150 µm	not reported	90s per layer
■	[15]	Hadipoespito	2003	DMD, 365 nm	20 µm	100 µm	not reported	not reported

Figure 2-6 and Table 2-4 presents systems using a DMD dynamic mask to project images from above, while employing alternative solutions to achieve recoating.

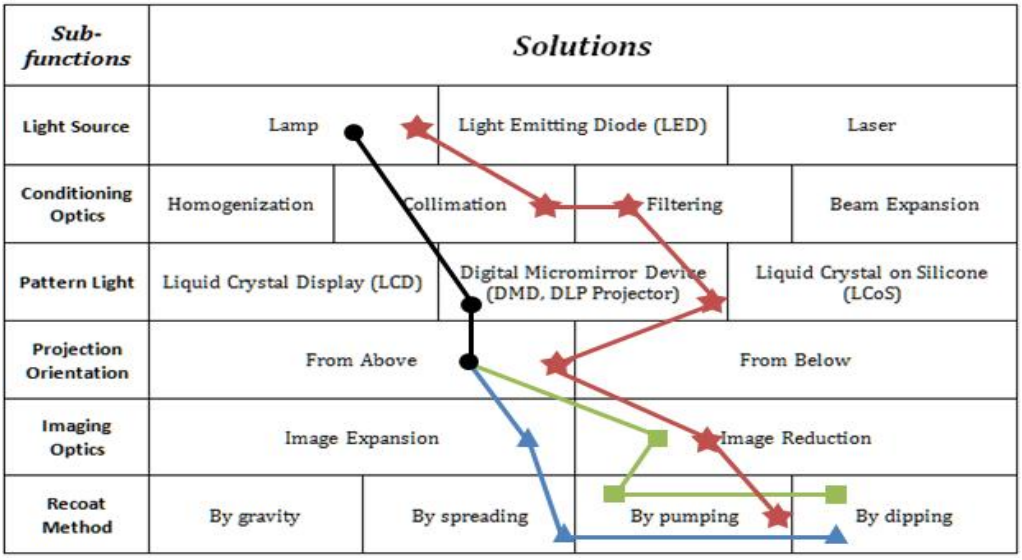

Figure 2-6. Morphological matrix categorizing PSL machines that use alternative recoat methods.

Table 2-4. Performance parameters for the PSL systems categorized in Figure 2-6.

	Ref	Research Group	Year	Special Feature	Min. Feature Size	Min. Layer Thickness	Part Size	Vertical Build Rate
★	[31]	Wicker	2009	DMD, 365 nm, multi material	~50 µm	21 µm	~ 2 x 2 x 4 mm^3	8-12s per layer
▲	[17]	Takahashi	2000	DMD, 365 nm	50 µm	200 µm	~ 2 x 2 x 2 mm^3	not reported
■	[16]	Roy	2008	DMD, 355 nm	50 µm	50 µm	not reported	60s per layer

Comparing the systems' performances listed in Table 2-2 and Table 2-3 versus Table 2-4Table 1-1 (which primarily differ by recoat method) suggests that systems that do not use recoat by dipping generally have larger minimum feature sizes (approximately 50 µm) and layer thicknesses ranging from 21 µm to 200 µm. This indicates that dipping may be the preferable method for recoating if the goal of system is to achieve a minimum feature sizes (as discussed in 2.2.5).

2.3.3 Third Generation

As the embodiment of second generation systems became a standard, some researchers have begun experimenting with alternative projection orientation in the effort to reduce build time. The system architecture presented in Figure 2-7 and Table 2-5 is unique as it projects from below and recoats by gravity.

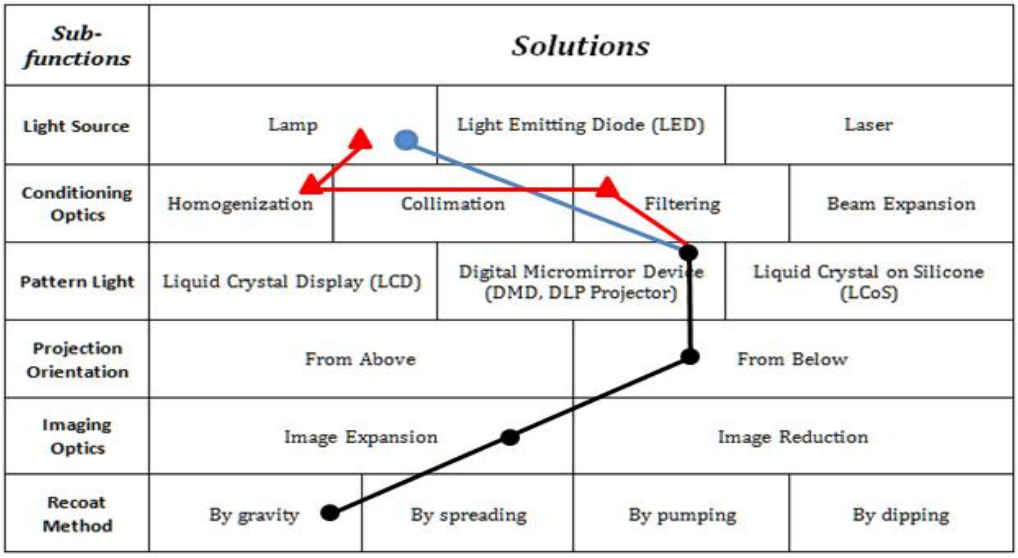

Figure 2-7. Morphological matrix categorizing PSL system that use a DMD device to project images

Table 2-5. Performance parameters for the PSL systems categorized in Figure 2-7.

	Ref	Research Group	Year	Special Features	Min. Feature Size	Min. Layer Thickness	Maximum Part Size	Vertical Build Rate
●	[32]	Chen	2012	DMD, Lamp, visible	400 µm	100 µm	48 x 36 mm^2	180 mm per hour
▲	[19]	Kang	2012	DMD, Lamp, UV	Not reported	Not reported	14.6 x 10.9 mm^2	Not reported

The feature sizes reported in Table 2-5 are much larger than those of the systems listed in Table 2-2 through Table 2-4 but the part size is also much larger. The print speed is the quickest of all systems analyzed [32]. Chen et al indeed show that projecting from below is quicker but also cannot achieve the resolution of top down projection systems because of the peeling force [36]. Work in this system embodiment still developing, and there is room for further improvement based on the performance parameters advantages.

2.3.4 Alternative Embodiments

The last system is unique in that it is the only published system that utilizes an LED light source, and is the only published system that uses an LCoS device to digitally pattern light. Figure 2-8 and Table 2-6 outline this system and characterizes its performance. This unique system achieves very small feature sizes, comparable layer thickness and part size of other projection from above, recoat by dipping systems. It follows the trend that high resolution is achievable by combining recoating via dipping with the top-down orientation.

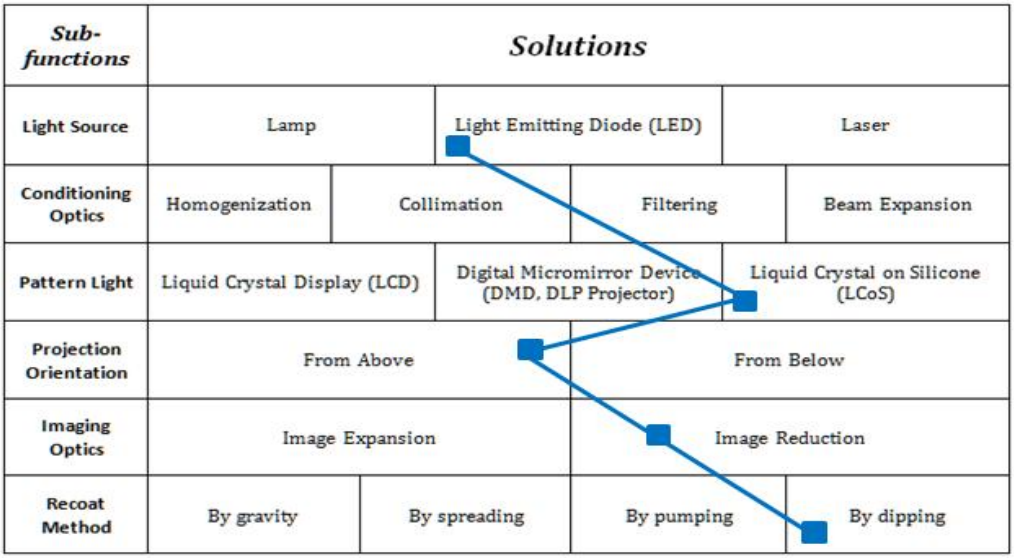

Figure 2-8. Morphological matrix categorizing PSL systems that use a LCoS device to project images.

Table 2-6. Performance parameters for the PSL system categorized in Figure 2-8.

	Ref	Research Group	Year	Special Features	Min. Feature Size	Min. Layer Thickness	Maximum Part Size	Vertical Build Rate
■	[26]	Zheng	2012	LCoS, LED, 395nm	1.3 µm	10 µm	2.56 x 1.44 mm^2	Not reported

2.4 Reflection on the Results

This section presents a PSL morphological matrix that is designed to functionally categorize and compare the fundamental design decisions solved in the realization of PSL systems. Using this matrix, several published PSL systems are analyzed in terms of critical PSL performance parameters: minimum feature size (µm), layer thickness (µm), build volume (mm^3), and vertical build time (mm/s). These performance parameters are expressed in units that serve as a standard benchmark to promote direct quantitative comparisons between PSL systems. From this analysis, relationships between system performance and the corresponding subsystems solutions have been identified to indicate general trends and tradeoffs.

- The most common system embodiments project images from above the photopolymer container and dip the build platform to achieve recoating. These systems are capable of achieving the smallest feature sizes, which are close to 1 µm.
- Dynamic mask selection does not significantly affect the minimum achievable feature size. While pixel pitch is a relevant design consideration, final feature size is ultimately determined by the imaging optics.
- Dynamic mask selection significantly affects the vertical build rate of a PSL system. LCD masks transmit only 12.5% of UV light, which can increase build time by a factor of 7 when compared to using a DMD with the same light source.
- The relationship between part size and feature size is equivalent to the relationship between aspect ratio and pixel pitch for any dynamic mask. Future dynamic masks with an equivalent pixel pitch but with greater resolution will enable creation of smaller feature sizes on equally sized parts, or the same feature sizes on larger parts.
- If a fast vertical build rate is priority, then system embodiment should project images from below the photopolymer vat. By using a gravity-assisted recoat approach, vertical build rates can be improved by an order of magnitude.
- The type of light source is noncritical provided that emission properties (wavelength and intensity) are suitable, and appropriate light conditioning is performed.

Amongst published PSL systems, design trends have changed historically. Exploration of novel form factors and embodiments has been limited. An area for future research is in exploring more unique embodiments and subsystem solutions. In doing so, the relationships between PSL performance parameters and subsystem solutions can be more broadly and quantitatively compared. These relationships are used to develop a PSL process optimized for fabrication with nanocomposites in Chapter 3, and ultimately these relationships can be used to aid other engineers in the design of PSL systems for their unique applications.

3. Design of the PSL System

A formal design process was used to translate research needs into a functional system capable of creating 3D objects from nanocomposite photopolymer. This process began with identification of the system requirements and translating those requirements into performance specifications (Figure 3-1). These specifications were used to determine appropriate design tradeoffs during the conceptual design of the system, and later for the detailed system design of subcomponents and their embodiment.

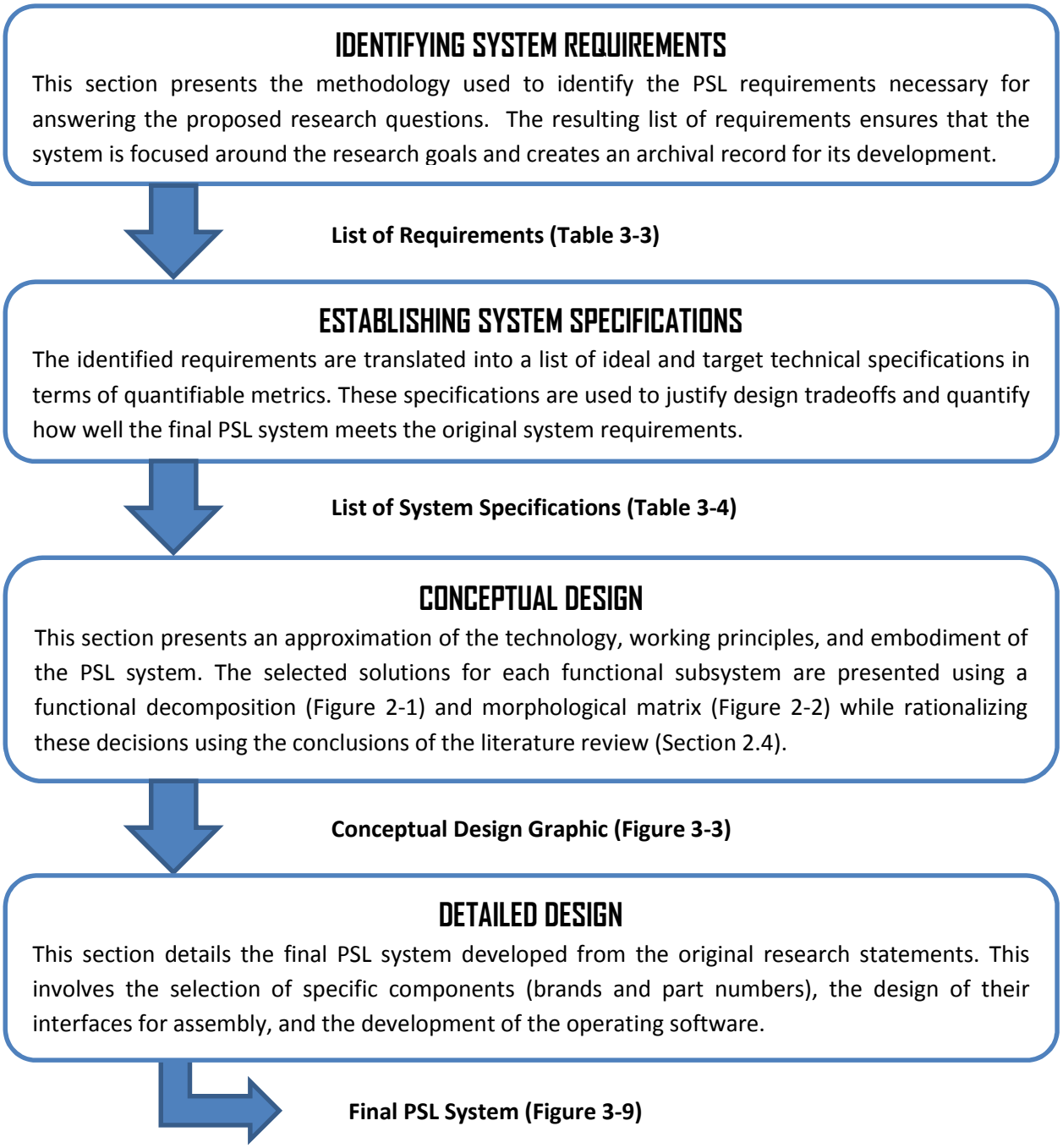

Figure 3-1. Flowchart of the design process used to develop the PSL system presented in this thesis. This flowchart also serves as an outline of the sections in this chapter, showing their outcomes.

By following this design process, a PSL system will be created specifically for fabricating three dimensional components from nanocomposite photopolymers with embedded MWCNT. This system is the answer Developmental Question #1:

Developmental Question #1: What features and components does a PSL system designed to process nanocomposites possess and what is their embodiment?

3.1 Identifying System Requirements

The process of identifying system requirements is an important part of the larger PSL development process and is a prerequisite to the establishment of PSL specifications and eventual concept generation. System requirements are general statements concerning revealing the expectations for the performance, appearance, embodiment, operation, and other properties of the system. Comprehensive identification of these requirements is important to ensure that this PSL system addresses all of the hidden and explicit requirements. The same requirements also provide a fact base for justifying the PSL specifications. This process was performed in five steps.

1. *Gather Raw Data*– Data was gathered through informal discussions and one on one interviews with Dr. Christopher Williams of the research team. During these discussions a series of statements regarding various topics were recorded. The results of these discussions are shown in Table 3-1.

2. *Interpret Raw Data in Terms of Research Needs* - Research needs were then derived by translating each statement or observation into one or more research needs, also shown in Table 3-1. These needs are expressed without implying solutions using the same level of specificity apparent in the original comment.

3. *Organize the Needs into a Hierarchy* - The 32 research needs were categorized and identified as primary and secondary needs, then organized into the intuitive hierarchy shown in Table 3-2. Primary needs represent the most general needs, while secondary needs provide additional detail of varying importance.

4. *Establish the Relative Importance of the Needs* – Because the design process sometimes requires conflicting design trade-offs, understanding the relative importance of these research needs is required to make the appropriate design decisions. The research needs are weighed numerically in Table 3-3 below using intuitive judgment of the original needs statements.

5. *Reflection on the Results and the Process* - It is evident that the most critical needs are concerned with the manufacturing quality of nanocomposite objects; specifically their resolution, precision, and repeatability. The PSL machine must also promote ease of maintenance, component accessibility, robustness; and secondarily, portability and ease of assembly.

Table 3-1. Research needs statements and the interpreted research needs.

Research Group:	Dr. Thomas Campbell, Dr. Christopher Williams, Earl Campaigne	
Question/ Prompt	**Statement**	**Interpreted Need**
Geometry	Levelness to ground is important for part consistency. It would be nice to transport this for demonstrations. “ Stability is important for a portable device. The resin elevator will move higher for taller build parts.	The resin elevator and vat are level. The machine travels easily and be transportable. The total height, width, and length can be carried. The machine does not fall over easily. The vertical actuator does not limit part height.
Kinematics	Recoating submerges the entire build part in the resin. Controlling light exposure aids in process optimization. We would like to manufacture wearable sensors. “ Dependable fabrication is an important benchmark. The wearable sensors will have micro-scale features.	The resin container covers the projection area. The machine controls light exposure. The machine possesses adequate fabrication volume. The machine projects over an adequate surface area. The machine creates accurate and precise features. The machine produces micro-scale features.
Energy	A portable machine must work in any office setting. Photopolymers are typically cured using UV light. Stray UV light can be harmful to operators over time.	The machine operates using minimum power supplies. The machine projects UV light of sufficient intensity. The machine prevents stray UV light.
Material	Cure depth, depth of penetration, and critical exposure are important material properties we will characterize.	The machine characterizes the polymer’s material properties.
Signals	Users must supply their part information. System parameters may need to be adjusted per resin. Machine might communicate build information back users. Control software must coordinate DOFs with the mask.	The machine possesses ports to transfer data. The software possesses an easy to use input UI. The software possesses an informative output UI. The machine is coordinated by control software.
Safety	User exposure to toxic photopolymers is unhealthy. Users should have a means for a safety over ride. This machine will be used in an office or classroom setting. Sensor feedback is important for safer machine operation.	The machine contains photopolymer securely. The machine requires an emergency off switch. The machine is safe to use in an office or classroom. The machine possesses feedback sensors.

Ergonomics	The product must promote demonstration and outreach. High learning curve is a barrier to accessibility. Visible internal components improve demonstration quality.	The machine serves as a demonstration showpiece. The setup process is straightforward and simple. The machine shows the internal components.
Production	We should utilize our additive manufacturing capabilities. System requirements will evolve over time.	AM is the preferred method of manufacturing. The machine is designed on a modular infrastructure.
Assembly/ Disassembly	Tools are not always accessible at hand when traveling. Assembly needs to be performed quickly when deployed. Using universal components quickens assembly.	The machine requires few tools for assembly. The machine assembles and sets up quickly, on demand. The machine uses common components for fasteners.
Transport	Must be moved and deployed by a single individual. Durability is important for trouble free transportation. Constant use and transport will create wear and tear.	The machine is light weight and disassembles. The machine is entirely encased for protection. The machine requires little regular maintenance.
Operation	External light sources can prematurely cure resins. Machine must operate in the classroom or office space. The finished part must be removed without damage. Build time is very important.	The machine isolates photopolymer from external light. The machine produces little noise during operation. Manufactured part must be removable without damaging. The machine prints vertical height quickly.
Maintenance	Manual calibration needs to be kept to a minimum. Replacing a light source is very expensive.	The optical components and mounting are robust. The light source operates for a realistic life time.
Costs	The budgetary restraints are important to consider. Resin and nanoparticles are expensive materials. We want to optimize machine performance per cost.	The machine costs do not surpass the appropriated budget. The machine wastes little photopolymer. The machine is economically and commercially viable.

Table 3-2. Hierarchical list of primary and secondary needs for the PSL system. Asterisks are used to identify the importance of secondary needs; one asterisk is of minimum importance while three asterisks are of critical importance. Latent needs are identified by an exclamation point.

	The system travels easily and be transportable.
*!	The total dimensions can be carried.
**	The system does not fall over easily
*	The system operates using minimum power supplies.
***	The system must be light weight and/or disassemble.
*	The system is entirely encased for protection.
	The system assembles and sets up quickly, on demand.
*	The system requires few tools for assembly.
**	The system is designed on a modular infrastructure.
*	The system uses common components for fasteners.
***	The system is light weight and disassembles.
	The system possesses adequate fabrication volume.
*	The vertical actuator does not limit part height.
***	The resin container covers the projection area.
***!	The system projects over an adequate surface area.
	The system produces micro-scale features.
**	The resin elevator and vat are level.
**	The system creates accurate and precise features.
***	Manufactured part must be removable without damaging.
***	The system projects UV light of sufficient intensity.
*	The system prevents stray UV light.
	The system can characterize the polymer's material properties.
**	The system controls light exposure.
*	The system isolates photopolymer from external light.
	The system is coordinated by control software.
***	The **system** possesses ports to transfer data.
***	The software possesses an intuitive input UI.
*	The software possesses an intuitive output UI.
	The system serves as a demonstration showpiece.
**	The setup process is straightforward and simple.
*	The system shows the internal components.

The system is safe to use in an office or classroom.

*** The system contains photopolymer securely.

* The system requires an emergency off switch.

** The system possesses feedback sensors.

* The system produces little noise during operation.

AM is the preferred method of manufacturing.

The system requires little regular maintenance.

*** The optical components are robustly mounted.

The system is economically and commercially viable.

** The system prints vertical height quickly.

*** The system costs do not surpass the appropriated budget.

* The system wastes little photopolymer.

* The light source operates for a realistic life time.

Table 3-3. Research needs identified with relative importance.

No.		Need	Imp.
1	The total dimensions	can be carried.	1
2	The system	does not fall over easily	2
3	The system	operates using minimum power supplies.	1
4	The system	is entirely encased for protection.	1
5	The system	requires few tools for assembly.	1
6	The system	is designed on a modular infrastructure.	3
7	The system	uses common components for fasteners.	2
8	The system	is light weight and disassembles.	4
9	The vertical actuator	does not limit part height.	3
10	The resin container	covers the projection area.	5
11	The system	projects over an adequate surface area.	5
12	The resin elevator and vat	are level.	3
13	The system	creates accurate and precise features.	4
14	Manufactured parts	must be removable without damaging.	5
15	The system	projects UV light of sufficient intensity.	5
16	The system	prevents stray UV light.	1
17	The system	controls light exposure.	3
18	The system	isolates photopolymer from external light.	2
19	The system	possesses ports to transfer data.	5
20	The software	possesses an easy to use input UI.	4
21	The software	possesses an informative output UI.	1
22	The system	contains photopolymer securely.	4
23	The system	requires an emergency off switch.	3
24	The system	possesses feedback sensors.	2
25	The system	produces little noise during operation.	1
26	The setup process	is straightforward and simple.	3
27	The system	shows the internal components.	2
28	The optical components	are robustly mounted.	5
29	The system	prints vertical height quickly.	4
30	The system costs	do not surpass the appropriated budget.	5
31	The system	wastes little photopolymer.	2
32	The light source	operates for a realistic life time.	3

3.2 Establishing System Specifications

Having evaluated the state of the art in PSL and having determined the research needs of this project, the next step in the design process is to determine this PSL system's specifications. A product specification is a set of target specifications that defines what the PSL machine is supposed to do by describing the research needs using measurable units and numeric value. The working principle is that translating needs to set of measurable product specifications is possible, and that meeting the target specifications will satisfy the corresponding needs.

1. *Prepare the List of Metrics* – Metrics are determined by considering each research need and deciding upon a precise, measurable characteristic that will reflect the degree to which the PSL machine will satisfy that need. Table 3-4 lists the metrics along with the research needs they represent, their importance, and the unit of measurement.
2. Table 3-5 illustrates the same information in the form of a needs-metrics matrix. This matrix represents the relationship between the needs in rows and metrics in columns.

3. *Collect Competitive Benchmarking Information* – Competitive benchmarking information was collected for 18 PSL systems as part of the literature review in Section 2.3, Categorization and Analysis of PSL Systems. Figure 3-2 and
4. Table 3-6 highlight five PSL systems from the literature review. These systems are representative of the diversity found in PSL architecture. Table 3-7 shows the performance parameters of the same five systems as reported in their technical publications.

5. *Set Ideal and Marginally Acceptable Values* –Table 3-8 shows the ideal and marginally acceptable target metrics for each specification. The exact values were chosen based on the research needs using intuition, along with experience acquired from performing the literature review. Not all of these values will be achieved because there are inherent design tradeoffs that force compromise. However, these values will guide the conceptual design of this PSL system and later be used to evaluate its success in fulfilling the product specifications.

6. *Reflect on the Results* – By benchmarking other PSL systems through a formal literature review, realistic ideal and marginally acceptable target values were determined to provide a guideline for the conceptual design of the physical system. The most important product specifications (feature accuracy, feature precision, area of fabricated parts, and vertical build rate, vertical build rate, etc.) come from the most critical research needs and have some of the most ambitious and demanding target specifications.

Table 3-4. List of metrics for the PSL system with units of meaurement and relative importance.

Metric No.	Need No.	Metric	Imp.	Units.
1	1	Total length	1	in
2	1	Total width	1	in
3	1, 2	Total height	2	in
4	2	Footprint area of the base	2	in^2
5	3	Power supply voltages	1	V
6	4	Total weight	1	lbs
7	5	Percentage of components encased	1	%
8	6, 8	Number of tools required for assembly	4	#
9	4, 6, 7	Number of components when disassembled	3	#
10	6, 7, 8	Number of different fasteners used	3	#
11	9	Vertical travel of the build platform	3	mm
12	10	Area of the build platform	5	$inch^2$
13	10, 11	Area of fabricated parts footprint	5	$inch^2$
14	12	Levelness of the photopolymer resin	3	%
15	13	Feature accuracy	4	um
16	13	Feature precision	4	um
17	14	Effort required to remove part	4	s
18	14, 15, 17	UV light intensity at projection plane	5	mW/cm^2
19	16	Maximum UV light intensity 6" from machine	1	mW/cm^2
20	17	Intensity range adjusted across	3	mW/cm^2
21	18	Ambient UV intensity at projection plane	2	mW/cm^2
22	19, 20, 21, 26	Number of data ports/connections	3	#
23	20, 26	Number of Input data fields	3	#
24	21, 24, 26	Number of output data fields	3	#
25	22	Volume of photopolymer that may leak	4	$inch^3$
26	23	Requires an emergency off switch	3	Y/N
27	24	Number of feedback sensors	2	#
28	25	Maximum sound volume 1' away from machine	1	dB
29	26	Time to start a build	3	min
30	26	Number of steps required to begin a print	3	#
31	27	Percentage of internal components visible	2	%
32	28	Degrees of freedom for optical components	5	# DOF
33	29	Vertical build rate	4	mm/min
34	30	Development cost of the machine	5	$
35	31	Volume of photopolymer wasted per build	2	$inch^3$
36	32	Operating lifetime of the machine	3	hrs

Table 3-5. The needs-metrics matrix showing the relationship between needs and metrics.

	Need	1 Total length	2 Total width	3 Total height	4 Footprint area of the base	5 Power supply voltages	6 Total weight	7 Percentage of components encased	8 Number of tools required for assembly	9 Number of compoenents when dissassembled	10 Number of different fasteners used	11 Vertical travel of the build platform	12 Area of the build platform	13 Area of fabricated parts footprint	14 Levelness of the photopolymer resin	15 Feature accuracy	16 Feature Precision	17 Force required to remove part	18 UV light intensity at projection plane	19 Maximum UV light intensity 6" from machine	20 Intensity range adjusted across	21 Ambient UV intensity at projeciton plane	22 Number of data ports/connections/sensors	23 Number of Input data fields	24 Number of output data fields	25 Volume of photopolymer that leaks during operation	26 Requires an emergency off switch	27 Number of feedback sensors	28 Maximum sound volume 1' away from machine	29 Time to start a build	30 Number of steps required to begin a print	31 Percentage of internal components visible	32 Total degrees of freedom for all optical components	33 Vertical build rate	34 Development cost of the machine	35 Volume of photopolymer wasted per build	36 Operating lifetime of the machine
	Metric																																					
1	Can be carried	•	•	•																																		
2	Does not fall over easily			•	•																																	
3	Operates using minimum power supplies					•																																
4	Is light weight and disassembles						•			•																												
5	Is entirely encased for protection							•																														
6	Requires few tools for assembly								•	•	•																											
7	Is designed on a modular infrastructure									•	•																											
8	Uses common components for fasteners								•		•																											
9	Does not limit part height											•																										
10	Covers the projection area												•	•																								
11	Projects over an adequate surface area													•																								
12	Is level														•																							
13	Creates accurate and precise features															•	•																					
14	Must be removable without damaging																	•	•																			
15	Projects UV light of sufficient intensity																		•																			
16	Prevents stray UV light																			•																		
17	Controls light exposure																		•		•																	
18	Isolates photopolymer from external light																					•																
19	Possesses ports to transfer data																						•															
20	Possesses a easy to use input UI																						•	•														
21	Possesses an infromative output UI																						•		•													
22	Contains photopolymer securely																									•												
23	Requires an emergency off switch																										•											
24	Possesses feedback sensors																								•			•										
25	Produces little noise during operation																												•									
26	Is straightforward and simple																						•	•	•					•	•							
27	Shows the internal components																															•						
28	Is robustly mounted																																•					
29	Prints vertical height quickly																																	•				
30	Does not surpass the appropriated budget																																		•			
31	Wastes little photopolymer																																			•		
32	Operates for a realistic life time																																				•	

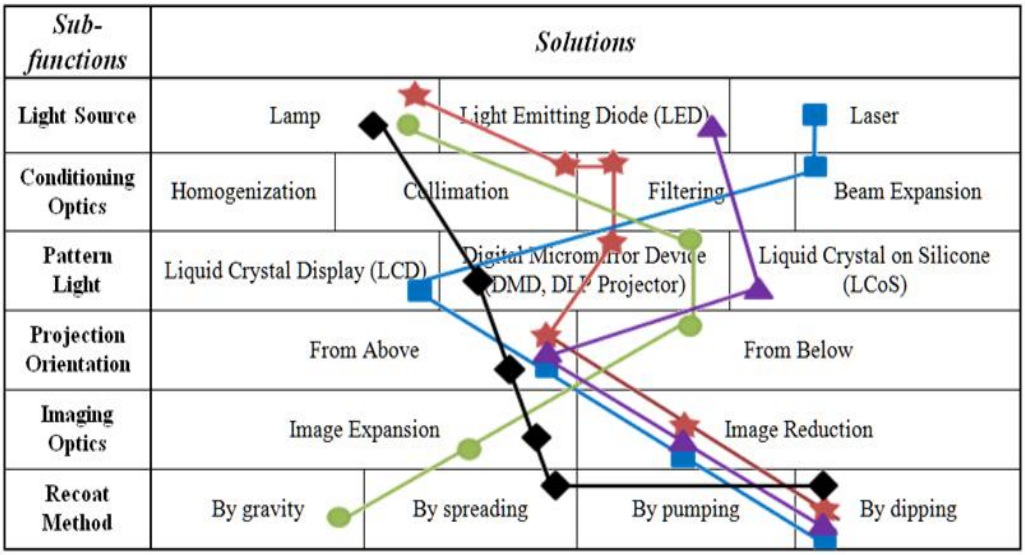

Figure 3-2. A morphelogical matrix showing the PSL system architectures from Section 2.3.

Table 3-6. A list view of the PSL systems categorized in Figure 3-2.

Research Group	Year Published	Light Source	Conditioning Optics	Pattern Light	Projection Orientation	Imaging Optics	Recoat Method
Bertsch	1997	Laser	Beam Expansion	LCD	Above	Reduction	Dipping
Bertsch	1999	Lamp	Collimation Filtering	DMD	Above	Reduction	Dipping
Takahashi	2000	Lamp	N/A	DMD	Above	Reduction	Spreading & Dipping
Zheng	2012	LED	N/A	LCoS	Above	Expansion	Dipping
Chen	2012	Lamp	N/A	DMD	Below	Expansion	Gravity

Table 3-7. The performance parameters of the PSL systems in Figure 3-2 and repeated in Table **3-6**.

Research Group	Year Published	Minimum Feature Size	Layer Thickness	Build Volume	Vertical Build Rate
Bertsch	1997	5 μm	5 μm	1.3 x 1.3 x 10 mm^3	73 layers per hr
Bertsch	1999	5 μm	5 μm	6 x 8 x 15 mm^3	280 layers per hr
Takahashi	2000	50 μm	200 μm	2 x 2 x 2 mm^3	Not reported
Zheng	2012	1.3 μm	10 μm	2.56 x 1.44 mm^2	Not reported
Chen	2012	400 μm	100 μm	48 x 36 mm^2	180 mm per hr

Table 3-8. Target specifications added to the previous list of product specifications.

Metric No.	Need No.	Metric	Imp.	Units.	Marginal Value	Ideal Value
1	1	Total length	1	in	< 48	< 24
2	1	Total width	1	in	< 48	< 24
3	1, 2	Total height	2	in	< 36	< 24
4	2	Footprint area of the base	2	in^2	< 1152	< 576
5	3	Power supply voltages	1	V	5, 12, 125	125
6	4	Total weight	1	lbs	< 50	< 35
7	5	Percentage of components encased	1	%	> 50%	> 60%
8	6, 8	Number of tools required for assembly	4	#	< 10	< 5
9	4, 6, 7	Number of components when disassembled	3	#	$4 \leq x \leq 10$	$4 \leq x \leq 6$
10	6, 7, 8	Number of different fasteners used	3	#	< 5	< 3
11	9	Vertical travel of the build platform	3	mm	> 50	> 100
12	10	Area of the build platform	5	$inch^2$	> 1.5	> 5
13	10, 11	Area of fabricated parts footprint	5	$inch^2$	> 1	> 4
14	12	Levelness of the photopolymer resin	3	%	< 5	0
15	13	Feature accuracy	4	um	< 50	< 20
16	13	Feature precision	4	um	< 25	< 10
17	14	Effort required to remove part	4	s	< 30	< 10
18	14, 15, 17	UV light intensity at projection plane	5	mW/cm^2	> 5	> 7.5
19	16	Maximum UV light intensity 6" from machine	1	mW/cm^2	< 1	0
20	17	Intensity range adjusted across	3	mW/cm^2	> 10	> 25
21	18	Ambient UV intensity at projection plane	2	mW/cm^2	< 0.25	< 0.0
22	19, 20, 21, 26	Number of data ports/connections	3	#	< 5	< 2
23	20, 26	Number of Input data fields	3	#	< 5	< 2
24	21, 24, 26	Number of output data fields	3	#	> 5	> 8
25	22	Volume of photopolymer that may leak	4	$inch^3$	< 50	< 30
26	23	Requires an emergency off switch	3	Y/N	N	Y
27	24	Number of feedback sensors	2	#	> 3	> 5
28	25	Maximum sound volume 1' away from machine	1	dB	< 60	< 40
29	26	Time to start a build	3	min	< 5	< 3
30	26	Number of steps required to begin a print	3	#	< 10	< 6
31	27	Percentage of internal components visible	2	%	> 50%	> 75%
32	28	Degrees of freedom for optical components	5	# DOF	< 14	< 8
33	29	Vertical build rate	4	mm/min	> 0.5	>1
34	30	Development cost of the machine	5	$	< 25000	< 20000
35	31	Volume of photopolymer wasted per build	2	$inch^3$	< 1	< 0.75
36	32	Operating lifetime of the machine	3	hrs	> 100	> 150

3.3 Conceptual Design

A conceptual design is an approximation of the technology, working principles, and embodiment of a product. Using the structure of the functional decomposition (Figure 2-1) and morphological matrix (Figure 2-2) previously presented in the literature review, this chapter presents the selected solutions for each functional subsystem while rationalizing these decisions using the conclusions of the literature review (Section 2.4) and the established target specifications (Table 3-8).

1. *Light Source* - A controllable lamp based light source was selected for this PSL system. Because lamp based light sources emit a broad spectrum of light, with multiple intensity peaks, they may work with a greater variety of photopolymers. Lamps have also been used heavily in PSL systems so they carry less inherent risk than LEDs or lasers since there is more prior literature for reference.

2. *Conditioning Light* – Light output intensity from a lamp based source typically follows a Gaussian profile from the center of the beam. A homogenizing optical rod takes light input and reflects it repeatedly, along the length of the rod to create light with a homogenous intensity. Lamp based light sources typically deliver highly divergent (high numeric aperture) light using a liquid light guide. An optical lens should be used to collimate the divergent light into a parallel beam, so sufficient intensity can be focused directly onto the digital light processor. These conditioning optical are largely responsible for the repeatability, accuracy, and precision of fabricated parts.

3. *Pattern Light* – A DMD was selected to digitally pattern and project cross sectional images. DMD chipsets transmit UV light more efficiently then LCD chipsets and are more established in prior literature than LCoS chipsets. DMDs are also cheaper and more accessible; they are even available in convenient developer board form factors.

4. *Imaging Optics* - A set of lenses will serve as the imaging optics for this PSL system, resizing the image reflected by the DMD. The projected print area can be designed by choosing lenses with proper diameter and focal length. The level of magnification at the build plane restricts the resolution of the projected image, the light intensity, and therefore the build speed. It is important that these tradeoffs are appropriately balanced for this PSL system.

5. *Projection Orientation and Recoating* – Projecting cross sectional images from below the build plane constrains curing between the container surface and the build platform such that parts are not submerged in a vat. This require less photopolymer material during fabrication and makes projecting from below the most appropriate embodiment for this PSL system. This technique also uses gravity to achieve higher vertical build rates and throughput, while simultaneously serving as a mechanism for controlling layer thickness. Its simplicity also makes assembly and maintenance easier. It does, however, impose a limit on the achievable feature sizes because the object layers have to be peeled from the constraining surface.

6. *Reflect on the Results*- Figure 3-3 below shows a summary of the chosen conceptual design. This system uses a lamp based light source with conditioning optics that homogenize and collimate light before it reaches a DMD digital light processor. The images will be projected from the DMD below the build plane, which relies on gravity to recoat the surface with photopolymer. The next step in the design process is the detail design, the selection of specific components as well their exact embodiment with regards to one another.

Sub-functions	***Solutions***			
Light Source	Lamp	Light Emitting Diode (LED)	Laser	
Conditioning Optics	Homogenization	Collimation	Filtering	Beam Expansion
Pattern Light	Liquid Crystal Display (LCD)	Digital Micromirror Device (DMD, DLP Projector)	Liquid Crystal on Silicone (LCoS)	
Projection Orientation	From Above		From Below	
Imaging Optics	Image Expansion		Image Reduction	
Recoat Method	By gravity	By spreading	By pumping	By dipping

Figure 3-3. Morphological matrix illustrating the chosen conceptual design.

3.4 Detailed Design

Having identified the subsystem solutions categorically, the detailed design step presents the final PSL system developed from the original research statements. This involves the selection of specific components (brands and part numbers) and the design of their interfaces for assembly. Several prototype systems were developed and tested using a DMD controller (FlexLight X3 DLP Controller sold by Keynote Photonics) in combination with different optical assemblies. Limited success with unsatisfactory image clarity further motivated the final system implementation. The entire bill of materials is included in Appendix A and the drafting drawings for all custom components are included in Appendix B.

3.4.1 Components

1. *Light Source* – A Dymax BluWave 75 was chosen as the light source for its ability to output 9W/cm^2 across the UVA spectrum (320-395nm) with peak intensity at 365nm. It also possesses a manual intensity adjustment from 1% to 100%, a programmable LCD timer, and shutter foot switch which allow for increased exposure control and automation [37].

2. *Conditioning Optics* – Selection of conditioning optics amongst published PSL works varies tremendously and the details of these components are often under reported and de-emphasized. After testing several prototypes, it was determined that the most effective solution is to use the conditioning optics and DMD chip inside a commercially available projector. A BenQ EP5920 DLP projector was selected for its availability and performance specifications. Figure 3-4 illustrates the conditioning optics inside the projector:

    - *Color Wheel* - Filters light into specific wavelengths using a series of dichroic filters. These filters attenuate the intensity of UV wavelengths and therefore must be removed.
    - *Integrator* - Redistributes the Gaussian intensity profile of the lamp by repeatedly reflecting light along the rod, spatially randomizing the input to create a flat intensity distribution.
    - Relay Optics – Transfers light from the integrator to the DMD mask while matching the numerical aperture of the integrator with the numerical aperture subsequent optics.
    - *Mirror Lens* – Redirects light to the DMD mask such that the DMD is positioned parallel to the projection surface. This prevents undesirable keystone effects on the projected image.

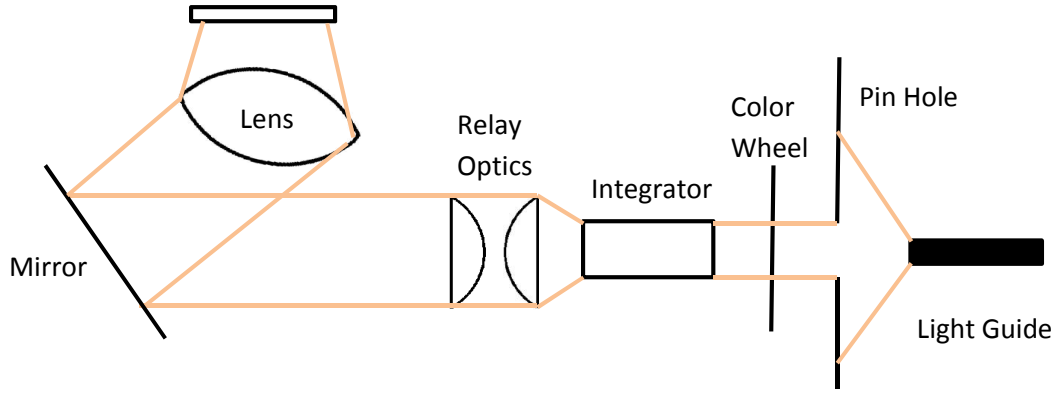

Figure 3-4. Diagram illustrating the conditioning optics inside the BenQ EP5920 DLP projector.

3. *Pattern Light* – The BenQ EP5920 DLP projector possesses a 8.1 x 14.4mm DMD with 1920 x 1080 micromirrors arranged along the surface [38]. Geometry shows that the micromirrors of the DMD are approximately 7.5 x 7.5µm squares. The DMD mirrors measure 14.4mm x 8.1mm in total.

Imaging Optics – The PSL pairs imaging optics native to the BenQ projector with additional optical components to achieve the desired output.

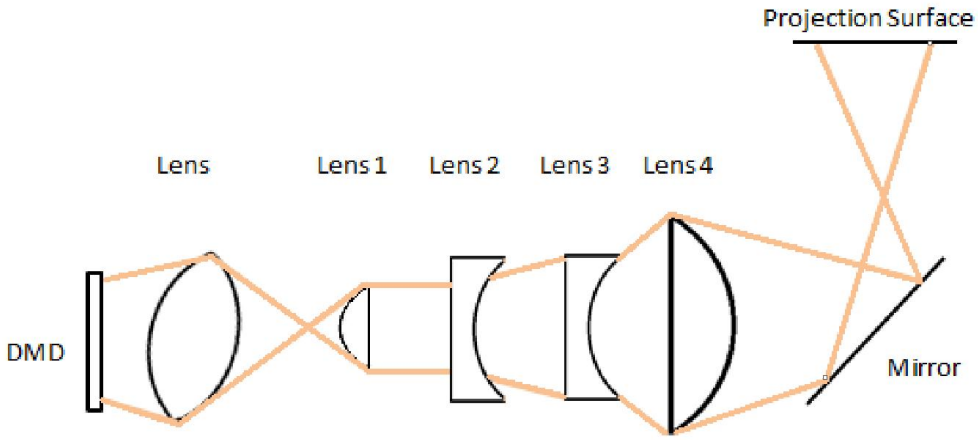

4. Figure 3-5 illustrates how these optical components are positioned relative to one another as well as their effects on the light path. Table 3-9 lists the diameter and focal lengths of these optical components as well as the distances between them.

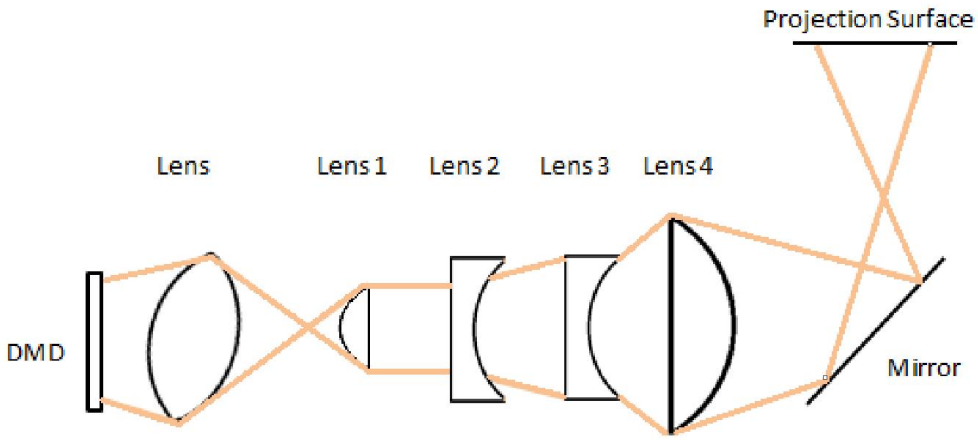

Figure 3-5. Diagram illustrating the imaging optics inside the benQ EP5920 DLP Projector. The prospective is rotated 90^{o} from Figure 3-4.

Table 3-9. Details concerning the optical components used for imaging in the PSL system.

Optical Component	Diameter (mm)	Focal Length (mm)	Distance (mm)
Lens 0	NA	~16	NA
Lens 1 - Convex	15	~16	~32
Lens 2 – Concave	25	-42	25
Lens 3 – Concave	25	-50	25
Lens 4 - Convex	50	50	25
Mirror	50 X 50 square	45^{o} angle	30
Projection Surface	43.18 x 25.4 rectangle	NA	100

Lenses 0, 1, and 2 are all optical components that are native to the projector. The focal lengths of these lenses were characterized by moving them relative to the DMD and a projection surface until they created a focused image. Lenses 0, 1, and 2 are used to relay and magnify the image projected off of the DMD mask for further magnification.

Lenses 3 and 4 are optical components added to the projector to achieve magnification while maintaining a reasonable exposure. Lens 3 exists only to increase the divergence provided by lens 2 and decrease the packaging size of the optical components. Without this lens, the distance between lenses 2 and 4 would be much greater and would increase the length of the machine while increasing intensity loss. The general lens equation is presented as Equation 3-1 and can be used to calculate the magnification provided by two lenses in series.

$$\frac{X_1}{X_2} = \frac{f_1}{f_2} \tag{3-1}$$

where *X* is the height of the image for lenses 1 and 2, while *f* is the focal lengths of lenses 1 and 2. The focal length of Lens 4 is 50mm and the focal length of Lenses 0 and 1 are 16mm each. Equation 3-1 may be solved for the projected width by also knowing that the DMD is 14.4mm wide and has a 1920 x 1080 aspect ratio:

$$\frac{X_1}{14.4} = \frac{50}{16} \qquad X_1 = 45mm \tag{3-2}$$

The final projection size is therefore 45mm x 25mm and has a measured uniform intensity of 0.23mJ/cm^2 as measured by a UV radiometer sold by Stratasys for use with their Objet machines. It is important to note that these values can be tailored for applications with specific resolution, build area, and intensity requirement by replacing components of the imaging optics.

5. *Intermediate Layer* – When using a constraining surface, adhesion between the photopolymer layers and the photopolymer vat may become so strong that features deform or break during separation as the build platform rises. Chen [39] shows that applying an intermediate Teflon coating can reduce separation force of cursed resin, and machines from Denken [40] and EnvisionTEC [41] have similarly used coated Teflon coatings to reduce the separation force. Huang and Jiang [42]have investigated the effects of silicone elastic layers on pulling force as a function of area, finding that a 60x60mm square may require over 60N for separation. However, Chen reports that easier separation between build parts and the polymer tank can be achieved by using a polydimethylsiloxane (PDMS) coating [32]. The observed reduction in separation force stems from the PDMS's ability to create a thin oxygen layer (~2.5µm) that inhibits free-radical polymerization at the interfacing surface, as shown by Dendukuri et al. [43]. Based on these research findings, a PDMS layer of Sylgard 184 by Dow Corning is used as an intermediate layer between the build part and polymer vat.

6. *Polymer Vat* - Glass petri dishes with a 3-7/8" diameter and ¾" height are used for to contain photopolymer during the fabrication process. Glass dishes were chosen because they are a suitable substrate for PDMS adhesion and because they are more rigid than their plastic counter parts, preventing warping to reduce variations in repeatability and accuracy. They are also disposable because they are cheap and easier to acquire, which makes waste management for carbon nanotubes composite photopolymer easier.

7. *Build Platform* - The build platform is manufactured with glossy surfaces using the Objet Connex 350 and VeroWhite material. The Connex Polyjet process was selected because it creates level parts and the glossy surface finish is suspected to reduce the force required for separating build parts. A printed platform also has the advantage of being easy to replace and dispose of. A brass threaded insert is adhered into the platform for attachment to the linear actuator using a ¼"-20 screw and right angle bracket.

8. *Linear Actuator* – A Zaber motorized linear slide with 75mm of travel was selected for the linear actuator connected to the build platform. This stepper motor based system has a resolution of 6.35µm per step, a unidirectional accuracy of 23µm, and a 2.5µm repeatability which is sufficient for the desirable vertical system resolution. The peak thrust of 300N and Maximum Continuous thrust of 300N are also more than sufficient for achieving reported separating forces [44].

3.4.2 Projector Modifications

Through experimentation it was determined that using the optical assemblies in a consumer projector provide the best performance opportunity. However using consumer projectors, such as the selected BenQ EP5920, with UV light in a PSL process requires modifications to the filter, color wheel, and lamp sensor as identified in Figure *3-6*.

The BenQ EP5920 uses a band pass filter to protect the DMD from the consequential damages of excessive UV and IR exposure. This filter was removed so the projector can pass UV light for curing commercial photopolymers sensitive to the 365nm wavelength. This necessity has an unknown effect on the operating life on the DMD chip, as there are no published specifications regarding UV light exposure on visible light DMD chips. There is no risk of IR exposure damage because the BluWave light source does not emit IR wavelengths.

The BenQ color wheel filters white light into its red, blue, yellow, green, cyan, ,and magenta components at a high rate such that their superposition creates the broader spectrum of visible colors (Figure 3-7). Each filter attenuates the UV wavelengths, reducing the projected UV intensity. However, this color wheel cannot be completely removed because the projector uses sensor feedback to check color wheel functionality for errors. The chosen solution is to remove the glass filters from the frame, such that the frame still spins on the projector.

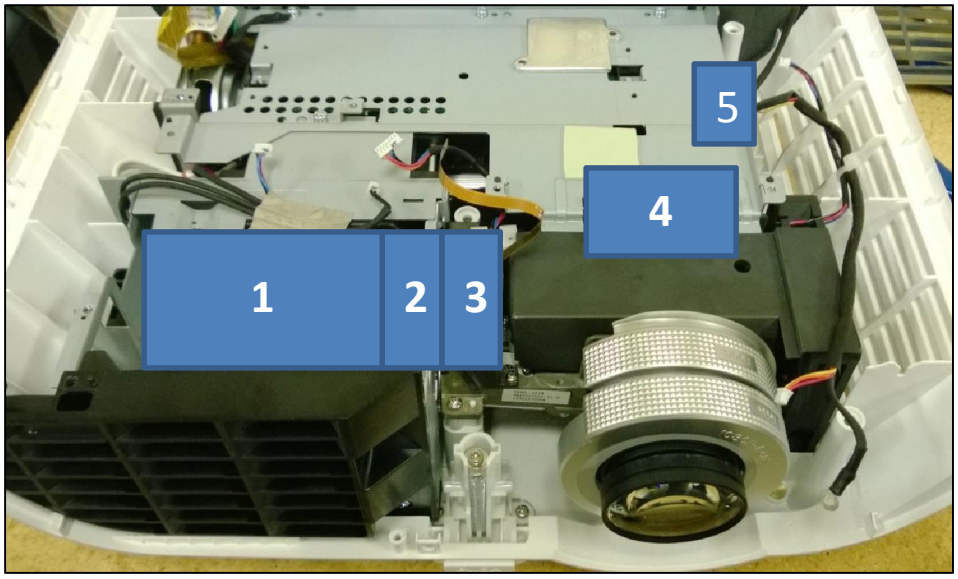

Figure 3-6. Location of various modified components within the projector: (1) Light source (2) Band pass filter (3) Color wheel (4) DMD chip (5) Lamp sensor.

Figure 3-7. The color wheel and bandpass filter are located in the projector's optical engine and identified by the red circle. Access to these components requires full dissassembly of the projector.

To use the BluWave light source with this projector, the projector's original light source has to be removed. All projectors use sensor feedback to check for light source errors, such as improper installation, before operation. Undergraduate students working on a similar project identified the bulb check sensor and corresponding wires. By measuring the voltage across each wire when the bulb was connected and when it was removed, they identified that the black wire rises from 0.17V to 3.3V when the bulb is missing with negligible difference in the other voltage signals. All bulb check errors can therefore be prevented by grounding the black wire to create a constant low voltage signal. In this way, the projector can operate using the BluWave light source with the original bulb removed.

3.4.3 Light Source Modifications

The BlueWave 75 light guide possesses a mechanical shutter controlled by a foot pedal to deliver timed exposures. Manual operation of this shutter is not idea an otherwise autonomous system. Software triggering of the mechanical shutter was achieved by disassembling the foot pedal and wiring the inner switch to an NI USB-6525 digital relay as seen in Figure 3-8. In this way one unified software program can control the light source shutter, the projected images, and the stepper motor.

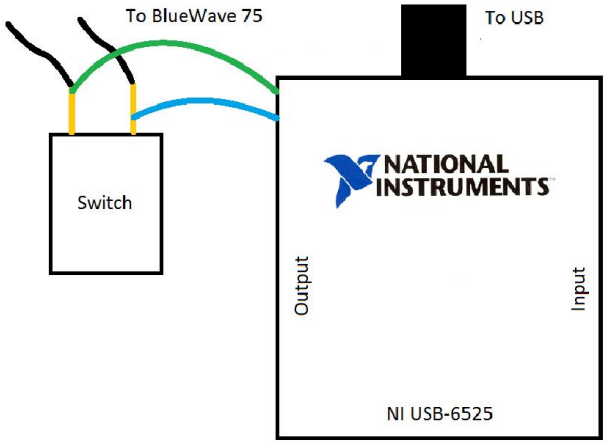

Figure 3-8. Diagram showing the foot pedal switch as wired to the Natoinal Instruments digital relay.

3.4.4 System Embodiment

The Projection Stereolithography system requires additional features to position and secure these individual subcomponents. Off the shelf components were selected when appropriate; but interfacing components had to be designed specifically for this application.

Off the shelf components including a breadboard, posts, right angle brackets, and lens mounts were used to position and secure the various imaging optics. Extruded 8020 aluminum was used in combination with right angle brackets to create a gantry-like structure. The x and y-axis degrees of freedom are used to position the petri dishes over the projected image. The z-axis degree of freedom is used to adjust the petri dish height and ensure focus of the projected image. The final embodiment is shown in Figure 3-9.

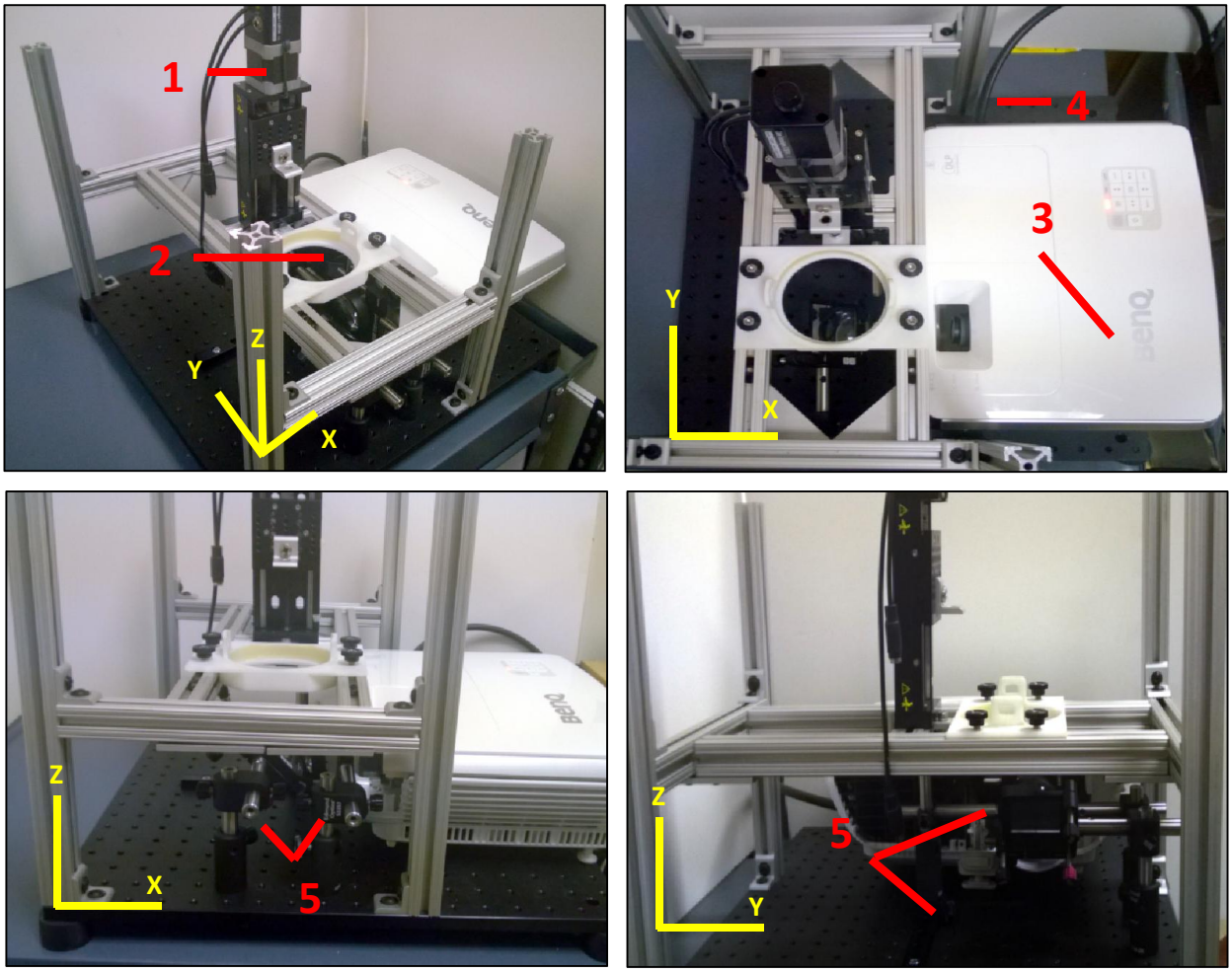

Figure 3-9. The final embodiment for this PSL system. The various components previously discussed can be identified throughout the different perspectives: 1) Stepper motor, 2) Petri dish holder, 3) DLP projector, 4) UV light guide, 5) Imaging optics. Axis are labeled to establish a orientation.

Custom components were fabricated using Additive Manufacturing methods for its accessibility, quick turnaround time, and design freedom. A mount for the light guide is required to ensure consistent positioning, as minor displacements lead to large changes in intensity. A new optical mount is used to achieve closer lens placement. And a petri dish holder is also required to secure petri dishes and prevent displacement from layer peeling. Figure 3-10 shows the CAD models and final printed parts used in the PSL system. Appendix A shows the engineering drawings with dimensions.

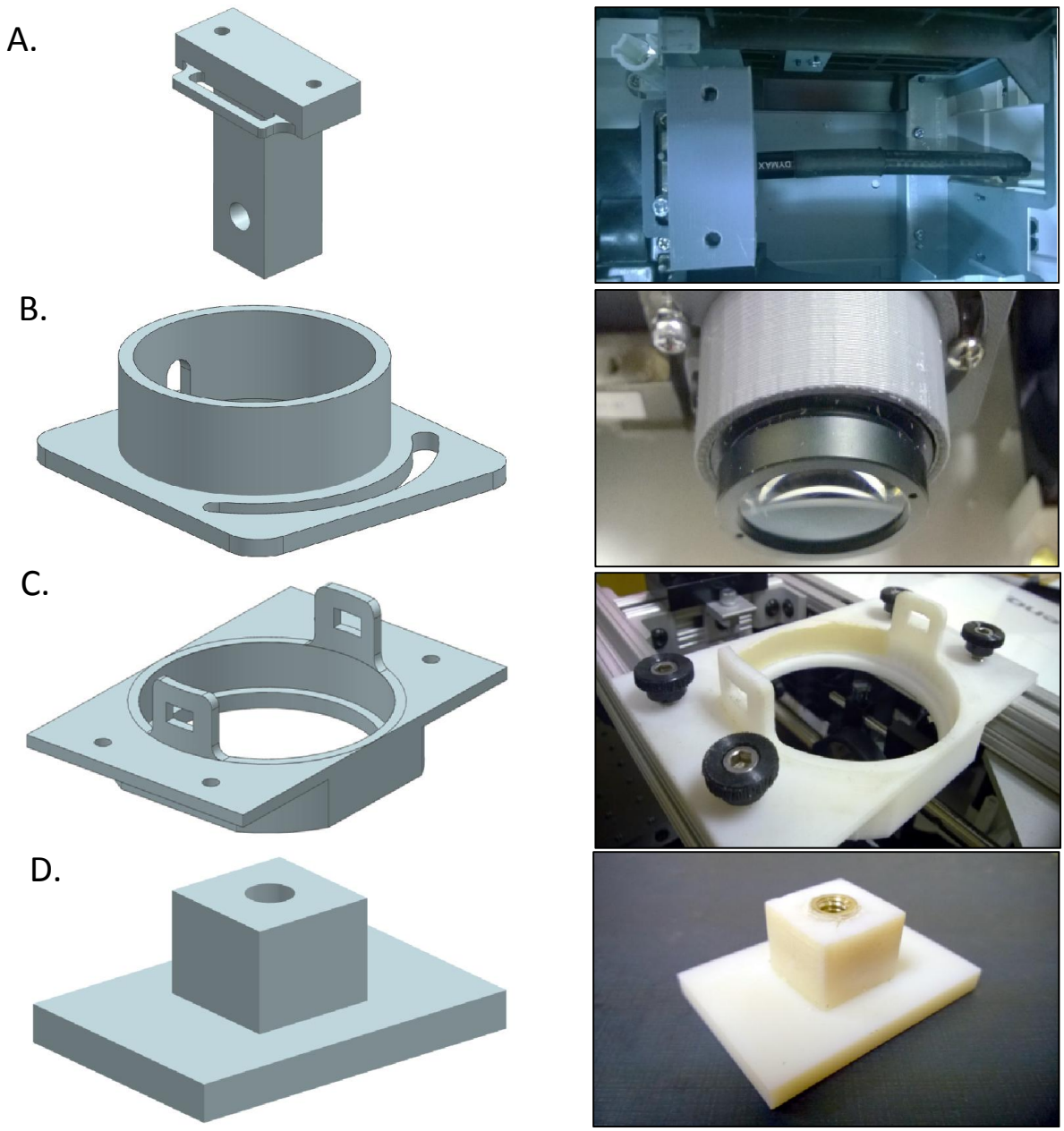

Figure 3-10. Images of the custom parts in as modeled in CAD and as fabricated using a Stratasys SST 776 or Objet Connex 360 for the build platform. Images are not in scale with one another. **A)** Light guide holder that replaces the original mercury bulb, **B)** Lens holder that replaces the interior optics of the projector, **C)** Petri dish holder that prevents displacement from peeling, **D)** Built platform that attached to motor with a threaded screw and insert.

3.4.5 Operating Software

The operating software for this PSL system coordinates the exposure of images with the actuation of the build platform, to ensure that accurate and precise layer thicknesses are achieved. The PSL control software was programmed as a set of virtual instruments (VI's) using National Instruments' LabVIEW software. To use the current PSL operating software a licensed version of LabVIEW must be installed with the NI USB DAQ hardware drivers and VISA communication package. Noteworthy aspects of the operating software are its user interface and software architecture.

Cross-sectional images can be created in many ways, but Netfabb Studio Pro was used to slice STL models for this research. Netfabb Studio Pro can set image resolution, size, and position; as well as the slicing intervals, filling hatch marks, and line thickness. The resulting image files are named using a standard format of "fileName_imageNumber.imageExtension".

3.4.5.1 User Interface

The user interface (UI) of the operating software must be intuitive to create an easy learning curve for new users. In doing so, demonstration of the working principles becomes more apparent and pre-fabrication setup becomes less complex. Figure 3-11 shows the UI of the operating software. The controls and indicators above the separating line are set and adjusted prior to starting the software, while those below should be used and monitored while the software is operating.

Input Controls:

1. *VISA In* – Sets the VISA port to communicate with the stepper motor.
2. *Folder Path* – Sets the file path to the folder containing the cross sectional images.
3. *Extrude A Signle Image* – Sets the software to repeatedly project the first image in the folder path.
4. *Peel Distance (µm)* – Sets the height traveled by the stepper motor to peel the fabricated object.
5. *Starting Image* – Sets the number of the first image to project.
6. *Layer Thickness (µm)* – Sets the desired layer thickness per exposed image.
7. *Pause* – Pauses the program by setting it to an idle state.
8. *Stop* – Stops the program after the current layer is complete.
9. *Turn on BlueWave* - Enables or disables the light source during fabrication. Used to trouble shoot.

Output Indicators:

1. *Elapsed Build Time* – Shows the elapsed total build time in a hh:mm:ss format.
2. *Exposure Time (ms)* - Shows the exposure time per layer calculated from thelayer thickness input.
3. *Dialog Box* – Shows the current softwre state of the operating software.
4. *Motor Active* – Shows whether the motor is in motion or not for safety.
5. *Image Indicator* – Shows the currently projected image.
6. *Total Layers* – Shows the total number of layers that have been projected.
7. *Current layer* – Shows the number of the currently projected layer.
8. *Percent Complete* – Shows the calculated percent completion.
9. *Approximate part Height (mm)* – Shows the calculated approximate part height.

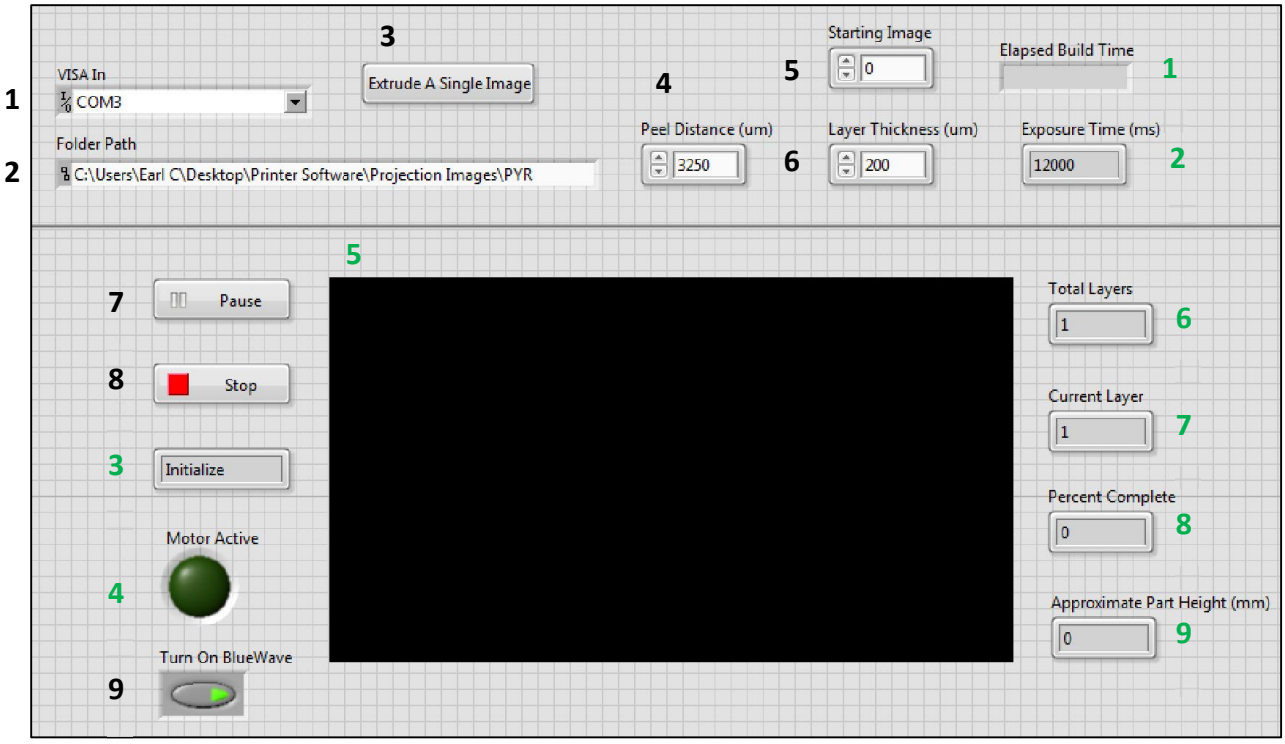

Figure 3-11- The UI of the operating software. The different numbered components are explained in more detail below. Black numbers indicate user controls. Green numbers indicate program indicators.

3.4.5.2 Software Architecture

This graphical programming environment coordinates the subfunctions of the PSL system, accurately controlling both the exposure time and platform actuation using three components:

The Global Controls.vi - This VI defines the global variables that must remain synced between the other components: a *2D Picture* indicator, a *Stop Everything* indicator, and a *Motor Active* Indicator.

Image Display.vi - This VI displays the 2D Picture indicator in full screen by matching the indicators resolution to that of the display, while removing the window boarders and tool bars typical of LabVIEW VIs. The *Stop Everything* and *Motor Active Indicators* are used to handle pausing and stopping image projection as necessary.

Main Driver.vi - This VI communicates with the stepper motor and solid state relay of the PSL system using a state machine framework that handles actions based the system's current state and the user's input. Each state performs operations that makeup the larger PSL process as described in Table 3-10.

Table 3-10 – The various system states of the main driver VI for operating the PSL system.

State	Description
Start	Begins fabrication using the input values for desired layer thickness and the image folder location. The Display Image VI is also maximized in preparation for fabrication.
Initialize	Retrieves the first image in the sequence and retrieves the file name format. This step also calculates the exposure time from the user entered layer thickness using the depth of penetration and critical exposure values for the photopolymer.
Project	Updates the 2D picture global variable to the next image in the sequence and opens the mechanical shutter, projecting the new image and exposing the photopolymer. The filename of the next image is determined and the PSL system enters the next state.
Platform	Once the set exposure time is reached, the image is reset to black and the shutter is closed to prevent low intensity accumulation reflecting out the projector. The stepper motor raises the build part, separating it, and lowers it to the appropriate layer thickness.
Update	If the program has been paused, the software enters the idle state. Otherwise the indicators are updated to show the current layer and percent completion. The height of the part is also estimated by multiplying the image number by the desired layer thickness.
Idle	Entered when the pause button is pressed. Ensures that the projected image is blank and closes the shutter for the duration of the state. Returns to previous state when unpaused.
Cleanup	Begins after the final image is projected. This state resets many of the controls and indicators in preparation for future fabrication. The program then ends.

3.5 Reflection on the Results

A formal design process was followed to create a PSL system designed and built specifically for fabricating three dimensional objects from nanocomposite photopolymers with embedded MWCNT. This process began with identifying a set of system requirements and ended with a physical manifestation of the conceptual design. The design details answer Developmental Question #1: (1) The tradeoff between resolution, print area, light intensity, and vertical print speed is even more important for PSL systems processing nanocomposites due to the increase in critical exposure and decrease in depth of penetration detailed in Chapter 5. (2) Projecting images from below the platform and peeling layers is the ideal projection orientation when working with nanocomposite photopolymers because it reduces material consumption, saving money and limiting exposure to harmful substances. (3) Using disposable build platforms and polymer vats reduces contamination when switching fabrication materials and simultaneously limits exposure to harmful substances by preventing the need to clean. Next the final performance parameters of the system need to be quantified to validate the design of the system and answer the second developmental question.

4. PSL System Validation

Having developed a PSL system for processing nanocomposites photopolymers, the next research task is to quantify the final performance metrics of the PSL system relative to the established marginal and ideal values. This benchmark allows for validation of the design and serves as a means for comparison with other PSL systems. It also addresses the second developmental question:

Developmental Question #2: What is the resolution, accuracy, precision, and vertical print speed of a PSL system designed to process nanocomposites?

Resolution, accuracy, precision, and vertical print speed metrics were focused on because they are the most widely reported performance parameters amongst PSL systems and other AM processes, so they serve as a universal basis for comparison. Section 4.1 reports the minimum feature resolution of the machine. Section 4.2 discusses the systems accuracy and precision in dimensioning and locating fabricated features. Section 4.3 simulates and calculates the optimal vertical print speed of the system based on layer thickness. Section 4.4 compiles all of the data regarding the machine in terms of the established performance specifications to draw a final conclusion on system performance. Some examples of fabricated parts are shown in Section 4.5. Note that system validation and fabrication of three dimensional parts requires characterization of the photopolymer, the details of which are presented in Chapter 5.

System validation regarding resolution, accuracy, precision, and vertical print speed was performed using benchmark parts fabricated from Objet VeroClear FullCure 810. The results of this section are therefore unique to using VeroClear FullCure 810 material with this PSL system. Other systems using the same photopolymers or similar systems using different photopolymers will likely achieve different performance metrics.

Similarly, there is no standardization for measuring these performance parameters on a PSL system. While there are parts designed for benchmarking the various other AM systems, their features are too small for fabrication and too difficult to measure when scaled down for fabrication using PSL. So while the techniques outlined below were created to quantify performance parameters of interest, they are not entirely comprehensive.

4.1 Resolution (Minimum Feature Size)

Knowing the resolution and part size of the PSL system is important to understand its limitations in fabricating microscale features. The maximum projection size for this system is measured as 45 x 25.3mm with a resolution of 1920 x 1080 pixels, such that each pixel corresponds to 23.5µm. However, this theoretical number is not necessarily achievable because force undergone during peeling may destroy small features. The destruction of these features is made analogous to a beam under deflection as described by Chen [45] and can be modeled by the beam bending equation:

$$\sigma = \pi 6FL/b^3 \tag{4-1}$$

where *F* if the applied force, *L* is the length of the beam, and *b* is the cross section length. Because of discrepancies due to anisotropic material properties of AM fabricated features, it is important to experimentally quantify the minimum feature size to understand the actual resolution of the system and material. This was done by repeatedly projecting circles of different pixel diameters to create thin rods, such that the smallest rod surviving the peeling process is indicative of the maximum resolution for the system.

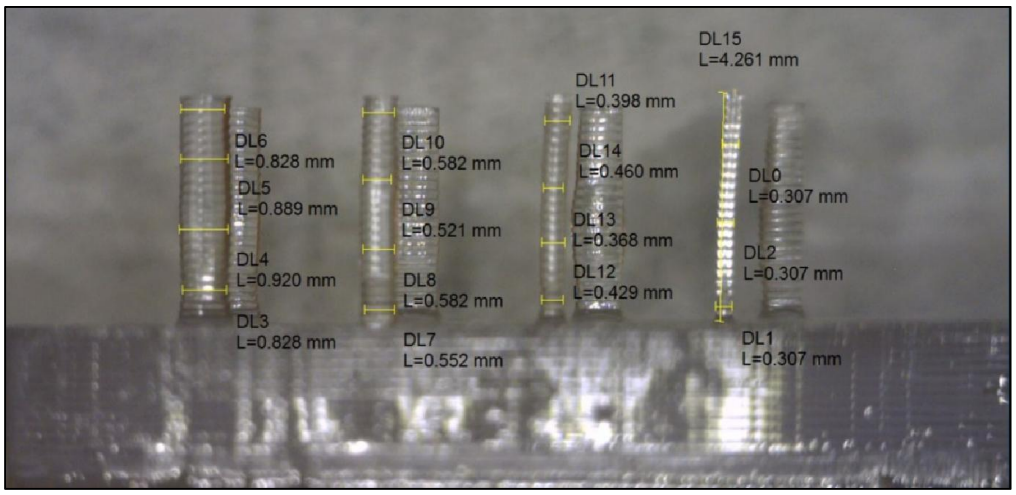

Figure 4-1 below shows these printed cylinders as viewed from the side under a DinoLite Pro optical microscope. The smallest reproducible feature is a cylinder with a 13 pixel diameter which is equal to a 305.5µm diameter. This test part was fabricated four times and the optical microscope was sued to measure diameters of 307µm, 307µm, 310µm. The discrepancy between the calculated resolution and measured resolution may be from limited resolution of the optical microscope.

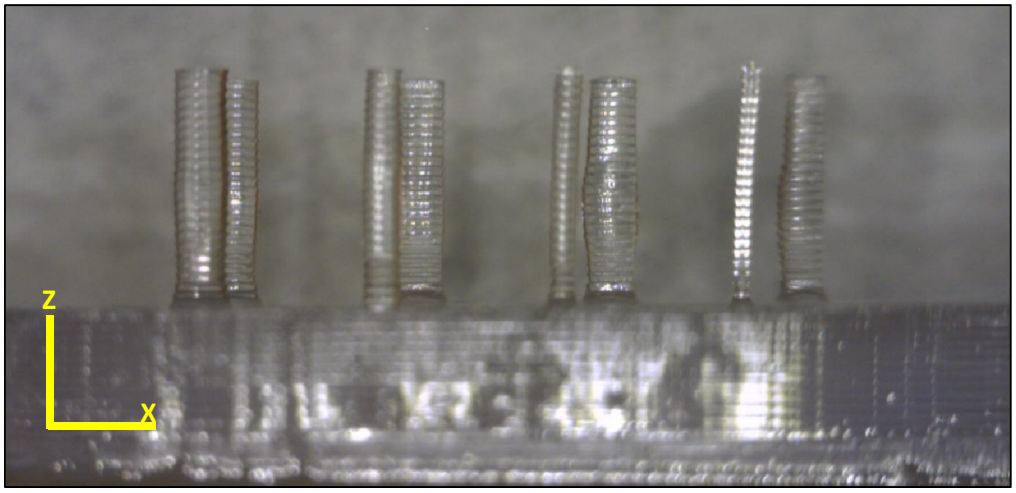

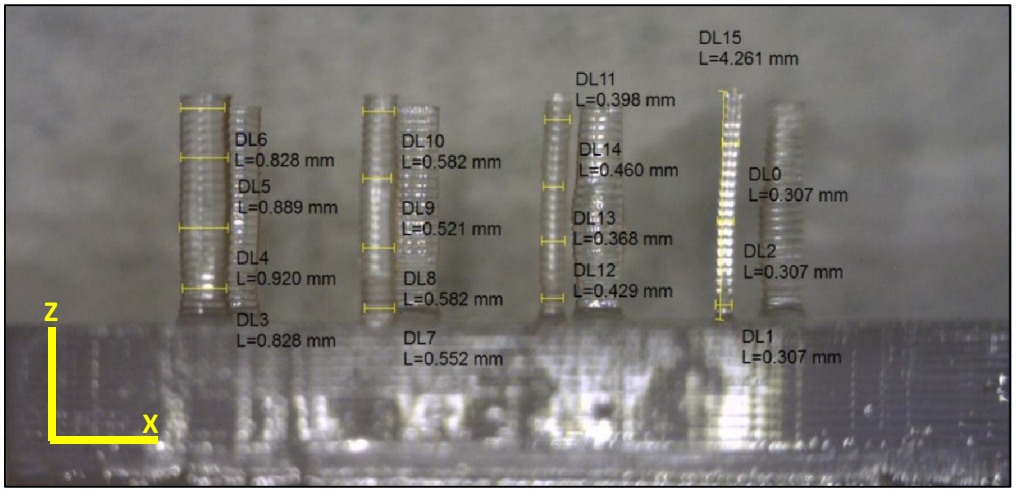

Figure 4-1. Cylinders printed along two rows to test system resolution, as viewed from the side under a DinoLite Pro optical microscope. The bottom image overlays thickness measurements of the thinnest cylinders in the foreground to measure resolution.

4.2 Accuracy and Precision

Quantifying accuracy and precision for both feature size and feature location was done using the test part shown in Figure 4-2. The test part features six square features distributed across the build area, designed to test the effects of location on accuracy and precision. These features are connected by a base that is notched to create a point of reference for measurement consistency. For these test parts on this system, the notch faced the stepper motor and the projector during fabrication. Test parts were fabricated from twenty 200µm layers. All of the dimensions identified in Figure 4-2 were measured for three different samples shown in Figure 4-3 using calipers with a 10µm resolution. Locational dimensions E, F, G, H, I, and J were measured for each square feature as appropriate.

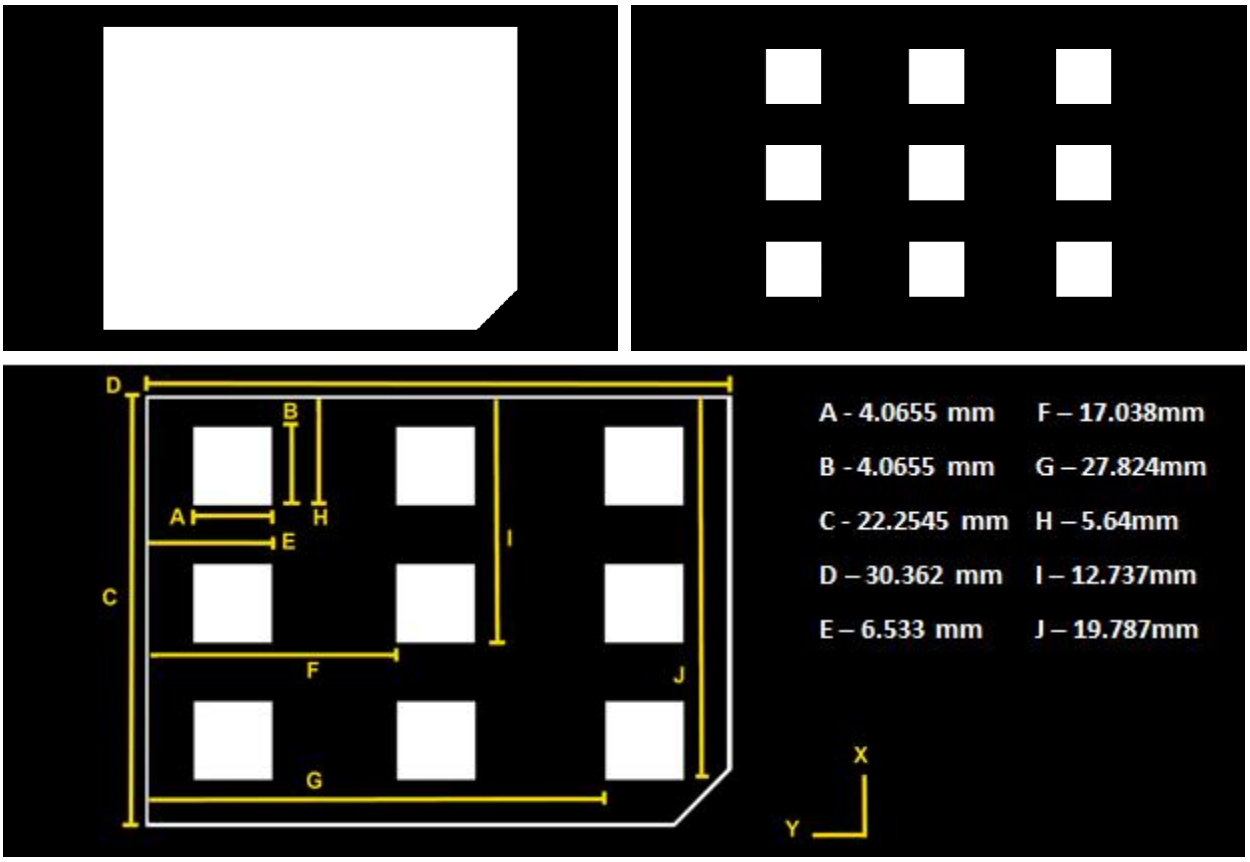

Figure 4-2. Images of the test part fabricated to quantify accuracy and precision of the PSL system. The top two pictures are the images projected to fabricate the part. The bottom two images identify the dimensions throughout the part calculated by multiplying the pixel count by magnified pixel size.

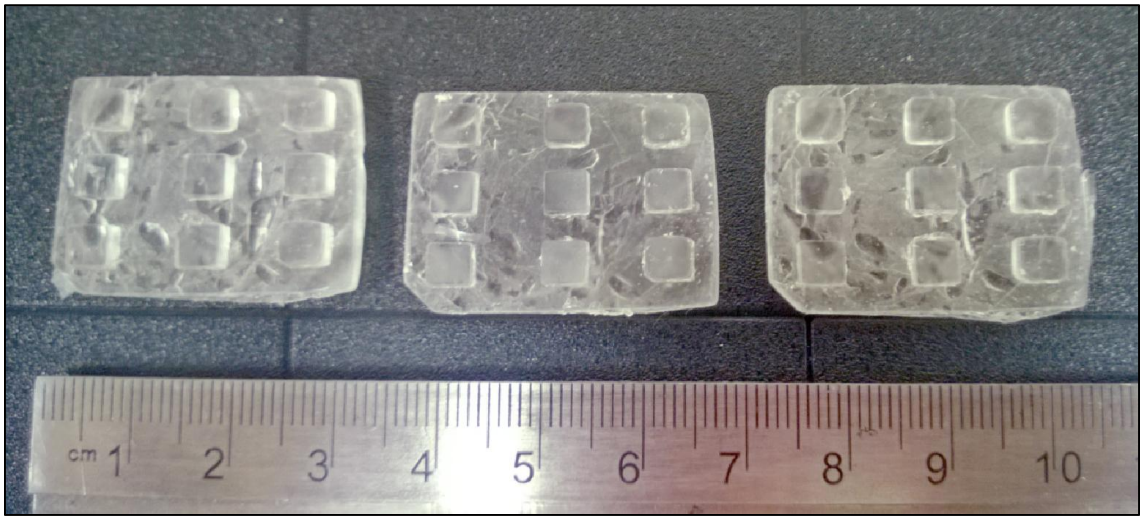

Figure 4-3. The three test parts fabricated to quantify accuracy and precision. The parts have cracks and defects along the bottom obtained during seperation from the build platform because the parts are brittle. This is a potential source of error that is unaccounted for.

The collected data is included in Appendix D and the resulting analysis is included as

Table 4-1 through Table 4-4. The average dimensional error is 492µm and the average standard deviation is 223µm across all measurements. There are also qualitative trends that can be identified by looking at the individual measurements:

- The three square features along the x-edge closest to the notch were ~150µm longer in dimension A then dimension B (the y-dimension is ~150µm longer than the x-dimension) making them rectangular. Dimensions A and B (the length and width) of the other square features were within ~50µm of each other making them closer to perfect squares.
- Dimension C, the width of the base in the x-dimension, is greatest in the center of the y-axis, while measurements to the left and right of center are generally equivalent.
- Dimension D, the height of the base in the y-direction, increases moving along the x-axis, with the greater values on the notched side.
- Vertical dimensions E, F, and G locating the square features along the y-dimension have decreasing error moving along the x-axis away from the notched edge.
- Horizontal dimensions H, I, and J locating the square features along the x-dimension have decreasing error moving along the y-axis away from the notched edge.
- The base thickness increases along the y-axis moving towards the notch and decreases along the x-axis moving away from the notch. The thicket points are generally closest to the notch and the thinnest points are generally in the opposite corner of the notch.

Table 4-1. Accuracy and standard deviations calculated from the dimensions of A and B. Dimension A was measured parallel to the y-axis and dimension B was measured parallel to the x-axis. Thickness is meassured along the z-axis at different points around the perimeter of the part.

Sample	Average A Error (mm)	Standard Deviation in A (mm)	Average B Error (mm)	Standard Deviation in B (mm)	Avg Thickness (mm)	Standard Deviation in Thickness (mm)
1	0.40	0.1	0.55	0.12	-0.591	0.299
2	0.17	0.08	0.38	0.12	-0.203	0.240
3	0.39	0.15	0.39	0.14	-0.586	0.229
AVG	**0.32**	**0.11**	**0.44**	**0.13**	**-0.46**	**0.26**

Table 4-2. Accuracy and standard deviations calculated from the dimensions of C and D. Dimension C was measured parallel to the x-axis and dimension D was measured parallel to the y-axis.

Sample	Average C Error (mm)	Standard Deviation in C (mm)	Average D Error (mm)	Standard Deviation in D (mm)
1	1.249	0.035	1.435	0.414
2	0.125	0.236	0.611	0.424
3	0.462	0.225	0.778	0.523
AVG	**0.61**	**0.17**	**0.94**	**0.45**

Table 4-3. Accuracy and standard deviations calculated from the vertical dimensions of E, F, and G. Distances were measured along the y-axis from each square feature to the far edge parallel to the x-axis.

Sample	Average E Error (mm)	Standard Deviation in E (mm)	Average F Error (mm)	Standard Deviation in F (mm)	Average G Error (mm)	Standard Deviation in G (mm)
1	0.627	0.151	1.495	0.087	1.326	0.308
2	0.387	0.056	0.962	0.242	0.559	0.523
3	0.357	0.066	1.169	0.363	0.869	0.291
AVG	**0.457**	**0.091**	**1.209**	**0.231**	**0.918**	**0.374**

Table 4-4. Accuracy and standard deviations calculated from the horiztonal dimensions of H, I, and J. Distances were measured along the x-axis from each square feature to the far edge parallel to the y-axis.

Sample	Average H Error (mm)	Standard Deviation in H (mm)	Average I Error (mm)	Standard Deviation in I (mm)	Average J Error (mm)	Standard Deviation in J (mm)
1	0.390	0.236	0.660	0.212	0.913	0.320
2	0.553	0.408	0.180	0.274	0.053	0.263
3	0.160	0.254	-0.077	0.375	0.070	0.215
AVG	**0.368**	**0.299**	**0.254**	**0.287**	**0.345**	**0.266**

The quantitative results can best be compared to the system's resolution of 300µm. The dimensional accuracy of the system is represented by the average dimensional error, which typically falls within twice the resolution of the system (0~600µm). These accuracy errors are likely caused by imprecise positioning of the petri dish surface relative to the final imaging lens. While an exact distance of 100mm provides a magnification of 3.125, a slight error in setting this distance can greater change the magnification. Because all of the features are larger and further apart than expected, it is reasonable to conclude that the petri dish needs to be slightly lowered to achieve the calculated feature sizes and reduce the average dimensional error. However, this is extremely difficult given the physical embodiment of the system and measurement tools available.

The dimensional precision is reflected by the standard deviations calculated and these typically fall within the feature resolution of the system (0~300 µm). The peeling process likely contributes to the standard deviation by deforming shapes in an unpredictable manner. The other potential sources of error that affect standard deviation may also be used to explain the qualitative trends:

- Leveling the build platform is one source of error. The rotation of the build platform must be leveled before every print using a standard carpenter's level (where a bubble is aligned between two guiding lines.) The limited resolution of this method promotes uneven layer thicknesses thickness that account for poor vertical accuracy and precision. Because of this the thinner side is over exposed and its features will grow in the two-dimensional plane beyond the projected image; this phenomena is a qualitative observation noticed while working with VeroClear FullCure 810 and will be referred to as cure creep. It is important to note that this is not a problem on PolyJet systems because the material is patterned instead of the light.
- Setting the correct distance between the build platform and the petri dish is another opportunity for error. There is no distance measurement to confirm the offset of the build platform and no visual frame of reference because of the photopolymer's transparency. Therefore the build platform is typically set too close to the petri dish such that the layers are overexposed and experience cure creep. This also increases the peeling force and may introduce excessive stresses introduce dimensional errors throughout fabrication.
- It's also possible that there exists minor misalignment within the optical components undetectable by the human eye. Minor positioning errors may introduce subtle key-stoning effects that slightly exaggerate some features and not others. This could explain why the greatest sources of dimensional error consistently exist closest to the notched corner.
- The curvature along the bottom of the glass petri dish is another source of error, causing the build plane to exist at variable distances from the imaging optics. This creates variations in magnification, which may account for the consistently greater error near the notched corner. The build platform also skews against the curvature of the petri dish during alignment introducing rotational problems as previously discussed. Similarly the PTFE Teflon coating may have varying effects on the projected image due to changing optical properties associated with changing thickness to accommodate the curvature.

- It is also possible that there are minor variations in the UV light intensity at the projection plane that go unmeasured by the UV radiometer. These variations could account for consistently greater area near the notched edge of the test part if exposure is greater there. Similarly the NI USB Relay timing may produce variable exposure or consistently increased exposures that go unquantified.

Ways to mitigate these sources of error are discussed in Section 4.6.

4.3 Vertical Print Speed and Optimal Layer Thickness

The vertical print speed of this PSL system has many contributing factors including the exposure time, the time to reposition the motor, and the number of layers or total part height. Mathematically this can be expressed as:

$$t_{total} = n_{layers}\left(t_{exposure} + t_{motor}\right), \tag{4-2}$$

$$n_{layers} = \frac{h_{part}}{h_{layer}} \tag{4-3}$$

where *t* is time, *n* is a whole number rounded, and *h* is height. Print speed is therefore a tradeoff between the layer thickness and number of layers printed: Many thin layers must be printed to achieve a specific height, so the motor most peel and reposition the build platform many times. This drastically increases the total build time for a part. Fewer thicker layers must be printed to achieve that same height, but the increased exposure time is exponentially greater and eventually becomes impractical. Equations 4-2 and 4-3 can be used to model the print speed of this PSL system, allowing for the prediction and optimization of print speed and throughput.

The operating time of the stepper motor across its operating range must be known to accurately model the vertical print speed of the PSL system. The model in Figure 4-4 was created experimentally by moving the motor the motor and timing the motion programmatically using a LabVIEW VI. Travel speed may vary due to the motors limitations in positional accuracy (23µm) and backlash (5µm), but these sources of error are practically insignificant.

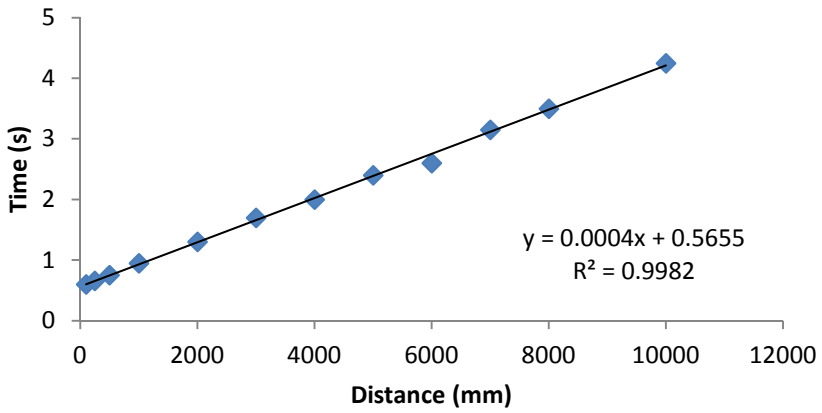

Figure 4-4. Operating time of the Zaber T-LSR75A stepper motor throughout its travel range.

To model the vertical print speeds a part height of 1 inch (25.4mm) was selected for the convenience of reporting print speed per vertical inch. To emulate realistic operation of the machine, a peel height of 3mm was included in the timing of the motor. Although excessive to achieve peeling, this height has the practical advantage of allowing the operator the opportunity to observe fabrication errors early. The experimental motor data was used to model the total operating time of the motor. The characteristic curve for Objet Fullcure Veroclear 810 (experimentally determined in Chapter 5) was used to calculate the exposure time and an additional 0.5 seconds was added to that time for over cure to ensure adhesion of consecutive layers. **Figure 4-5** below calculates the total print time over the range of layer thicknesses for VeroClear FullCure 810 using Equations 4-2 and 4-3. The minimum print time (which is the absolute minimum) was calculated as 7.8 minutes and the optimal layer thickness setting was calculated as 720µm.

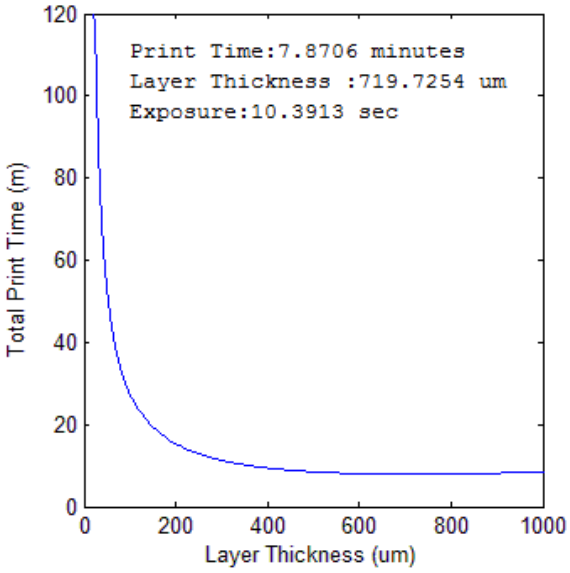

Figure 4-5. Print speed visualizations for a range of layer thicknesses and MWCNT weightings.

In practice, however, these values are not practical for fabrication with this PSL system. The discrepancy stems from the peeling process required by projecting images from below the build platform. While long exposure times create thick layers and increase vertical print speed, the photopolymer molecules closest to the PTFE coated petri dish adhere stronger to the PTFE coating and the stepper motor cannot overcome the adhesion force. It was determined experimentally that using layer thickness of ~180µm (¼ of the ideal value) provided the best balance between layer thickness and peeling ability. This corresponds to a print time of ~18.5 minutes per vertical inch and has been confirmed in practice on the system.

4.4 Validation of System Performance Parameters

The success of the system can is quantified by how well it meets the ideal and marginal values established for each performance specification established in Chapter 3. The final value is reported in Table 4-5 for each performance metric. Metrics whose ideal values are achieved by the system are highlighted in green, while metrics whose marginal values are achieved are highlighted in yellow. Red highlighting is used to identify any metrics with unachieved marginal and ideal values. These values were either measured directly from the system or were measured from parts fabricated by the system. This PSL system addresses 78% of all the performance metrics satisfactory. Although established after performing the literature review, performance metrics 13, 18, and 20 were recognized as unrealistic after having hands on experience from designing the machine. With these metrics ignored, the system satisfied 82% of the performance metrics. Overall, the system is a successful design but leaves room for performance particularly regarding accuracy and precision of dimensional reproduction.

Table 4-5. Final performance parameters of the PSL system compared to the ideal and marginal values. Green highlights indicate achieved ideal values, yellow highlights identify achieved marginal, and red highlights show metrics not met in either capacity.

Metric No.	Need No.	Metric	Imp.	Units.	Marginal Value	Ideal Value	Actual Value
1	1	Total length	1	in	< 48	< 24	18
2	1	Total width	1	in	< 48	< 24	18
3	1, 2	Total height	2	in	< 36	< 24	18
4	2	Footprint area of the base	2	in^2	< 1152	< 576	324
5	3	Power supply voltages	1	V	5, 12,125	125	5, 125
6	4	Total weight	1	lbs	< 50	< 35	~25
7	5	Percentage of components encased	1	%	> 50%	> 60%	60
8	6, 8	Number of tools required for assembly	4	#	< 10	< 5	3
9	4, 6, 7	Number of components when disassembled	3	#	≤ 10	≤ 6	3
10	6, 7, 8	Number of different fasteners used	3	#	≤ 5	≤ 3	5
11	9	Vertical travel of the build platform	3	mm	> 50	> 100	75
12	10	Area of the build platform	5	$inch^2$	> 1.5	> 5	3.5687
13	10, 11	Area of fabricated parts footprint	5	$inch^2$	> 1	> 4	1.117
14	12	Levelness of the photopolymer resin	3	%	< 5	0	0
15	13	Feature accuracy	4	um	< 50	< 20	492
16	13	Feature precision	4	um	< 25	< 10	223
17	14	Effort required to remove part	4	s	< 30	< 10	15
18	14, 15, 17	UV light intensity at projection plane	5	mW/cm^2	> 5	> 7.5	0.23
19	16	Maximum UV light intensity 6" from machine	1	mW/cm^2	< 1	0	0
20	17	Intensity range adjusted across	3	mW/cm^2	> 10	> 25	0
21	18	Ambient UV intensity at projection plane	2	mW/cm^2	< 0.25	< 0.0	0
22	19, 20, 21, 26	Number of data ports/connections	3	#	< 5	< 2	2
23	20, 26	Number of Input data fields	3	#	< 5	< 2	2
24	21, 24, 26	Number of output data fields	3	#	> 5	> 8	9
25	22	Volume of photopolymer that may leak	4	$inch^3$	< 50	< 30	1.344
26	23	Requires an emergency off switch	3	Y/N	N	Y	N
27	24	Number of feedback sensors	2	#	> 3	> 5	0
28	25	Maximum sound volume 1' away	1	dB	< 60	< 40	65
29	26	Time to start a build	3	min	< 5	< 3	2
30	26	Number of steps required to begin a print	3	#	< 10	< 6	4
31	27	Percentage of internal components visible	2	%	> 50%	> 75%	60
32	28	Degrees of freedom for optical components	5	# DOF	< 14	< 8	6
33	29	Vertical build rate	4	mm/min	> 0.5	>1	1.27
34	30	Development cost of the machine	5	$	< 25000	< 20000	9,093.14
35	31	Volume of photopolymer wasted per build	2	$inch^3$	< 1	< 0.75	0.25
36	32	Operating lifetime of the machine	3	hrs	> 100	> 150	NA

4.5 Fabricated Parts

Figure 4-6 and Figure 4-7 below show images of parts fabricated using the PSL system designed in Chapter 3. Each part was made from Objet VeroClear Fullcure 810 with the process parameters detailed in Table 4-6. As seen in the pictures, each part is fabricated with a sacrificial base to increase part adhesion to the build platform. The early layers of the base also accumulate and compensate for any deviation in perfect levelness of the build platform.

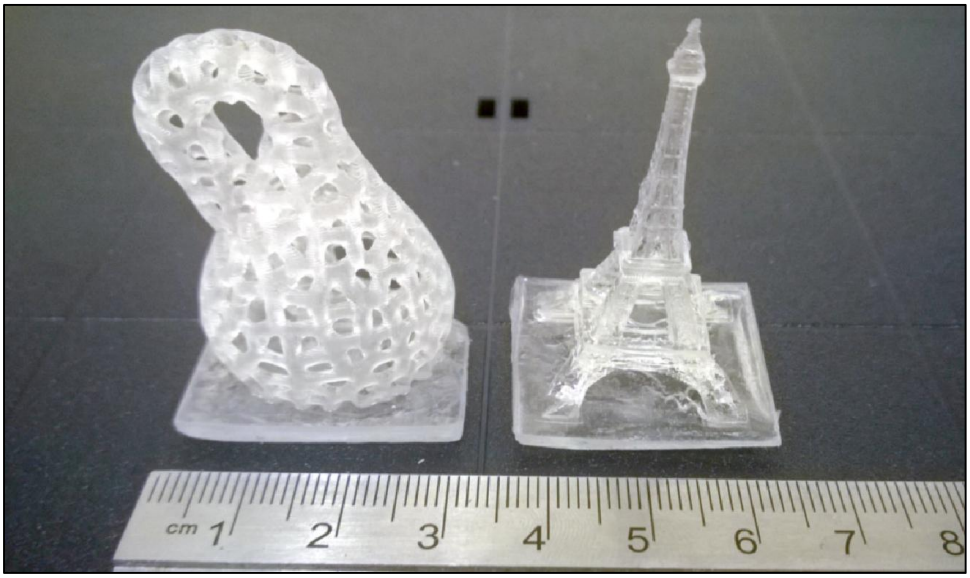

Figure 4-6. A cellular klein bottle and the Eiffle Tower fabricated from VeroClear FullCure 810.

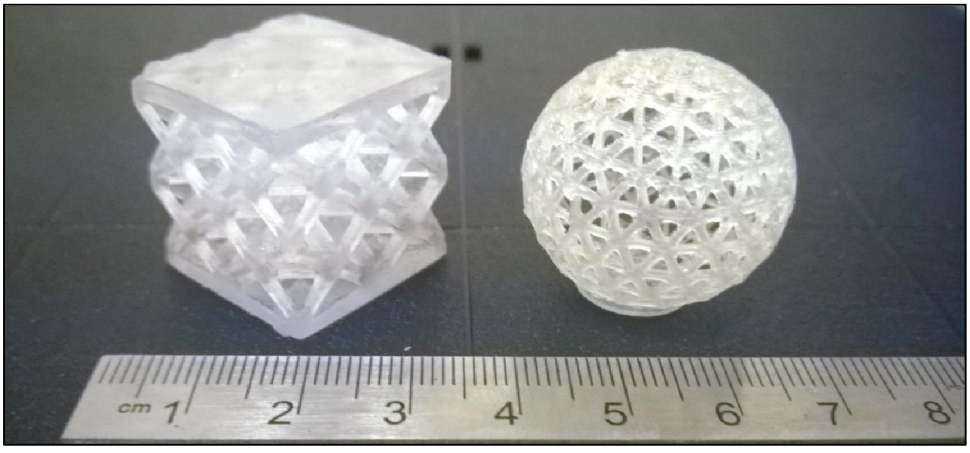

Figure 4-7. A cellular square and sphere fabricated from VeroClear FullCure 810.

Table 4-6. Process parameters for fabricating the objects in Figure 4-6 and Figure 4-7.

Layer Thickness:	200µm
Part Height:	1 – 1.3”
Fabrication Time:	25 - 30 minutes in total
Exposure Time Per Layer:	4.23 seconds
Incident Light Intensity:	0.23 mW/cm^2
Exposure Per Layer:	0.9729 mJ/cm^2 per second

4.6 Reflection on the Results

This machine is best compared with the PSL system developed by Chen [32] in 2012 since both machines pattern UV light from a lamp using the DMD inside a projector. Both systems project images from below the build plane and peel successive layers to separate them from a PDMS coating. Table 4-7. Comparison between the key performance parameters of this system and that of the system developed by Chen [32]. Comparisons are not exact given potential differences in testing methods and measurement techniques.Table 4-7 shows the key performance metrics of the two systems. It’s important to note that these comparisons are not absolute because different fabrication, testing, and measurement techniques may have been employed. Vertical build rate is the most difficult to compare because this is determined by the critical exposure and depth of penetration for the photopolymer. Different photopolymers in the same system could dramatically change the vertical build rate. This may also be said for the other metrics but with much less effect.

Table 4-7. Comparison between the key performance parameters of this system and that of the system developed by Chen [32]. Comparisons are not exact given potential differences in testing methods and measurement techniques.

Research Group	Year Developed	Min. Feature Size (µm)	Min. Layer Thickness (µm)	Maximum Part Size (mm^2)	Vertical Build Rate (mm per hours)
Chen [32]	2012	400	100	48 x 36	180
Campaigne	2014	300	100	45 x 25	80

Incorporating a multi-axis accelerometer along the build platform to programmatically determine level-ness with greater resolution would greatly improve accuracy and precision. A CCD camera could be used to passively measure dimensions within the projected image and digitally compensate for errors in the projection software. The addition of force/distance sensors could aid, or even automate, the initial positioning of the build platform relative to the projection plane, preventing over exposure of layers and ensuring constant thickness. The addition of these sensors would provide more information regarding the subtleties in system performance. However their incorporation will require drastic and fundamental changes in the embodiment of the system in ways that could introduce unforeseen sources of error. These options need to be researched further before being incorporated into the system.

5. Curing Characterization of Nanocomposite Photopolymer

The addition of nanocomposite materials into photopolymer may allow for the fabrication of three dimensional objects with enhanced material properties, which could provide new opportunities for creating functional end-use devices. This chapter addresses the Research Questions #1:

Research Question #1 (RQ1): How does the addition of multi-walled carbon nanotubes by weight percent change the curing characteristics of the photopolymer?

Section 5.1.1 discusses the basics of photopolymerization theory, including the baseline model and relevant material characteristics. Section 5.1.2 then presents a literature review on how others have processed nanoparticles using stereolithography. Section 5.2 presents the materials and procedures used to create MWCNT nanocomposite photopolymers. Section 5.3 describes the experimental steps used to characterize the photopolymerization of these nanocomposites. Section 5.4 presents the experimental results and Section 5.5 qualitatively discusses these results using existing models.

5.1 Existing Photopolymerization Models

The PSL system must be programmed with knowledge regarding the curing characteristics of a photopolymer to calculate the exposure necessary for a desired layer thickness and ultimately fabricate three-dimensional models. This section presents the most prevalent photopolymerization model and discusses the current state of the art in the photopolymerization of nanocomposites.

5.1.1 Modeling of Photopolymerization

Photoplymermization is a specific form of polymerization in which energy from incident light initiates monomer bonding and is often colloquially described as curing or solidification. More specifically, light of particular wavelengths trigger the release of free radicals from photoiniators and these radicals create covalent bonds between monomers because of their unpaired valence electrons [7]. The Beer-Lambert law is used to model how light intensity diminishes as the light penetrates through a media:

$$z = \frac{1}{\gamma}\ln\left(\frac{I_o}{I(z)}\right) \tag{5-1}$$

In this equation I_o is the incident light intensity, z is the cure depth, and γ is the extinction coefficient indicative of light absorption. When applied to stereolithography of photopolymers, the Beer-Lambert equation can be rewritten as the Jacobs equation [48]:

$$C_d = D_p \ln\left(\frac{E_o}{E_c}\right) \tag{5-2}$$

C_d = cure depth (mm), the depth of resin cure as a result of laser irradiation and is equivalent

D_p = depth of penetration (mm) replaces the extinction coefficient γ and defines the penetration of light into the resin until a reduction in irradiance of $1/e$ is reached

E = exposure (mJ/cm^2) is the exposed light energy over time such that $E=I*t$

E_c = critical exposure (mJ/cm^2) is the exposure at which resin solidification starts to occur

These properties are acquired experimentally by curing thin films across a range of exposures and creating a plot like the one shown in Figure 5-1. When these values are plotted on a semi-logarithmic scale, the depth of penetration is represented by the slope of the fit line and the critical exposure by the x-intercept. The equation of the trend line itself follows the format of Equation 5-2, which allows for the experimental determination and modeling of critical exposure and depth of penetration. As such, these material properties define how a photopolymer reacts to light exposure and are used to control the exposure in a stereolithography system.

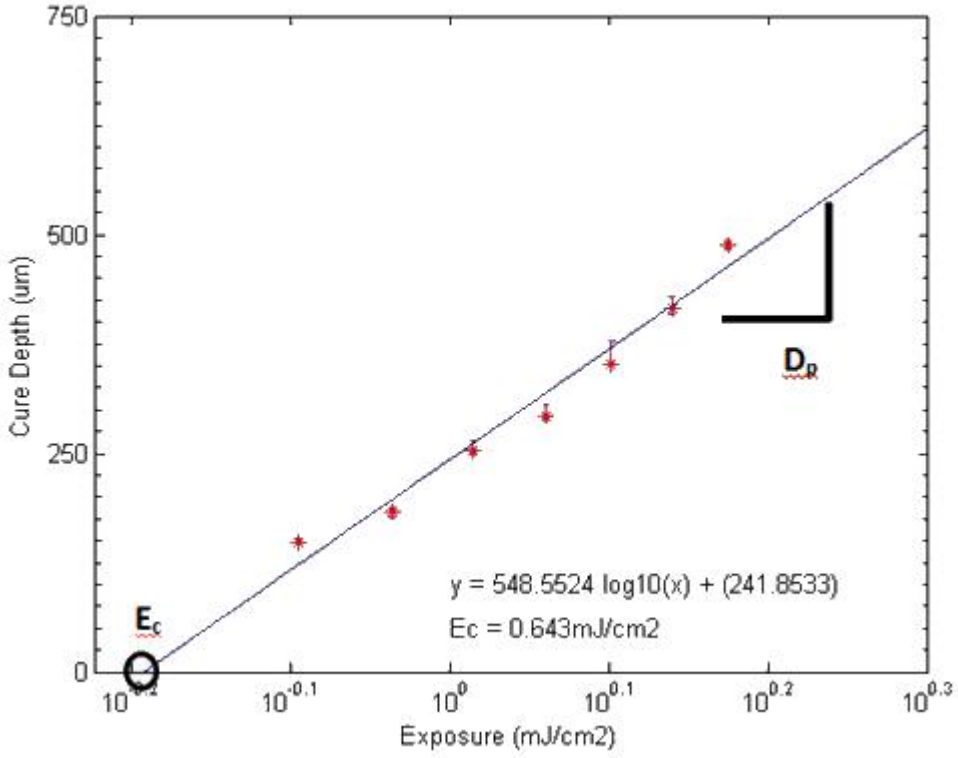

Figure 5-1. Characteristic (working) curve illustrating cure depth and depth of penetration.

5.1.2 Modeling of Nanocomposite Photopolymers in AM

Within the context of additive manufacturing, other researchers have characterized material properties and curing characteristics of photopolymer/CNT mixtures. These efforts include Sandoval and Wicker who used stereolithography to fabricate composite parts featuring 0.05wt% Multi-Walled Carbon Nanotubes (MWCNT) in DSM Somos® WaterShed™ 11120 resin [5]. Experimentally they determined that the nanocomposite mixture increased the critical exposure from 11.5 mJ/cm^2 to 60 mJ/cm^2 and depth of

penetration from 0.16mm to 6.5mm for the DSM Somos® WaterShed™ 11120. The authors' work was focused on quantifying the increases in material strength, however no modeling was performed to quantify the relationship between critical exposure and depth of penetration for varying MWCNT concentrations.

Elliot developed a model to quantify the effects of varying quantum dot nanoparticles on the photopolymerization properties of Polyjet VeroClear photopolymer [46]. As the nanoparticle s agglomerated in her mixtures, her model shows that Mie scattering principles can be used to mathematically predict a decrease in critical exposure with an increase in quantum dot loading. She also shows that quantum dots have no effect on the depth of penetration for the nanocomposite and concludes that the depth of penetration term is not significant for the Polyjet VeroClear photopolymer. **However, an analogous model for CNT does not exist and must be developed before CNT nanocomposite photopolymers can be reliably processed using vat photopolymerization techniques**. This gap in current knowledge motivates Research Question #2:

Research Question #1: How does the addition of multi-walled carbon nanotubes by weight percent change the curing characteristics of the photopolymer?

Leveraging prior photopolymerization models, the following hypothesis is formed:

RQ1 Hypothesis: The addition of multi-walled carbon nanotubes into a photopolymer will decrease its depth of penetration and critical exposure. These results are expected due to the scattering and absorption properties of suspended particles, and can be qualitatively justified using prior models by Elliot and Griffith [46], [47].

5.2 Experimental Setup and Procedure

To quantify the effects of nanocomposite on the curing characteristics of photopolymer, nanocomposite materials must be prepared from a selected nanocomposite and base photopolymer resin. Section 5.2.1 details what materials were used, why they were chosen, and how they were prepared. Section 5.2.2 describes the experimental procedure used to create the characterization curves of the nanocomposite photopolymers.

5.2.1 Nanocomposite Materials and Preparation

To determine the influence of MWCNT on the critical exposure and depth of penetration for a commercially available photopolymer, nanocomposite mixtures with different particle loadings must be created. The MWCNT used in this research (Catalog No. PD30L520 from Nano-Lab Inc. in Waltham, MA) were produced by Chemical Vapor Deposition (CVD) with a ceramic oxide support and purified to >95% by mass by means of acid etching. These MWCNT have a reported diameter of 35nm $\pm$ 15nm and a reported length of 5-20µm. They were selected because they have been used in prior literature [5]. Commercially available Polyjet VeroClear FullCure 810 was used as the matrix material for the nanocomposite. This photopolymer was chosen for its transparency and low critical exposure, which

enhance the qualitative visual perception of suspended MWCNT. The low exposure time also facilitates greater vertical build speed and throughput.

Nanocomposite mixtures were created by adding MWCNT into the VeroClear FullCure 810 using a scale and paddle. These constituents were then mixed using non-localized bath sonication for one hour to evenly distribute the MWCNT, similar to the process used by Sandoval [8]. The nanocomposites were held approximately at room temperature during sonication by continuously cycling water at ambient temperature into the bath. Precipitation and sedimentation was observed approximately 8 hours after sonication and can be attributed to the low viscosity of the photopolymer (~160 cps at ambient temperature). The MWCNT were re-dispersed using the same sonication method whenever sedimentation was observed. Nanocomposite mixtures were created with 0.1, 0.2, and 0.5wt% MWCNT.

5.2.2 Experimental Procedure for Material Characterization

Figure 5-2 illustrates the process used to characterize the nanocomposite material. Approximately 4 mL of the nanocomposite mixture was placed into a small petri dish. Next the photopolymer was exposed to the image of a circle via PSL until the desired exposure was delivered (Figure 5-2a). The circle measures 6mm in diameter such that cured samples fit completely in the arms of the micrometer to ensure measurement consistency. The cured sample was then removed from the petri dish, cleaned of excess photopolymer using task wipes with IPA (Figure 5-2b), and the cure depth (thickness) of the sample was measured using a digital micrometer (Figure 5-2c). This process was repeated for seven different exposures, each exposure repeated three times, to create twenty-one samples per concentration. All other parameters of the system were held constant.

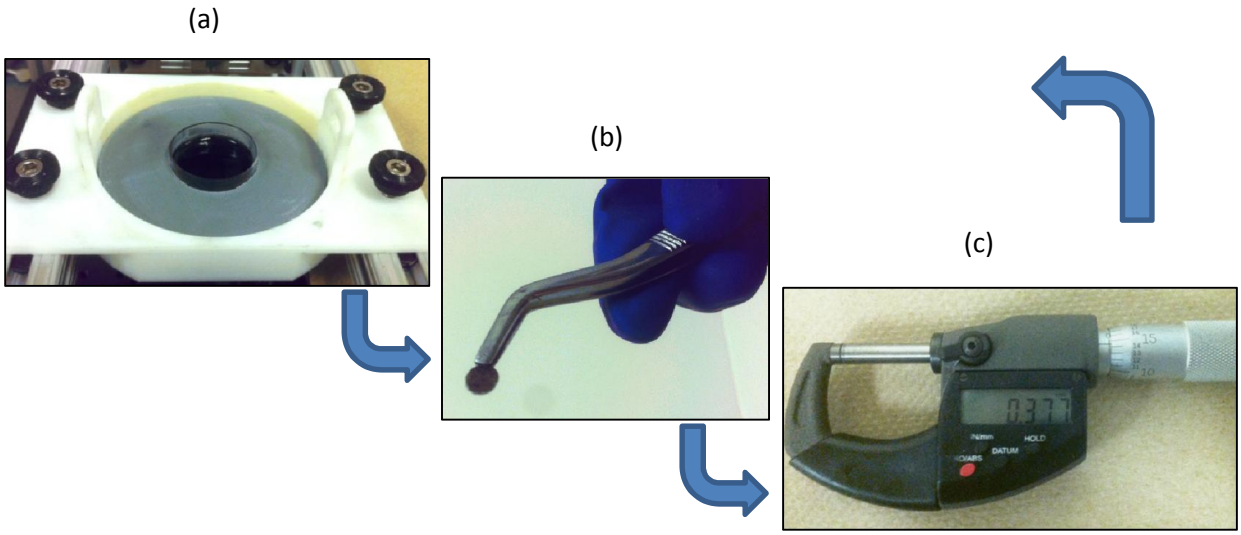

Figure 5-2. The data collection method used in this thesis for characterizing the Objet VeroClear FulLCure 810 photopolymer with and without MWCNT: (a) curing samples, (b) removing and cleaning a sample, (c) measuring sample with a digital micrometer.

5.3 Experimental Results

The depth of penetration and critical exposure of each concentration sample was found by plotting the cure depth against the exposure energy on a semi-logarithmic plot to create the characterization curve (as in Figure 5-1). All original experimental data is included in Appendix C. Table 5-1 summarizes the results of the collected data. The critical exposure and depth of penetration are reported using absolute values and relative percent increase to the control photopolymer. Figure 5-3 superimposes the individual characteristic curves included in Appendix C to illustrate the qualitative difference in critical exposure and depth of penetration.

Table 5-1. Characterization results for Objet VeroClear 810 with varying concentrations of MWCNT. The raw experimental data is included in Appendix C. Percent increase is relative to the 0wt% nanoparticle control photopolymer.

Weight Percent (%)	Average Standard Deviation (um)	Critical Exposure (mJ/cm2)	E_c Percent Increase (%)	Depth of Penetration (um/mJ)	D_p Percent Increase (%)
0	7.60	0.64	NA	549	NA
0.1	8.91	0.71	11%	329	40%
0.2	4.49	0.79	23%	189	66%
0.5	6.26	1.14	77%	110	80%

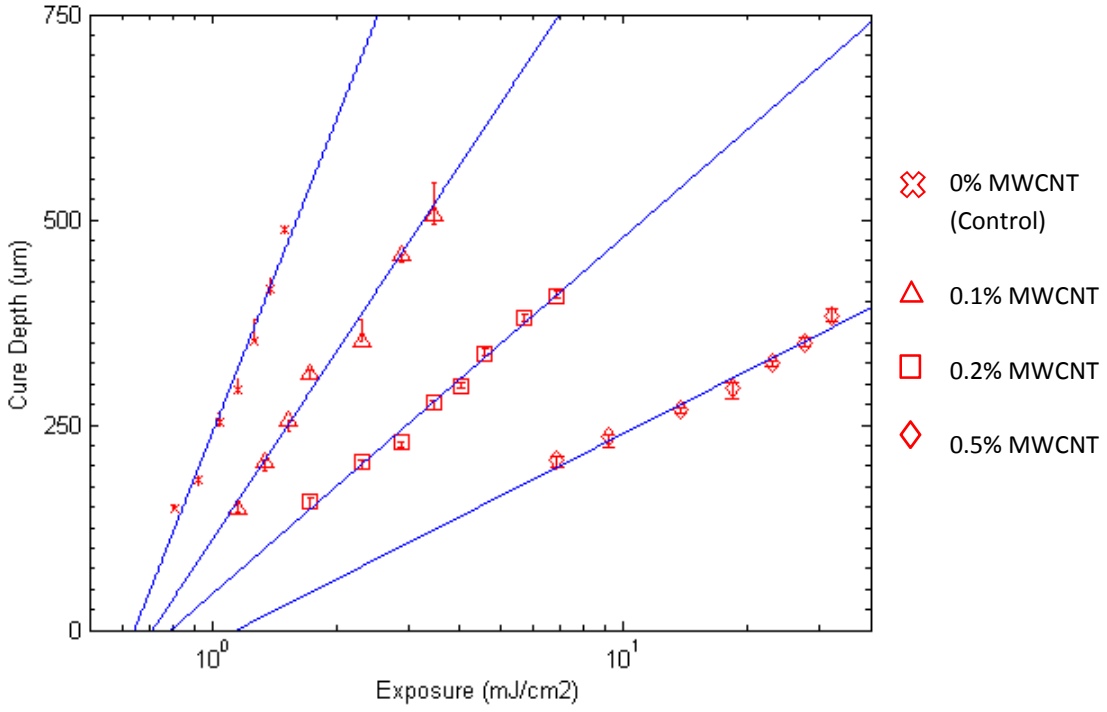

Figure 5-3. Characterization curves from Appendix C superimposed to illustrate the difference in critical exposure and depth of penetration.

5.4 Discussion and Analysis

5.5.1 MWNCT Effects on Critical Exposure

To analyze the effects of MWCNT on the amount of exposure needed to cure the photopolymer, critical exposure is plotted as a function of MWCNT concentration in Figure 5-4. From this plot, it is observed that there is a positive log-linear relationship between the MWCNT concentration and photopolymer critical exposure. The calculated percent increase in critical exposure relative to the control photopolymer without added MWCNT is shown in Table 5-1.

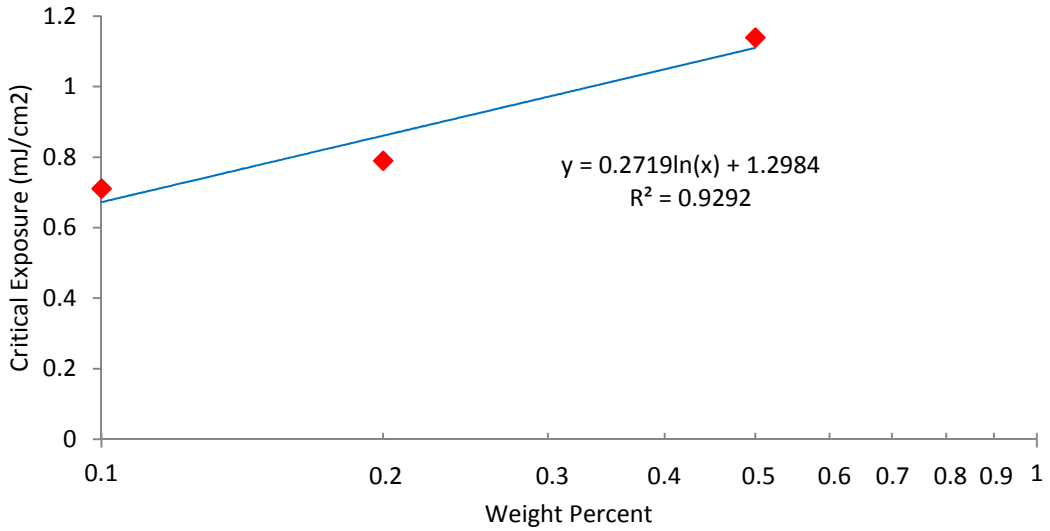

Figure 5-4. Critical exposure as a function of weight percent MWCNT in VeroClear 810.

These results can be qualitatively justified using existing models that characterize the effects of nanoparticles on a material's critical exposure. Elliot [46] presents such a model characterizing the effects of quantum dot particle loading on the critical exposure of Objet VeroClear FullCure 810shown as Equation 5-6. This model is derived by substituting the variables in Equations 5-4 and 5-5 into Equation 5-3. Because her study involved microscale agglomerates of quantum dots research, this model assumes that the agglomerates are spherical and have diameters of micrometers. These microscale agglomerates are the result of inter-particular attraction between the nanoscale quantum dots, and the agglomerates are treated as single particles by the size and shape assumptions. Therefore the exact equation is not applicable because those assumptions of scale and shape are not applicable to evenly dispersed MWCNT with nanometer diameters. Never-the-less, Equation 5-6 (whose variables are defined in Table 5-2) can be used to qualitatively justify the observed results:

$$E_c = E_{c,0}\,\gamma\,\ln(wt\%), \tag{5-3}$$

$$\gamma = \frac{4\,p_{media}}{3\,d\,p_{particles}}\,Q, \tag{5-4}$$

$$Q = 2\left(\frac{2\pi d}{\lambda_0}\right)^i \Delta n^2 \tag{5-5}$$

$$E_c \propto E_{c,0}\ \frac{4\ p_{media}}{3\ d\ p_{particle}}\left(\frac{2\pi d}{\lambda_0}\right)^i \Delta n^2 \ln(wt) \tag{5-6}$$

Table 5-2. Variables and values for Equations 5-3, 5-4, 5-5, and 5-6. Specified values were obtained through product documentation or measured experimentally as reported.

Term	Description	Value	Unit	Determination
E_c	Critical Exposure of Nanocomposite	Unknown	mJ/cm^2	Calculated
γ	Extinction Coefficient	Unknown	m^{-1}	Calculated
Q	Rayleigh Scattering Coefficient	Unknown	Dimensionless	Calculated
i	Empirical Term	Unknown	Dimensionless	Calculated
$E_{c,0}$	Critical Exposure of Pure Polymer	0.643	mJ/cm^2	Experimental
d	Average Particle Diameter	35	nm	Known
p_{media}	Density of Pure Polymer	1.145	g/ml	Experimental
$p_{particle}$	Density of Nanoparticle	2.1	g/ml	Known
$n_{polymer}$	Refractive Index of Polymer	1	Dimensionless	Assumption[1]
$n_{particle}$	Refractive Index of Particle	2.19	Dimensionless	Specified
λ_0	Wavelength of Incident Light	365	nm	Known

Given the above values are all constant, Equation 4-6 can be simplified into an equivalent form:

$$E_c \propto C\ \ln(wt) \tag{5-7}$$

where C is a constant equal to the mathematical result of all the constants in Equation 5-6. Equation 5-7 takes the same form as the best fit trend identified in Figure 5-4. Qualitatively, the observed trend is in agreement with the Elliot model: critical exposure increases with an increase in MWCNT loading. Conceptually this makes sense because MWCNT scatter and absorb light near UV radiation, providing less energy to initiate photopolymerization. These scattering and absorption effects should increase with greater concentrations of MWCNT, so intuitively the critical exposure should increase as concentration of MWCNT increases.

[1] The reported value for the refractive index of VeroClear is assumed to be one as an alternative Δn state as it could not be measured, and this is justifiable in most cases [50].

5.4.2 MWNCT Effects on Depth of Penetration

As stated in the hypothesis (Section 5.1.2), there is a suspected correlation between the concentration of MWCNT and the depth of penetration. Figure 5-5 plots MWCNT concentration against the depth of penetration to quantify this trend. The calculated percent increase in depth of penetration relative to the control photopolymer without added MWCNT is shown in Table 5-1.

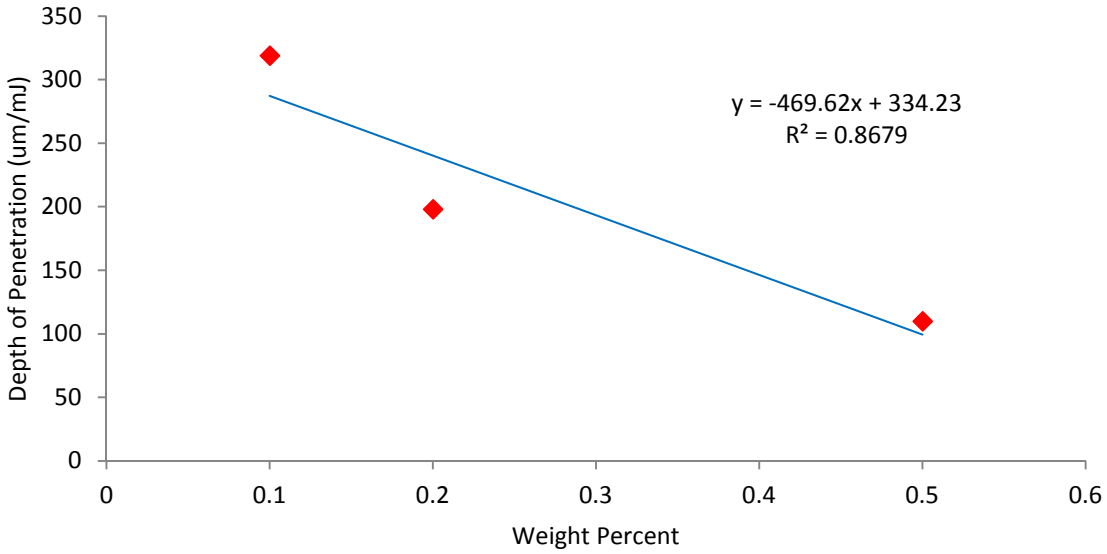

Figure 5-5. Depth of penetration as a function of MWCNT weight percent in VeroClear 810.

This observed trend in depth of penetration can be justified qualitatively using a theoretical model proposed by Griffith and coauthors to predict the cure depth of photopolymer suspensions of microscale ceramic particles. The goal of this model is to account for how suspended nanoparticles scatter light such that it penetrates the polymer less. The authors' model uses the established Mie and Raleigh-Gans light scattering models to redefine the Jacobs equation as:

$$C_d = d_p \ln\left(\frac{E_o}{E_c}\right) = \frac{d}{Q\phi}\ln\left(\frac{E_o}{E_c}\right) = \frac{d}{\beta\Delta n^2\phi}\ln\left(\frac{E_o}{E_c}\right) = \frac{C}{\phi}\ln\left(\frac{E_o}{E_c}\right) \quad (5\text{-}8)$$

such that depth of penetration is simply:

$$D_p = \frac{C}{\phi} \quad (5\text{-}9)$$

where the variables are all defined in Table 5-3. For the experiments characterizing MWCNT nancomposite photopolymers, all of the factors defining depth of penetration are held constant except for the volume fraction loading ϕ, which is equal to the product of the mass fraction loading and the constant density ratio:

$$\phi = \frac{V_{MWCNT}}{V_{Polymer}} = \frac{p_{media}}{p_{particle}}\frac{M_{particle}}{M_{media}} = C\frac{M_{particle}}{M_{media}} \quad (5\text{-}10)$$

such that volume fraction and mass fraction can be used interchangeably without consequence in the trend. The observed negative linear trend between depth of penetration and particle mass loading is therefore justified qualitatively by the relationship proposed by Griffith, shown in Equation 5-8 and simplified into Equation 5-9 whose values are included in Table 5-3. Conceptually, it makes sense that the scattering and UV absorption properties of MWCNT prevent near UV radiation from penetrating as deeply into the photopolymer, and thus lowering the depth of penetration. Furthermore, it is intuitive that increasing the concentration of MWCNT would increase the scattering and absorption effects to further reduce the depth of penetration.

Table 5-3. Variables and values for Equations 4-1 and 4-2. Specified values were obtained through product documentation or measured experimentally as reported.

Term	Description	Value	Unit	Determination
E_c	Critical Exposure of Nanocomposite	Unknown	mJ/cm^2	Calculated
$E_{c,0}$	Critical Exposure of Pure Polymer	0.643	mJ/cm^2	Experimental
Q	Rayleigh Scattering Coefficient	Unknown	Dimensionless	Calculated
ϕ	Volume or Mass Loading	Variable	Dimensionless	Known
β	Extinction Coefficient Constant	(S/λ)	Dimensionless	Unknown
d	Average Particle Diameter	35	nm	Known
p_{media}	Density of Pure Polymer	1.145	g/ml	Experimental
$p_{particle}$	Density of Nanoparticle	2.1	g/ml	Known
$n_{polymer}$	Refractive Index of Polymer	1	Dimensionless	Assumption[i]
$n_{particle}$	Refractive Index of Particle	2.19	Dimensionless	Specified

5.4.3 Difficulties with Quantitative Modeling of MWCNT Photocuring

Although the experimental results have strong correlations with justifiable results, there is still much uncertainty surrounding the effects of how MWCNT will affect the refractive index of nanocomposites. These uncertainties make the quantitative analysis of photocuring nanocomposites difficult to model:

1. All of the scattering models, including the Elliot model, apply the rule of mixtures to determine the effects of differences in refractive indices (the Δn term). However CNT can restructure the composite and change the local (~30nm) index of refraction unpredictably, such that the rule of mixtures is not necessarily applicable.
2. Graphene-based materials have a frequency cutoff in the low UV wavelengths, where their light absorption peaks tremendously. At these wavelengths, the index of refraction of and around the MWCNT may vary widely and unpredictably. This may introduce sources of error since all optical characterization is being performed with 365nm light.
3. The refractive index of MWCNT is based on the imaginary and real components of perpendicular and parallel orientations. The reported single value is calculated from these four components and may not be accurate for this application since the MWCNT have an unstructured orientation in the nanocomposite.

Therefore any attempt to mathematically model the photocuring of MWCNT must account for these sources of error. This is an area for future work that exceeds the scope and demands of this thesis project.

5.5 Reflection on Results

From these experiments it has been experimentally shown that: **(1) There exists a positive linear relationship between the critical exposure of a nanocomposite and the weight percent loading of the nanoparticle**. **(2) There is similarly a negative linear relationship between the depth of penetration for a nanocomposite and the weight percent loading of the nanoparticle**. Both of these observations are justified qualitatively by the models and findings of Elliot and Griffith.

These models can be used to optimize operational parameters of the PSL system, particularly allowing for programmatic control of layer thickness by controlling the exposure time. However, these results are only for single layer films and do not model stacking of the films to create three dimensional parts. So while these parameters are useful they do not account for details like overexposing layers to ensure adhesion between consecutive layers. It also does not account for the peeling process and the effects of high exposure times on adhesion to the PTFE petri dish coating. Never-the-less, the trends and characteristic curves developed here do accurately characterize the material and provide a starting point for the optimization and characterization of three dimensional fabrication, as evidenced by the fabricated parts presented in Section 5.7.

5.6 Fabrication of a Nanocomposite Structure

A nanocomposite cellular structure was printed using a nanocomposite mixture of Objet VeroClear FullCure 810 with 0.1wt% MWCNT. When using these nanocomposite materials, the layer thickness must be reduced to prevent over cure and high adhesion forces that prevent peeling. This effect is quantified by the observed decrease in depth of penetration and can be explained intuitively: Longer exposure times are required to create thicker layers using nanocomposite materials. Because of this, the photoinitiators immediately against the PTFE coating of the petri dish become increasingly over exposed and increasingly adhere to the coating. Therefore, process parameters must compensate for differences between experimental values and practical values for fabrication with nanocomposites. Table 5-4 shows the difference in process parameters for Objet VeroClear FullCure 810 without and with 0.1wt% MWCNT loading.

Table 5-4. Process parameters for fabricating the objects in Figure 5-6.

	VeroClear 0wt% MWCNT	**VeroClear 0.1wt% MWCNT**
Layer Thickness:	200µm	100µm
Part Height:	1”	1”
Fabrication Time:	25 minutes in total	45 minutes in total
Exposure Time Per Layer:	4.23 seconds	5.92 seconds
Incident Light Intensity:	0.23 mW/cm^2	0.23 mW/cm^2
Exposure Per Layer:	0.973 mJ/cm^2 per second	1.362 mJ/cm^2 per second

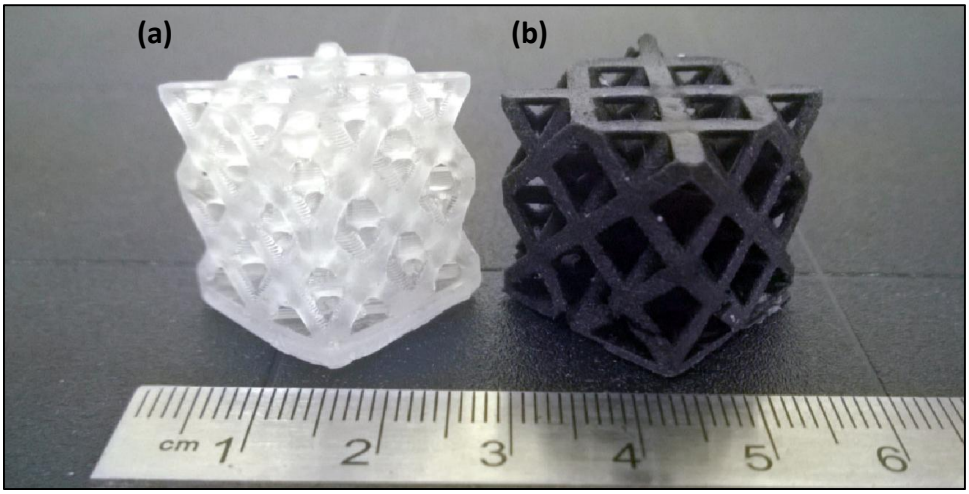

Figure 5-6. A cellular square fabricated using (a) the control photopolymer without any MWCNT and (b) the same sample printed from the nanocomposite photopolymer contianing 0.1wt% MWCNT.

5.7 Transmission Electron Microscopy (TEM) of Solid Nanocomposite

Knowing the distribution of MWCNT inside cured nancomposite photopolymer can be insightful to qualitatively understanding the effects of adding nanoparticles to photopolymers. Transmission Electron Microscopy (TEM) is a microscopy technique that transmits a beam of electrons through an ultra-thin specimen. The electrons interact with the specimen and expose a CCD camera behind the sample to generate the image. This imaging technique was used to acquire images of the MWCNT distribution inside cured photopolymer. As is common in microscopy, very thin cross sectional material samples were cut from a nanocomposite sample piece like that shown in Figure 5-6 using a microtome with diamond knives. Sample preparation was performed by Stephen McCartney at the Nanoscale Characterization and Fabrication Laboratory (NCFL) located with the Corporate Research Center (CRC) of Virginia Tech. Figure 5-7 illustrates where the sample were taken from.

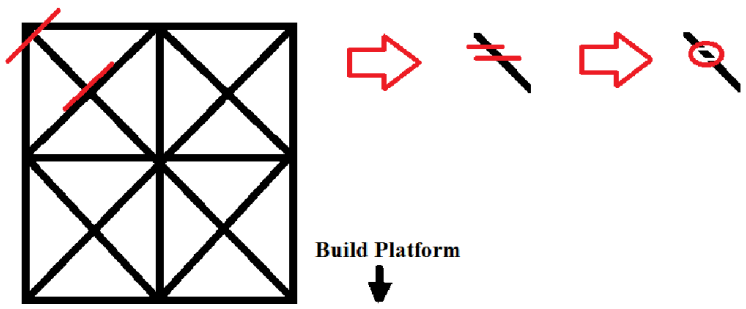

Figure 5-7. Illustration of how the TEM samples were obtained. Red lines indicate cuts in the material, such that samples are parallel to the build plane of the PSL system. Samples were cut from the approximate center (width, length, and height) of the sample part.

The pictures in Figure 5-8, Figure 5-9, Figure 5-10 were acquired by Christopher Winkler at NCFL using a Phillips EM420 TEM machine. Agglomerates of the MWCNT were found present in the cured photopolymer and are seen as concentrations of black in the images, due to the high density of MWCNT blocking electron transmission. Individual MWCNT are seen as grey wisps and always exists around agglomerates. Because the nanocomposite materials were always processed in the PSL system within an hour of mixing, these images imply that sonication does not generate enough force to overcome the inter-particle attractions of the MWCNT. Therefore the MWCNT agglomerate with each other with select few MWCNT separated from the periphery.

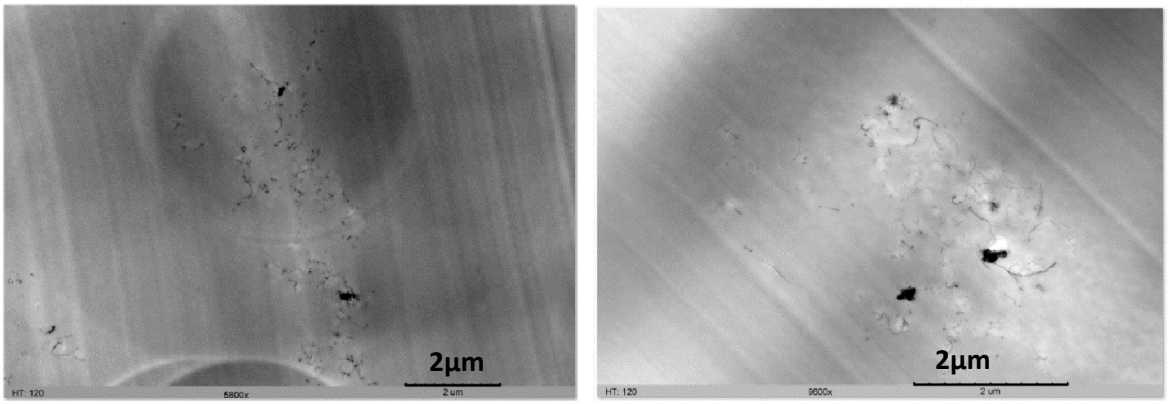

Figure 5-8. TEM images acquired from the test sample parts with a scale of 2µm.

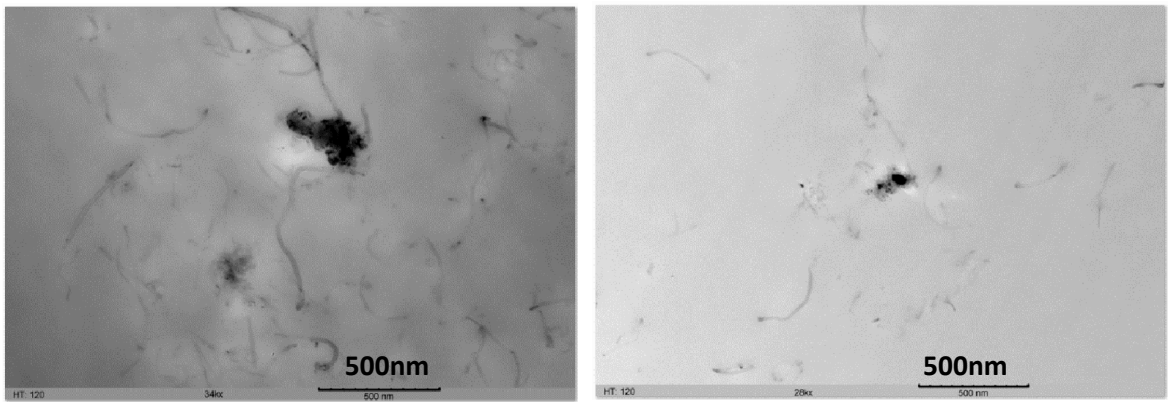

Figure 5-9. TEM images acquired from the test sample parts with a scale of 500nm.

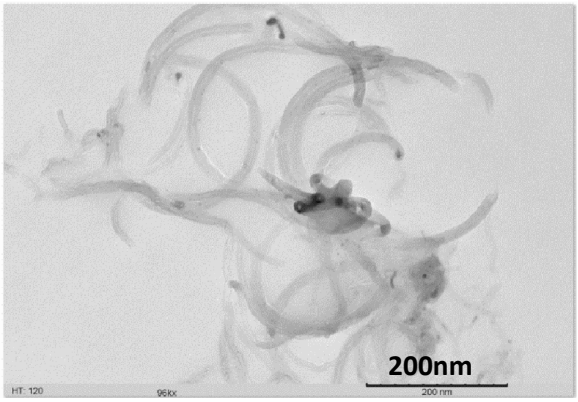

Figure 5-10. TEM images acquired from the test sample parts with a scale of 200nm.

It is important to restate the mixing procedure used to develop the nanocomposite photopolymers is almost identical to that used by Sandoval and Wicker [35]. Bath sonication was used in particular for both bodies of research because it is a non-localized method for mixing and does not directly interact with the MWCNT. A localized method such as stirring the materials would damage the MWCNT, breaking them into smaller lengths, and adversely affecting their material properties, as well as the material properties of the nanocomposite.

The same mixing methods were deployed in both sets of research, yet one yielded evenly dispersed MWCNT while one did not. The differentiating factor seems to therefore be the selection of base photopolymer and its viscosity: a more viscous photopolymer is able to overcome nanoparticle attraction and keep MWCNT separated. This is supported by the lower viscosity of Objet VeroClear FullCure 810 which is 160cps [46] compared to the higher viscosity of DSM Somos WaterShed Ultra 11120 of 260cps [30], both at 30^{o} C. This difference is understandable qualitatively because the VeroClear FullCure is developed for the Objet polyjet process that must spray the photopolymer through nozzles, while DSM Somos photopolymer is designed for stereolithography AM processes where the material is static. Because the cause of the agglomeration is suspected to be the low viscosity of the VeroClear Fullcure, no realistic amount of mixing could prevent the MWCNT from agglomerating in the photopolymer unless the viscosity is changed.

The effect of photopolymer viscosity on MWCNT agglomeration could be quantified by creating nanocomposite materials from photopolymers of various viscosities and obtaining TEM images of fabricated samples. This is one area of future work that may be worth investigating. Of particular interest if the photopolymers manufactured by Envisiontech for their PSL systems which is most similar to the one used in this research.

6. Material Property Characterization of Nanocomposite Photopolymer

Having fabricated three dimensional objects with embedded carbon nanotubes from a nanocomposite photopolymer, the next step in the scope of this work is to quantify the material properties of these materials. Tensile strength and electrical conductivity were focused on specifically to quantify the nanocomposites practicality for creating weight efficient load-bearing structures and electrically conductive geometries. This exploration is guided by Research Question #2:

Research Question #2 (RQ2): How do the multi-walled carbon nanotubes affect the PSL process and the material properties (tensile strength and electrical conductivity) of the photopolymer?

6.1 Tensile Strength of Nanocomposite Photopolymers

6.1.1 Existing Material Characterization of Nanocomposite Photopolymers

Sandoval and Wicker characterized printed three dimensional structures from a nanocompsite created by mixing DSM Somos WaterShed 11120 photopolymer with 0.05 weight percent multi-wall carbon nanotubes (MWCNT). The parts were created using a modified stereolithography machine from 3D systems (Model 250/50), cleaned with isopropyl alcohol, and post-cured in an oven for ~1 hour before testing. Experimentally Sandoval and Wicker quantified a 17% increase in the ultimate tensile stress, a 37% increase in the fracture stress, a ~16 increase in the hardness, and a ~30% decrease in fracture strain for objects made from the nancompsite materials as compared to those made from the control WaterShed resin. Testing data was collected from eight samples in total, four made from WaterShed 11120 and four from the nanocomposite mixture. This prior work is used to formulate a hypothesis for Research Question #2:

RQ2 Hypothesis: The addition of MWCNT to photopolymer will increase the tensile stress at break and decrease the fracture strain. This is suspected because of the results obtained by Wicker [5] and because of the stiffness and strength naturally attributed to MWCNT.

No work has been found quantifying the effects of MWCNT on electrical conductivity.

6.1.2 Experimental Setup and Procedure

Test samples were prepared using the following steps from Objet VeroClear FullCure 810 and nanocomposite mixtures of Objet VeroClear FullCure 810 with 0.1wt%, 0.2wt%, and 0.5wt% MWCNT. Figure 6-1 shows images illustrating these experimental procedures. The setup, procedure, and analysis were performed with aid of Alison Schultz working in Dr. Tim Long's polymer chemistry lab at Virginia Tech.

1. MWCNT were added to a known amount of Objet VeroClear FullCure 810 until the desired weight percentage was achieved. This mixture was then bath sonicated using non-localized means for one hour at room temperature, which was maintained by cycling fresh water into the bath sonicator.

2. Each photopolymer was added into a ceramic mold until a liquid height of ~700µm was achieved (as recommended by the residential expert). This puck was then passed through a Fusion Systems conveyor belt UV curing system repeatedly until the entire thickness was cured, checked by gently pealing one corner of the material to visually identify liquid photopolymer settled along the bottom. The number of passes was calculated using the curing characterization data from Chapter 6 and the known exposure of the conveyor belt as calculated using a UV radiometer. In practice, however, an extra pass was usually necessary to achieve full curing.
3. The solidified sheets were then cut into test strips using a razor blade. Typically this process is performed using a dog bone punch, but the material was too brittle to be punched and it fractured. While sample strips did vary in size, the dimensions of each test strip were put into the Instron's Blue Hill tensile test software to make calculations using exact values.
4. All of the test strips were pulled using an Instron 5500R which is designed for tensile testing of thin film materials and is often used to quantify material properties for photopolymer. This was done by lowering the grippers such that 1/3rd the length of the test strip separated them. Then 1/3rd of the length was secured in the top vice and 1.3rd of the length was secured in the bottom vice. The test then commenced as the sample was loaded until failure. The machine was calibrated and zeroed between each test.

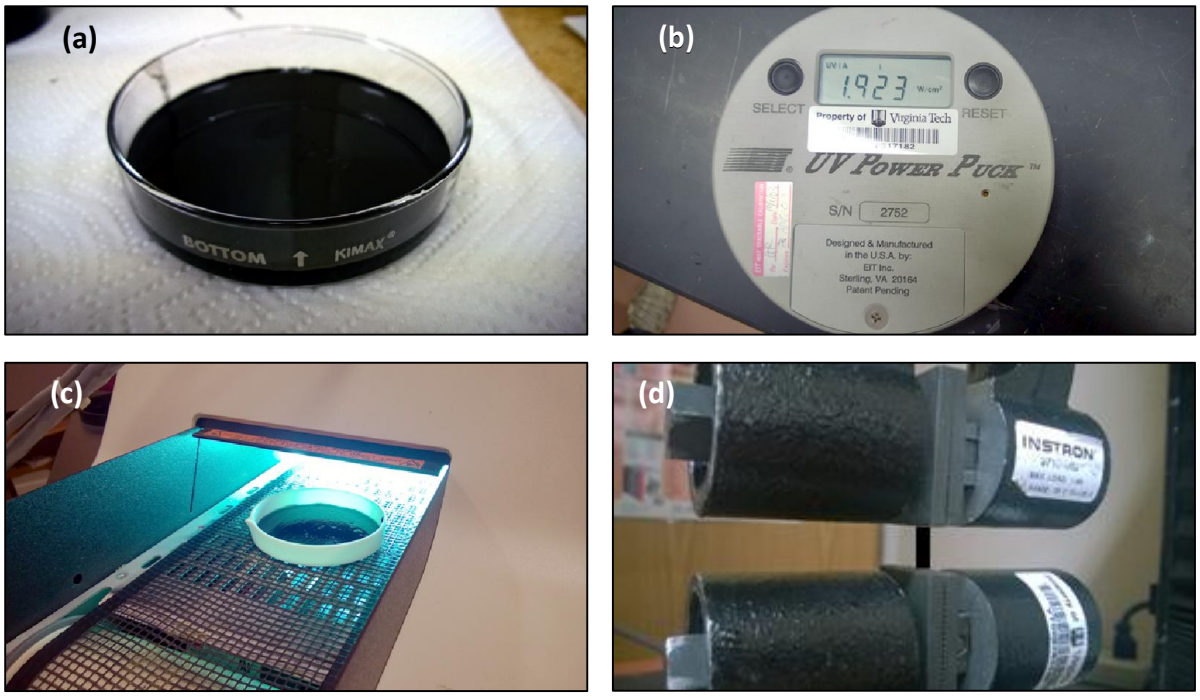

Figure 6-1. Images illustrating the procedure for the tensile test. **(a)** Nanocomposite mixture with 0.1 weight percent MWCNT after mixing. **(b)** UV radiometer used to measure the Fusion Systems conveyor UV curing system; it reads 1.923 mW/cm^2. **(c)** A cured sheet of nancompsite exiting the conveyor system inside the mold. **(d)** A sample strip fixtured in the Instron 5500R system.

Tensile test samples were not created using the developed PSL system because it is not able to achieve the layer thicknesses required by the Instron system for each nanocomposite concentration and stacking thinner layers would create anisotropic material properties dependent on interlayer adhesion. The implemented testing procedure ensures that the quantified material characteristics are process independent, ensuring less variation by eliminating sources of error introduced by the PSL system.

6.1.3 Experimental Results

The entirety of the experimental results are presented in Appendix E. Table 6-1 below summarizes all of this data and presents the mean and standard deviation for the tensile stress at break, tensile strain at break, and elastic modulus of Objet VeroClear FullCure 810 with 0, 0.1, 0.2, and 0.5wt% loading of MWCNT. Figure 6-2. Representative samples for each material are plotted with one another for a qualitative comparison. Conclusions either qualitative or quantitative should not be drawn from this plot since the variation between samples is not acounted for.plots representative samples for each material with one another to provide a visual representation of the tensile test results. Stratasys reports a tensile stress between 50-65MPa for Objet VeroClear FullCure 810 and an elongation at break of 10-25% [51]. The experimental tensile stress of the control samples made from VeroClear FullCure 810 fall within the reported tensile stress range. The experimental tensile strain for these samples is 8.79%, just under the reported 10% expected minimum. Stratasys does not report how these values are determined and do not describe how the test parts are made, it is therefore not possible to speculate on reasons for the discrepancy between observed and reported tensile strain.

Table 6-1. Summary of the experimental results for tensile tests of the various photopolymer mixutres.

		Maximum Load (N)	Tensile Stress at Break (MPa)	Tensile Strain at Break (%)	Elastic Modulus (MPa)
0.0wt%	**Mean:**	184.73	52.29	8.79	1138.66
	Standard Deviation:	21.18	4.79	1.65	178.34
	stdev/mean:	11.47 %	9.15 %	18.81 %	15.66 %
0.1wt%	**Mean:**	107.74	28.31	5.86	819.64
	Standard Deviation:	9.91	3.55	0.73	82.64
	stdev/mean:	9.19 %	12.55 %	12.50 %	10.08 %
0.2wt%	**Mean:**	75.59	17.68	4.46	589.5
	Standard Deviation:	14.75	2.27	0.4	134.48
	stdev/mean:	19.52 %	12.86 %	8.99 %	22.81 %
0.5wt%	**Mean:**	29.27	4.56	1.83	334.30
	Standard Deviation:	5.27	0.34	0.24	44.65
	stdev/mean:	17.99 %	7.48 %	13.21 %	13.36 %

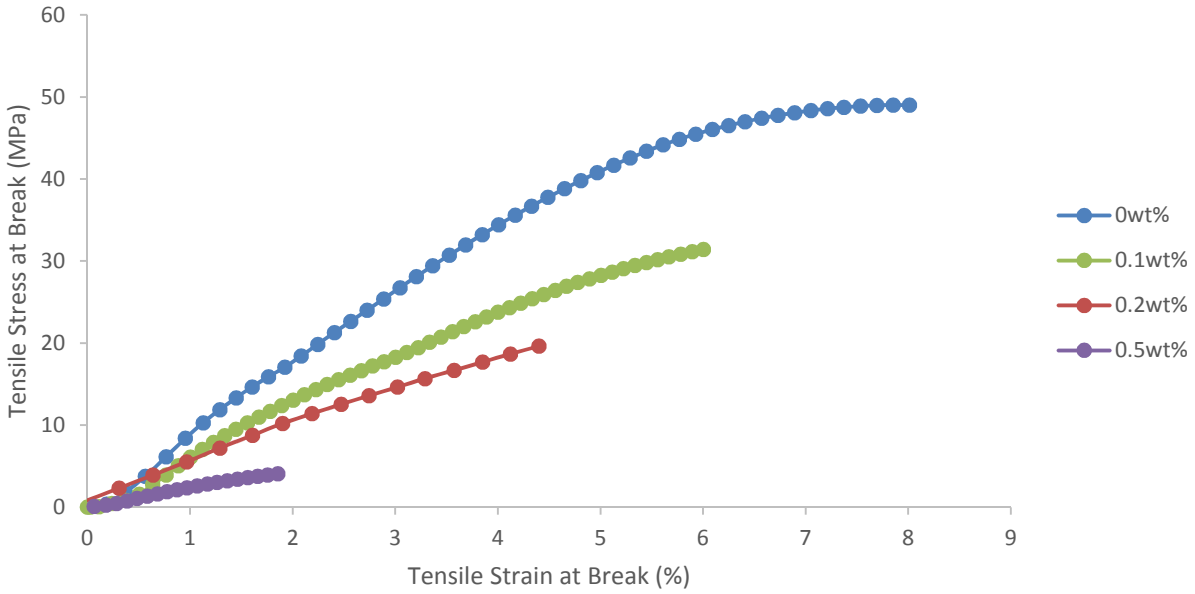

Figure 6-2. Representative samples for each material are plotted with one another for a qualitative comparison. Conclusions either qualitative or quantitative should not be drawn from this plot since the variation between samples is not acounted for.

6.1.4 Discussion and Analysis

Figure 6-3, Figure 6-4, and Figure 6-5 plot the tensile stress at break, tensile strain at break, and elastic modulus for the varying nanocomposites concentrations. Qualitatively these charts show that adding MWCNT filler to the VeroClear FullCure photopolymer decreases the polymer's tensile strength and elasticity. Although there is no strong quantitative trend, the higher concentrations of MWCNT appear to have an increasingly detrimental effect. Table 6-2 below shows the percent decrease in these material properties from each nanocomposite mixture relative to pure VeroClear.

Table 6-2. Precent decrease in tensile stress and strain at break along with the decrease in elastic modulus for the varrying concentrations of MWCNT relative to VeroClear.

Weight Percent MWCNT (wt%)	Decrease in Tensile Stress at Break (%)	Decrease in Tensile Strain at Break (%)	Decrease in Elastic Modulus (%)
0.1	45.89	33.33	28.01
0.2	66.19	49.26	48.23
0.5	91.27	79.19	70.64

These results are unexpected considering the positive results of Wicker and Sandoval, who observed a 17% increase in the ultimate tensile stress and a 30% decrease in fracture strain [5]. While a decrease in fracture strain was observed (33-79%), the ultimate tensile stress at break is shown to decrease with the addition of MWCNT (46-91%).

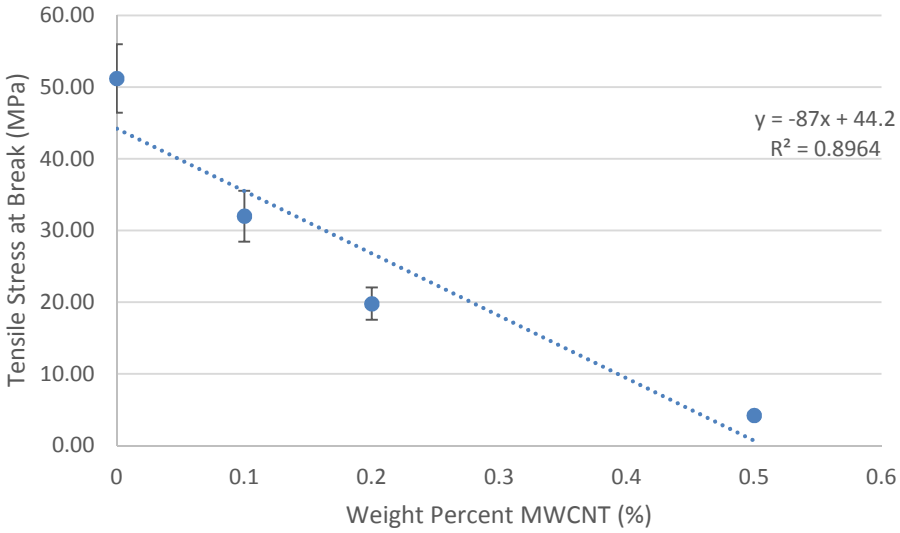

Figure 6-3. Tensile stress at break for the varying nanocomposite concentrations.

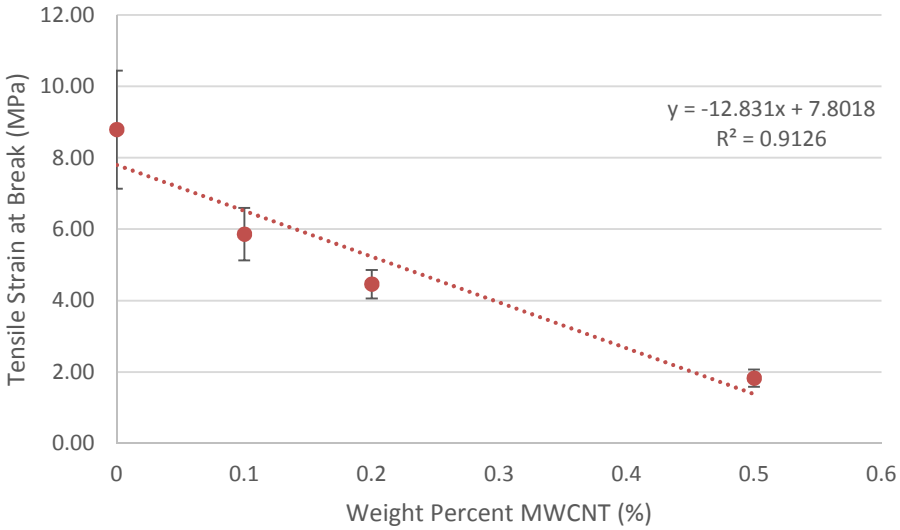

Figure 6-4. Tensile strain at break for the varying nanocomposite concentrations.

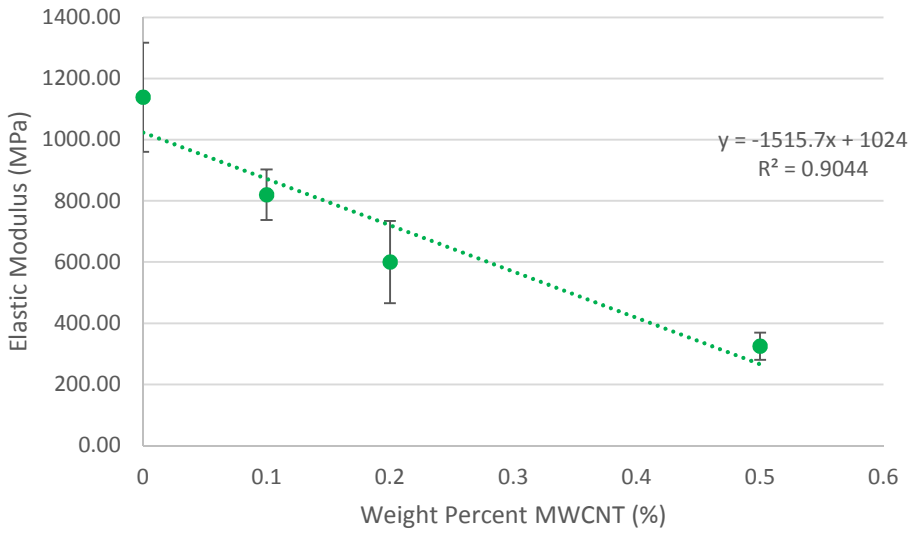

Figure 6-5. Elastic modulus for the varying nanocomposite concentrations.

There are some sources of potential error within these measurements that may account for this discrepancy. Potential solutions for these sources of error are also provided.

- VeroClear photopolymer is incredibly brittle when fully cured. This makes the creation of test strips for tensile tests very difficult. Using punching dies and razor blades to create test parts often fractures the material but may also introduce micro-cracks that hinder part strength during the tensile test. Even if the PSL system is used to fabricate these test parts, their forceful removal from the build platform would deform the samples and is even more likely to introduce structural defects like cracks and surface imperfections.

- All photopolymer tensile test samples (with and without nanocomposites) had a smooth glass-like surface finish which made them difficult to clamp using the Instron vices. The smooth surface often slipped out of the vices unless over tightened, however excessive tightening would occasionally fracture the sample from the point of contact and up. Even surviving samples may have introduced micro-cracks that made the samples weak. It is recommended that tensile tests are performed using larger test strips that can survive clamping, but these test strips would be even more difficult to fabricate.

- The MWCNT within the sample parts may be detrimental to the tensile strength of the material because the agglomerates create fracture propagation points analogous to other material impurities. This would make it easier for structural failures to begin and continue throughout the test parts. This is especially true given the difficulty in preparing and fixturing the test samples for the Instron tensile test.

6.2 Electrical Conductivity of Nanocomposite Photopolymers

Electrical conductivity of nanocomposite photopolymers would allow for the fabrication of three dimensional objects with electronic applications in portable sensing, particularly in wearable bio-physiological quantified-self devices. Nanocomposites for electrical conductivity testing were prepared using the same materials and procedures discussed in Section 5.2.1. Test parts were fabricated by controlled exposure using the PSL system to incorporate lead attachment points 19mm away from each other.

A digital multi-meter was used to measure the resistivity of each sample. A resistivity of 150kΩ or 8kΩ/mm was measured for VeroClear with 0.5wt% MWCNT. Resistivity was immeasurable for the other nanocomposite concentrations. These measurements were obtained with the help of Deba Saha working in Dr. Ben Knapp's maker lab. While MWCNT themselves are conductive, the MWCNT inside the test samples are present in agglomerated form that likely prevents the transfer of electrons. For conductivity there must be continuity along the MWCNT for the electrons to travel and there exists too much nonconductive photopolymer between the agglomerates. The agglomerate problem may be solved by using a more viscous base photopolymer to create the nanocomposites as discussed in Section 6.1.4. Otherwise, alignment of the MWCNT using an electro-magnetic field may ensure continuity and increase conductivity for evenly dispersed MWCNT in the photopolymer.

6.3 Reflection on the Results

The experimental results and analysis presented in this chapter show that increasing amounts of embedded MWCNT in VeroClear photopolymer have detrimental effects on the tensile strength and tensile strain at break, creating an overall decrease in elastic modulus. While the observations regarding the strain at break match the findings of Wicker and Sandoval [5], this research has found that the addition of MWCNT decreases the ultimate tensile stress of the part even though Wicker and Sandoval observed an increase in ultimate tensile stress. Table 6-3 below illustrates the differences between the experiments performed by Wicker and Sandoval and the experiments outlined in this chapter.

Table 6-3. Comparison between this research and prior literature concerning experimental details for quantifying tensile strength of nanocomposite photopolymers with embedded MWCNT.

	Sandoval and Wicker	**This Chapter**
Photocuring System:	Modified 3D Systems SL Model 250/50	Fusion Systems UV Conveyor Belt
Tensile Machine:	Instron 5500	Instron 5500R
Base Photopolymer:	DSM Somos WaterShed 11120	Objet VeroClear FullCure 810
Nanocomposite Filler:	Multi-wall carbon nanotubes	Multi-wall carbon nanotubes
Concentrations:	0 and 0.05 weight percent	0, 0.1, 0.2, and 0.5 weight percent
Samples Per Concentration:	4 per	4 per

The observed decrease in tensile strength may be explained by the presence of agglomerated nanoparticles with the cured nanocomposites. These agglomerates likely serve as fracture propagation points along the material samples that make failure more likely to begin and continue with increased severity. This is especially pertinent given the preparation and fixturing requirements of the Instron tensile test process and its tendency to damage samples. The measurable conductivity is the result of conductive MWCNT passing electrons within cured photopolymer, however this was only achieved at very high concentrations. Conductivity may be increased and require lower concentrations of MWCNT if they can be more evenly dispersed inside the cured samples.

It is suspected that agglomeration is promoted by the low viscosity of the Objet VeroClear FullCure 810 photopolymer compared to the higher viscosity of DSM Somos Watershed Ultra 11120 (160cps vs 260cps respectively at 30^{o} C). This suspicion arises from the different results of this research and Sandoval, which both used the same MWCNT with the same mixing process. Preventing agglomerations may therefore be possible by creating the nanocomposites from a more viscous photopolymer intended for use in PSL systems, such as the photopolymers offered by EnvisionTech.

Never the less, the results show that adding MWCNT to Objet VeroClear FullCure 810 is detrimental to the tensile strength and tensile strain of the resulting nanocomposite. It is also shown that electrical conductivity is possible, although very low, when VeroClear FullCure is mixed with 5wt% MWCNT. It is possible that the addition of MWCNT has other beneficial effects on material properties such as thermal efficiency. This would enable the fabrication of geometrically complex and optimized heat exchangers, but this is only a hypothesis that would need investigation.

7. Conclusions and Future Work

7.1 Summary of Research

The primary goal of this work was to fabricate three dimensional objects from nanocomposite photopolymers with embedded carbon nanotubes. This goal has been achieved by building a projection stereolithography (PSL) system designed to process such nanocomposite mixtures. This system was then used to characterize the curing and material properties of the nanocomposite mixtures and fabricate a three dimensional nanocomposite structure. The development of the system and characterization of the nanocomposites were motivated by two developmental questions and two research questions:

Developmental Question #1: What features and components does a PSL system designed to process nanocomposites possess and what is their embodiment?

> This projection stereolithography system combines a modified BenQ EP5920 DLP projector and Dymax BlueWave 75 light source with optical components and a stepper motor to digitally project light and cure stacked layers of photopolymer. Images are projected from below the petri dish containing photopolymer such that layers cure constrained between the petri dish and the build platform. The petri dish is coated with a PTFE Sylgard Coating (Dow Corning) to reduce adhesion to the polymer so it can be separated by the stepper motor. This embodiment allows for quicker vertical print speeds, finer control of layer thickness, and the use of less material but increases the minimum feature size by an order of magnitude. The machine is programmed in LabVIEW and highly automated with an intuitive user interface for ease of use (Section 3.4).

Developmental Question #2: What is the resolution, accuracy, precision, and vertical print speed of a PSL system designed to process nanocomposites

> This system meets 82% of the developed customer needs and performance specifications. The system projects a build plane 45mm x 25mm with a uniform light intensity of 0.23mJ/cm^2 at 365nm that capable of achieving 300µm features. When fabricating repetitive 4mm x 4mm features, the average system error is 492µm and the average standard deviation is 223µm. The system is also capable of achieving vertical print speeds of 76.2mm or 3". These results were obtained experimentally by fabricated and measuring test parts made from Objet VeroClear FullCure 810 (Table 4-5 in Section 4.5).

Research Question #1: How does the addition of multi-walled carbon nanotubes by weight percent change the curing characteristics of the photopolymer?

> Nanocomposite materials were developed through sonication of multi-walled carbon nanotubes (with a reported diameter of 35nm $\pm$ 15nm and a reported length of 5-20µm) into Objet VeroClear FullCure 810. The curing properties of VeroClear with 0, 0.1, 0.2, and 0.5 weight percent of multi-walled carbon nanotubes were characterized in terms of critical exposure and depth of penetration. As compared to the control sample of Objet VeroClear FullCure 810, the addition of

0.1wt% MWCNT increases the critical exposure by 0.069mJ/cm^2 (10.7%) while the addition of 0.2wt% MWCNT correlates to a 0.148mJ/cm^2 (23%) increase and the addition of 0.5wt%MWCNT correlates to a 0.497mJ/cm^2 (77.3%) increase. This trend can be qualitatively verified by the model proposed by Elliot who mathematically defines how the addition of nanoparticle agglomerates effect critical exposure of photopolymerization. By applying the Elliot model (Section 5.5.1) the experimental trend can be quantified as:

$$E_c = 0.2719 \ln(wt\%) + 1.2984 \quad (5\text{-}1)$$

The depth of penetration of VeroClear decreases by 220um/mJ (40.1%) with the addition of 0.1wt% MWCNT. The addition of 0.2wt% MWCNT correlates to a 360um/mJ (65.6%) decrease and the addition of 0.5wt% MWCNT correlates to a 439um/mJ (80%) decrease. These results are confirmed qualitatively by the Griffith model which demonstrates how the addition of nanoparticles affect the depth of penetration. The experimental trend can be quantified by applying the Griffith model (Section 5.5.2):

$$D_p = {}^{44.898}/_{wt\%} + 101.24 \quad (5\text{-}2)$$

Transmission Electron Microscopy (TEM) images were taken of the cured photopolymer samples and revealed particle agglomerations. These agglomerations have likely formed because the base photopolymer is not viscous enough to prevent the Van Der Whaals of mixed MWCNT from attracting each other and forming agglomerates.

Research Question #2: How do the multi-walled carbon nanotubes affect the PSL process and the material properties (tensile strength and electrical conductivity) of the photopolymer?

Test strips were made from the nanocomposite materials and tensile tested using an Instron 5500R (Section 6.1.3). It was found that adding 0.1wt% MWCNT decreased the tensile stress at break by 23.98MPa (41.67%), adding 0.2wt% MWCNT corresponded to a 34.61MPa (66.19%) decrease, and adding 0.5wt% MWCNT corresponded to a 47.73MPa (84.16%) decrease. The addition of MWCNT had a similar effect on decreasing the tensile strain at break: Adding 0.1wt% MWCNT decreased the tensile strain at break by 2.93MPa (33.33%), adding 0.2wt% MWCNT corresponded to a 4.33MPa (49.26%) decrease, and adding 0.5wt% MWCNT corresponded to a 6.96MPa (79.19%) decrease. The decrease in stress and strain corresponds to a decrease in elastic modulus as well: Adding 0.1wt% MWCNT decreased the elastic modulus at break by 319.02MPa (28.01%), adding 0.2wt% MWCNT corresponded to a 549.16MPa (48.23%) decrease, and adding 0.5wt% MWCNT corresponded to a 804.36MPa (70.64%) decrease. These trends are quantified in Figures 6-2, 6-3, and 6-4. Through measurement with a digital multi-meter it was also shown that VeroClear with 0, 0.1, and 0.2 weight percent MWCNT is non-conductive. VeroClear with 0.5 weight percent MWCNT is just barely conductive with a resistance of 8kΩ/mm, however this is

too great for any practical sensing applications (Section 6-2). It is believed that the decrease in tensile strength is due to the precense of agglomerations.

7.2 Research Contributions

The main contributions of this work are:

1. Creation of a functional decomposition and morphological matrix for the categorization of PSL systems based on their design criteria. Critical performance specifications are also presented to quantitatively compare these systems according to the identified system tradeoffs.

Functional decomposition and morphological matrix aid the conceptual design of a PSL system by establishing high level tradeoffs. The comparison in system performance specifications provides a quantitative benchmark for understanding how these tradeoffs affect final system performance. This work was performed in collaboration with Phillip Lambert. Future work may therefore use these tools to design PSL systems tailored to specific research needs. These tools, benchmarks, and design tradeoffs are detailed in Chapter 2 as well as in a peer reviewed paper published in the 2013 Solid Freeform Fabrication Symposium [49].

2. The design, development, and validation of a PSL system for fabricating three dimensional parts from nanocomposite mixtures of VeroClear and MWCNT.

This machine provides a means for fabricating structures out of photopolymer resins and can be used to characterize their curing properties. Because the system uses vat-photopolymerization any nanomaterials made from lower concentrations (<5wt%) of MWCNT and photopolymer can be embedded into fabricated objects. This system can therefore be used in future work with other commercial and novel photopolymers. The system validation also provides a benchmark for comparison with other AM processes and PSL systems to help identify appropriate applications in the future.

3. Modeling of the effect MWCNT have on critical exposure and depth of penetration for Objet VeroClear FullCure 810.

This research provides quantitative models that may be used to determine the critical exposure and depth of penetration for any nanocomposite created from VeroClear and MWCNT which may be used for any other PSL system or photo-based AM process. The Elliot and Griffith models were also applied qualitatively to justify the observed changes in critical exposure and depth of penetration for the developed nanocomposite photopolymers.

4. Analysis of how the addition of MWCNT affects the tensile strength and electrical conductivity of VeroClear photopolymer.

This analysis shows that the tensile stress at break, strain at break, and elastic modulus all decrease as more MWCNT are added to Objet VeroClear FullCure 810. This analysis also shows that only a 0.5 weight percent loading of MWCNT has any conductivity, although it is too low for practical sensing applications. These experimental results provide a benchmark case study for the effects of MWCNT on commercial photopolymer that may provide future researchers with a starting point for improving the material properties of photopolymers with nanomaterials.

7.3 Limitations and Future Work

The results of this research identify many system and material limitations that may be improved through future work. The analysis and reflection sections of each chapter go into great detail regarding the potential sources of error and areas of improvement for future work. However, these discussions can be categorized into two main areas of improvement with a few high priority suggestions for future work:

(i) There still exists gaps in the validation of the PSL system which may be quantified by incorporating closed loop feedback control into the operating software and selecting or building a new photopolymer vat.

- The accuracy and precision of the PSL system can be further characterized and compensated for using closed loop control with camera feedback. Through the addition of a CCD camera, digital image analysis can be performed to identify and correct discrepancies between the actual projected image and the digital image file. The observed effects of cure creep from over-exposure could be calculated and compensated for using such a method.

- An IR range sensor and accelerometer can be incorporated onto the build platform to provide closed loop feedback control of layer thickness. This would allow for consistent and repeatable positioning of the build platform in relation to the projection plane for the first and every sequential image. This would also reduce the effects of excessive curing and feature growth due to over exposure and may even be used to quantify it.

- The glass petri dish used as a photopolymer vat has a slight curvature along the bottom. For this reason, the build platform deforms to conform to this contour and is suspected of introducing adverse effects of the precision and accuracy of the PSL system. For this reason the glass petri dish should be replaced with a more level alternative, such that the build platform may remain consistently parallel to the projection plane.

(ii) There is a knowledge gap in understanding the polymer chemistry around nanomaterial fillers in photopolymers and more specifically their influence on the formation of polymer chains during photopolymerization.

- This research may be repeated for nanocomposites made from photopolymers more viscous than Objet VeroClear FullCure 810, ~160cps [45], and the same MWCNT. More viscous photopolymers should prevent the formation of agglomerates as evidenced by the results of Sandoval, who experienced no agglomeration using DSM Somos WaterShed Ultra 11120 with a 260cps viscosity [35]. The results may reveal quantifiable relationships between agglomeration and viscosity. Repeating the experiments using an EnvisionTech photopolymer as the base material in the nanocomposite mixtures is of particular interest since it is formulated for use in EnvisionTech PSL systems, most similar to the PSL system developed in this work.

- Future work may be done to functionalize the MWCNT such that they bond within the polymer chains. It is hypothesized that the MWCNT filler interrupts the development of long polymer chains and that functionalization would prevent the interruption of photopolymerization.

(iii) There is a discrepancy between the work of Sandoval and Wicker [5] and this research regarding the effect of MWCNT on the tensile stress at break for nanocomposite photopolymer test parts.

- Test parts should be created and tested in the future to obtain process dependent results. It is possible that processing the materials through a stereolithography system somehow structures the material to increase its tensile strength. A comparison between the process independent results of this thesis and process dependent results would reveal insight into the effects of MWCNT on the tensile strength of photopolymers.

- Future work could be to recreate the results of Sandoval and Wicker using the same MWCNT and DSM SomoS WaterShed 11120. Tensile tests could be performed with test parts created from the PSL system, from a commercial stereolithography system, and independent of any AM process. This may provide insight into how these various experimental procedures influence the tensile test results.

Works Cited

[1] A. Bertsch, “Microstereolithography: a Review,” in *Materials Research Society Symposium Proceedings*, 2002, vol. 758, p. 15.

[2] A. Bertsch, S. Zissi, and J. Y. Je, “Microstereophotolithography using a liquid crystal display as dynamic mask-generator,” 1997.

[3] A. Bertsch and J. C. Andr, “Study of the spatial resolution of a new 3D microfabrication process : the microstereophotolithography using a dynamic mask-generator technique,” vol. 107, pp. 275–281, 1997.

[4] O. Ivanova, C. Williams, and T. Campbell, “Additive manufacturing (AM) and nanotechnology: promises and challenges,” *Rapid Prototyp. J.*, pp. 733–749, 2013.

[5] J. H. Sandoval, K. F. Soto, L. E. Murr, and R. B. Wicker, “Nanotailoring photocrosslinkable epoxy resins with multi-walled carbon nanotubes for stereolithography layered manufacturing,” *J. Mater. Sci.*, vol. 42, no. 1, pp. 156–165, Dec. 2006.

[6] D. Yugang, Z. Yuan, T. Yiping, and L. Dichen, “Nano-TiO<DN>2</DN>-modified photosensitive resin for RP,” *Rapid Prototyp. J.*, vol. 17, no. 4, pp. 247–252, 2011.

[7] P. J. F. Harris, *Cabron Nanotubes and Related Structures: New Materials for the Twenty-first Century*. Cambridge, United Kingdom: Press Syndicate of the University of Cambridge, 1999, pp. 186–205.

[8] J. Sandoval and L. Ochoa, “Nanotailoring stereolithography resins for unique applications using carbon nanotubes,” *Proc. 16th …*, pp. 513–524, 2005.

[9] R. Andrews and M. . Weisenberger, “Carbon nanotube polymer composites,” *Curr. Opin. Solid State Mater. Sci.*, vol. 8, no. 1, pp. 31–37, Jan. 2004.

[10] C. B. Williams, F. Mistree, and D. W. Rosen, “A Functional Classification Framework for the Conceptual Design of Additive Manufacturing Technologies,” *J. Mech. Des.*, vol. 133, no. 12, p. 121002, 2011.

[11] B. M. Comeau, “Fabrication of Tissue Engineering Scaffolds Using Stereolithography,” Georgia Institute of Technology, 2007.

[12] J.-W. Choi, R. Wicker, S.-H. Lee, K.-H. Choi, C.-S. Ha, and I. Chung, “Fabrication of 3D biocompatible/biodegradable micro-scaffolds using dynamic mask projection microstereolithography,” *J. Mater. Process. Technol.*, vol. 209, no. 15–16, pp. 5494–5503, Aug. 2009.

[13] A. Bertsch, P. Bernhard, C. Vogt, and P. Renaud, “Rapid Prototyping Of Small Size Objects,” *Rapid Prototyp. J.*, vol. 6, no. 4, pp. 259–266, 2000.

[14] Y. Lu, G. Mapili, and G. Suhali, “A Digital Micromirror Device Based System for the Microfabrication of Complex, Spatially Patterned Tissue Engineering Scaffolds,” *… Res. Part A*, vol. 77, no. 2, pp. 396–405, May 2006.

[15] G. W. Hadipoespito, Y. Yang, H. Choi, G. Ning, and X. Li, “Digital Micromirror Device Based on Microstereolithography for Micro Structures of Transparent Photopolymer and Nanocomposites,” University of Wisconsin-Madison, Madison, Wisconsin, 2003.

[16] L.-H. Han, G. Mapili, S. Chen, and K. Roy, “Projection Microfabrication of Three-Dimensional Scaffolds for Tissue Engineering,” *J. Manuf. Sci. Eng.*, vol. Vol. 130, p. 021005: 1–4, 2008.

[17] K. Takahashi and J. Setoyama, “A UV Exposure System Using DMD,” *Electron. Commun. …*, vol. 83, no. 7, pp. 56–58, Jul. 2000.

[18] A. Bertsch, P. Bernhard, and P. Renaud, “Microstereolithography : Concepts and applications,” vol. 00, pp. 289–298, 2001.

[19] H.-W. Kang, J. H. Park, and D.-W. Cho, “A Pixel Based Solidification Model for Projection Based Stereolithography Technology,” *Sensors Actuators A Phys.*, vol. 178, pp. 223–229, May 2012.

[20] Y. M. Ha, J. W. Choi, and S. H. Lee, “Mass production of 3-D microstructures using projection microstereolithography,” *J. Mech. Sci. Technol.*, vol. 22, no. 3, pp. 514–521, May 2008.

[21] C. Sun, N. Fang, D. M. Wu, and X. Zhang, “Projection micro-stereolithography using digital micro-mirror dynamic mask,” *Sensors Actuators A Phys.*, vol. 121, no. 1, pp. 113–120, May 2005.

[22] A. Limaye and D. D. W. Rosen, “Multi-Objective Process Planning Method For Mask Projection Stereolithography,” Georgia Institute of Technology, 2007.

[23] a. Bertsch, H. Lorenz, and P. Renaud, “3D Microfabrication by Combining Microstereolithography and Thick Resist UV Lithography,” *Sensors Actuators A Phys.*, vol. 73, no. 1–2, pp. 14–23, Mar. 1999.

[24] A. Bertsch, L. Beluze, and P. Renaud, “Microstereolithography : A New Process To Build Complex 3D Objects,” vol. 3680, no. April, pp. 808–817, 1999.

[25] S. Monneret, “Microstereolithography Using a Dynamic Mask Generator and a Noncoherent Visible Light Source,” *Des. Test, …*, vol. 3680, no. April, pp. 553–561, 1999.

[26] X. Zheng, J. Deotte, M. P. Alonso, G. R. Farquar, T. H. Weisgraber, S. Gemberling, H. Lee, N. Fang, and C. M. Spadaccini, “Design and Optimization of a Light-Emitting Diode Projection Micro-Stereolithography Three-Dimensional Manufacturing System,” *Rev. Sci. Instrum.*, vol. 83, no. 12, p. 125001, Dec. 2012.

[27] C. Chatwin, M. Farsari, S. Huang, M. Heywood, P. Birch, R. Young, and J. Richardson, “UV Microstereolithography System that uses Spatial Light Modulator Technology.,” *Appl. Opt.*, vol. 37, no. 32, pp. 7514–22, Nov. 1998.

[28] C. Chatwin, M. Farsari, S. Huang, P. Birch, F. Claret-Tournier, R. Young, D. Budgett, and C. Bradfield, “Microfabrication by use of a Spatial Light Modulator in the Ultraviolet,” *Opt. Lett.*, vol. 24, no. 8, pp. 549–50, Apr. 1999.

[29] M. Farsari, F. Claret-Tournier, S. Huang, C. . Chatwin, D. . Budgett, P. . Birch, R. C. . Young, and J. . Richardson, “A Novel High-Accuracy Microstereolithography Method Employing An Adaptive Electro-Optic Mask,” *J. Mater. Process. Technol.*, vol. 107, no. 1–3, pp. 167–172, Nov. 2000.

[30] C. R. Chatwin, M. Farsari, S. Huang, M. I. Heywood, R. C. D. Young, P. M. Birch, F. Claret-Tournier, and J. D. Richardson, “Characterisation of Epoxy Resins for Microstereolithographic Rapid Prototyping,” *Int. J. Adv. Manuf. Technol.*, vol. 15, no. 4, pp. 281–286, Apr. 1999.

[31] J.-W. Choi, E. MacDonald, and R. Wicker, “Multi-material microstereolithography,” *Int. J. Adv. Manuf. Technol.*, vol. 49, no. 5–8, pp. 543–551, Dec. 2009.

[32] Y. Chen, Y. Pan, and C. Zhou, “A Fast Mask Projection Stereolithography Process for Fabricating Digital Models in Minutes,” *J. Manuf. Sci. Eng.*, vol. 134, no. 5, p. 051011, 2012.

[33] T. V. Wilson, “How LCoS Works.” [Online]. Available: http://electronics.howstuffworks.com/lcos.htm. [Accessed: 08-Jul-2013].

[34] “3D Systems,” 2013. [Online]. Available: http://www.3dsystems.com/. [Accessed: 08-Jul-2013].

[35] A. S. Limaye and D. W. Rosen, “Compensation zone approach to avoid print-through errors in mask projection stereolithography builds,” *Rapid Prototyp. J.*, vol. 12, no. 5, pp. 283–291, 2006.

[36] Y. Pan, C. Zhou, and Y. Chen, “A Fast Mask Projection Stereolithography Process for Fabricating Digital Models in Minutes,” *J. Manuf. Sci. Eng.*, vol. 134, no. 5, p. 051011, 2012.

[37] Dymax, “BlueWave® 75 UV Curing Spot Lamp with Intensity Adjustmenttle.” [Online]. Available: http://www.dymax.com/index.php/curing-systems/spot-lamps/bluewave-75.

[38] BenQ, “EP5920 Projector.” [Online]. Available: http://www2.benq.us/product/projector/ep5920/.

[39] Y. Chen, C. Zhou, and J. Lao, “A Layerless Additive Manufacturing Process Based on CNC Accumulation,” *Rapid Prototyp. J.*, vol. 17, no. 3, pp. 218–227, 2011.

[40] J. Denken Corp, “SLP-4000 Solid Laser Diode Plotter.” 1997.

[41] “EnvisionTEC.” [Online]. Available: http://envisiontec.com/.

[42] Y.-M. Huang and C.-P. Jiang, “On-LineForce Monitoring of Platform Ascending Rapid Prototyping System,” *J. Mater. Process. Technol.*, vol. 159, no. 2, pp. 257–264, Jan. 2005.

[43] D. Dendukuri, D. C. Pregibon, J. Collins, T. A. Hatton, and P. S. Doyle, “Continuous-Flow Lithography for High-Throughput Microparticle Synthesis,” *Nat. Mater.*, vol. 5, no. 5, pp. 365–9, May 2006.

[44] Zaber, “Motorized Linear Slide, 75 mm travel, RS-232 plus manual control.” [Online]. Available: http://www.zaber.com/products/product_detail.php?detail=T-LSR075A#tabs.

[45] Y. Cheng, M. Li, J. Lin, C. Ke, and Y. Huang, “Development of dynamic mask photolithography system,” *IEEE Int. Conf. Mechatronics, 2005. ICM ’05.*, vol. 4, pp. 467–471, 2005.

[46] A. M. Elliot, “Additively Manufactured Physical Unclonable Functions: The Effects of Quantum Dot Nanoparticles on Polyjet Direct 3D printing Process,” Virginia Polytechnic Institute and State University, 2014.

[47] J. W. H. Michelle L. Griffith, “Freeform Fabrication of Ceramics via Stereolithography.pdf,” *J. Am. Ceram. Soc.*, vol. 79, no. 10, 1996.

[48] B. S. Ian Gibson, David W. Rosen, *Additive Manufcaturing Technologies: Rapid Prototyping to Direct Digital Manufacturing*. Springer Science + Business Media, LLC, 2010, pp. 63–75.

[49] P. M. Lambert, E. A. C. Iii, and C. B. Williams, “DESIGN CONSIDERATIONS FOR MASK PROJECTION MICROSTEREOLITHOGRAPHY SYSTEMS,” pp. 1–20.

[50] S. Stanzione, “Cmos silicon physical unclonable functions based on intrinsic process variability,” *Solid-State Circuits, IEEE …*, vol. 46, no. 6, pp. 1456–1463, 2011.

[51] www.stratsys.com, "PolyJet Materials Data Sheet," May 2014.

Appendix A – Complete Bill of Materials

Table A1: Complete bill of materials for the PSL systems presented in this literature, costing $9,093.14 in total.

Vendor	Item	Identifier	Units	Unit Cost	Total Cost
Amazon	AmazonBasics High-Speed HDMI Cable with Ethernet (15 Feet)	NA	1	$12.71	$12.71
Amazon	AmazonBasics USB 2.0 Male to Female Extension Cable (9.8 Feet)	NA	1	$5.99	$5.99
Amazon	BenQ EP5920 Plug 'n Play 1080P Home Theater Projector	BenQ EP5920	1	$869.99	$869.99
Carolina Fluid Compo	80-20 Aluminum, 1x1", 10" long	10x10x10	6	$2.30	$13.80
Carolina Fluid Compo	80-20 Aluminum, 1x1", 16" long	10x10x16	2	$4.40	$8.80
Carolina Fluid Compo	80-20 cutting service	7005	6	$1.95	$11.70
Edmonds Optics	1/8" Hex Key Size, English Allen Wrench	03-662	2	$4.25	$8.50
Edmonds Optics	1/4-20 x 1/2" Setscrew, 12/Pack	03-644	2	$6.95	$13.90
Edmonds Optics	Steel Post, 4" Length, 1/4-20 Stud	59-000	4	$9.70	$38.80
Edmonds Optics	Post Holder, 2" Length, 1/4-20 Thread	58-978	2	$14.00	$28.00
Edmonds Optics	Right Angle Post Clamp, 12.7mm - 12.7mm (Fixed)	53-357	2	$16.00	$32.00
Edmonds Optics	Leveling Feet, 32-500lb Support (Package of 4)	62-682	1	$17.00	$17.00
Edmonds Optics	1/4-20 Hex Thumbscrew, PACK OF 10	58-681	2	$18.50	$37.00
Edmonds Optics	2" x 2" Kinematic Mount, 3 Screws	58-861	1	$129.00	$129.00
Edmonds Optics	Bench Plate, 18" x 18"	56-935	1	$299.00	$299.00
Edmonds Optics	Plano-Convex Lens 50.0mm Dia. x 50.0mm FL, Uncoated	32-970	1	$43.50	$43.50
Edmonds Optics	Plano-Concave Lens 25.0mm Dia. x -50 FL, Uncoated	45-028	1	$28.50	$28.50
Edmonds Optics	1/10 Wave Mirror, 50mm Square, Enhanced Aluminum Coating	64-020	1	$125.00	$125.00
Edmonds Optics	Optic Mount, 25mm Optic Diameter	#64-560	1	$40.00	$40.00
Edmonds Optics	Optic Mount, 50mm Optic Diameter	64-567	2	$49.00	$98.00
Ellsworth Adhesives	Light guide for spot curing, 5mm diameter, 1m long	57200	1	$422.34	$422.34
Ellsworth Adhesives	Dymax BlueWave 75-watt Mercury Lamp	40078	1	$2,795.00	$2,795.00
Krayden	Dow Chemical 184 SYLGARD 0.5KG 1.1LB KIT	DC4019862	1	$42.97	$42.97
McMaster-Carr	Glass Petri Dish, 3-7/8" Diameter, 3/4" Height	5027T91	50	$4.76	$238.00
McMaster-Carr	Aluminum Inch T-Slotted Framing System, Single End Cap, for 1" Extrusion	47065T91	4	$1.20	$4.80

McMaster-Carr	End-Feed Fastener, for 1" & 2" W, Aluminum Inch T-Slotted Framing System	47065T139	6	$1.85	$11.10
McMaster-Carr	90 Degree Bracket, Single, 2-Hole, for 1" Extrusion	47065T223	8	$3.98	$31.84
McMaster-Carr	90 Degree Plate, Single, 5-Hole, for 1" Extension	47065T177	4	$6.70	$26.80
Nano Lab	Multwall Carbon Nanotubes, Hollow Structure, OD 35+-15nm, Length 5-20um	PD30L520-5g	1	$500.00	$500.00
National Instruments	8 Solid-State Relays, 8 DI, Counter, Ch-to-Ch Isolated	NI USB-6525	1	$287.10	$287.10
Stratasys	KIT, FOR TOOL, UV G&R MEASURING DEVICE, TOL-00019-S	KIT-00019-S	1	$1,062.00	$1,062.00
Stratasys	Objet Veroclear Fullcure 810	RGD810	NA	NA	NA
Zaber	Motorized Linear Slide, 75 mm travel, RS-232 plus manual control	T-LSR075A-KT04	1	$1,810.00	$1,810.00
				Grand Sum:	**$9,093.14**

Appendix B – Custom Part Schematics

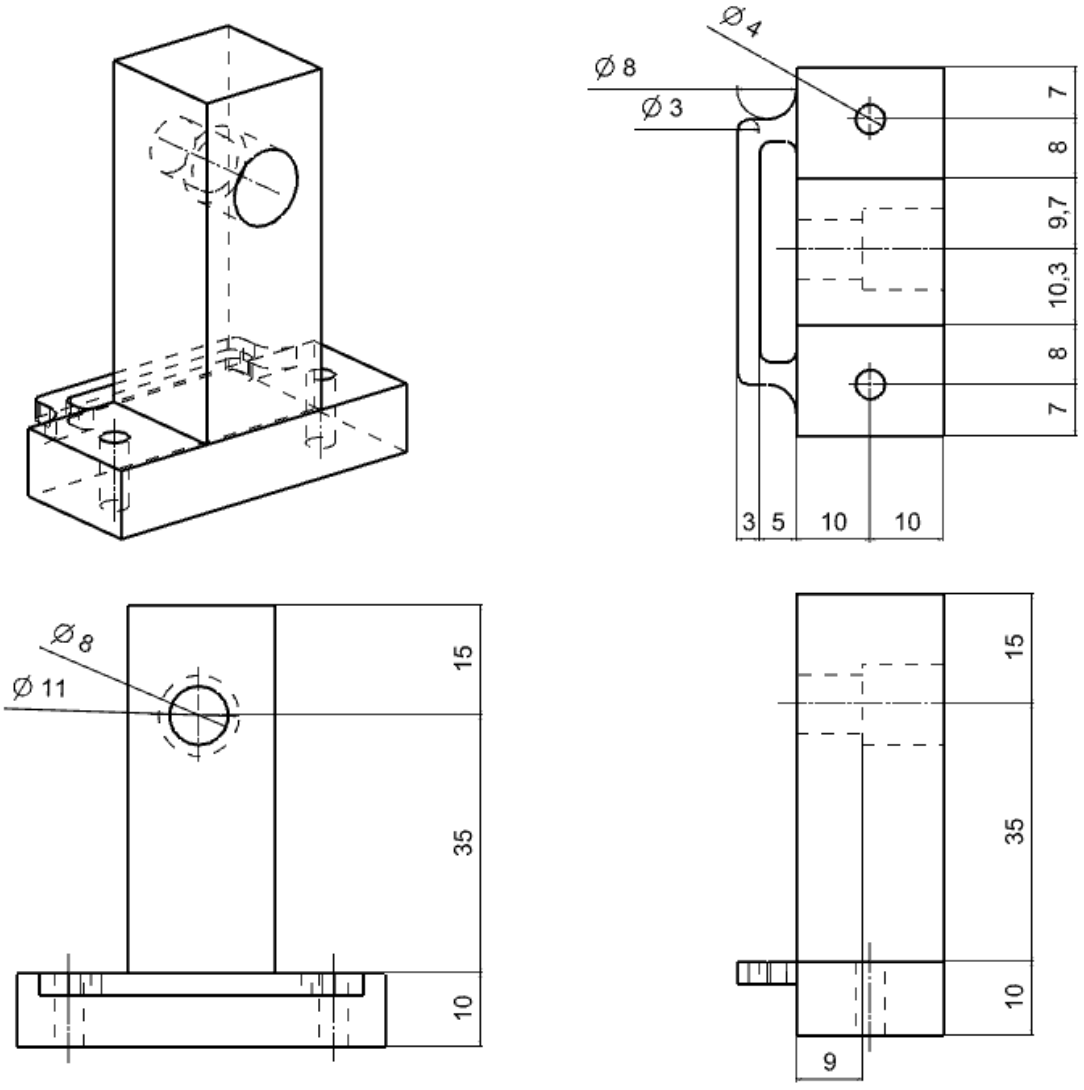

Figure B1. Schematic drawing of the projector light guide mount, all dimensions are shown in mm.

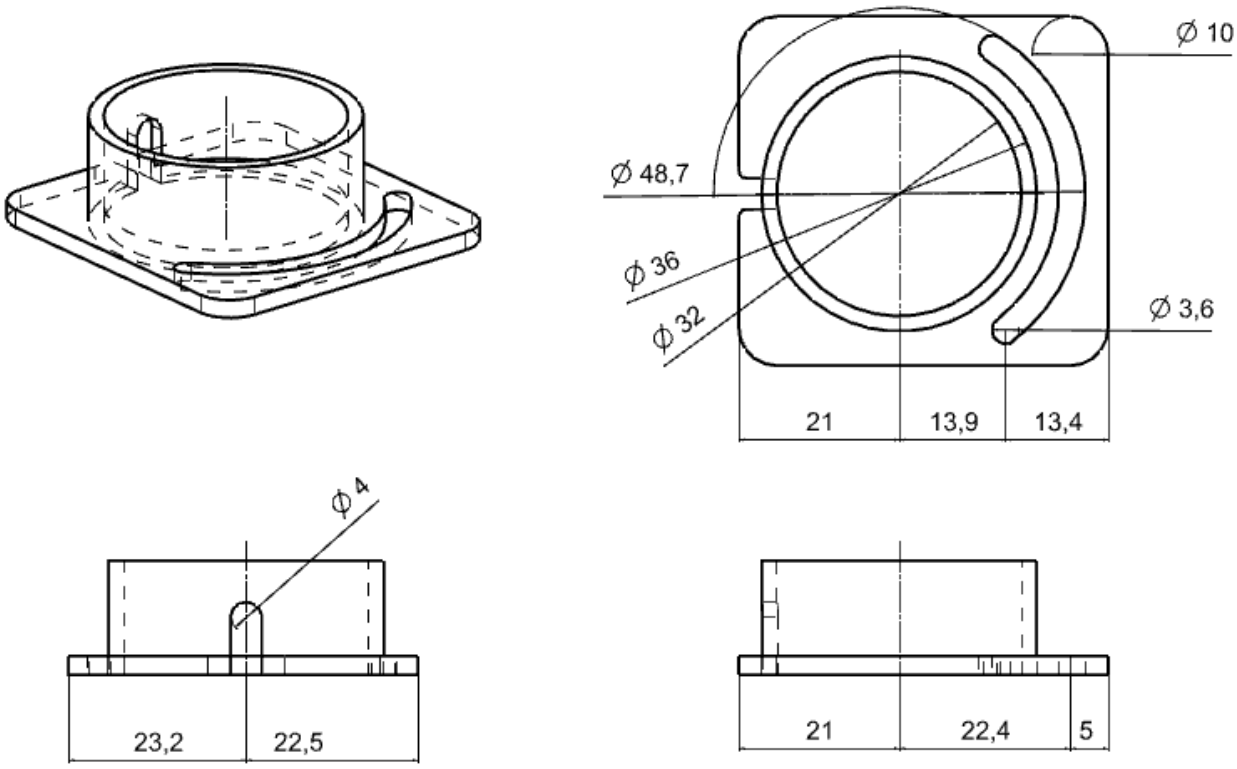

Figure B2. Schematic drawing of the projector optics mount, all dimensions are shown in mm.

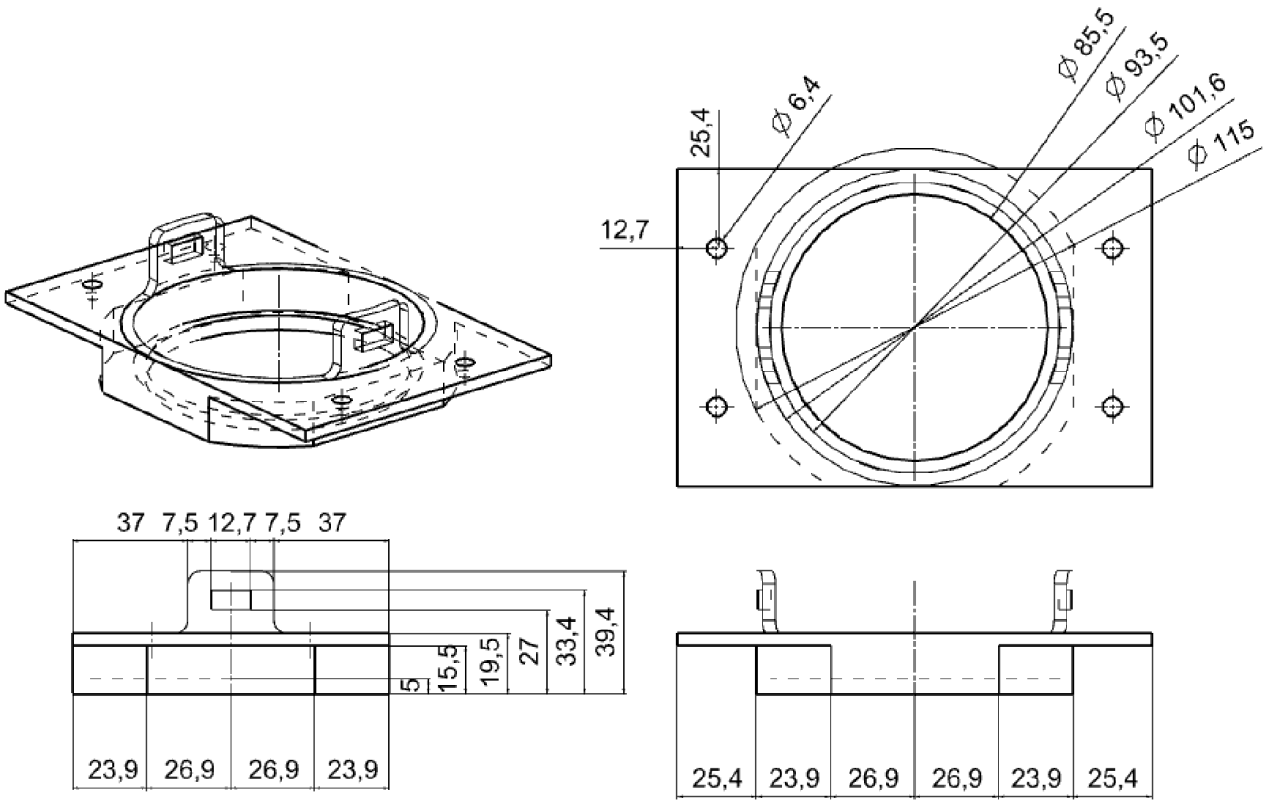

Figure B3. Schematic drawing of the petri dish mount, all dimensions are shown in mm.

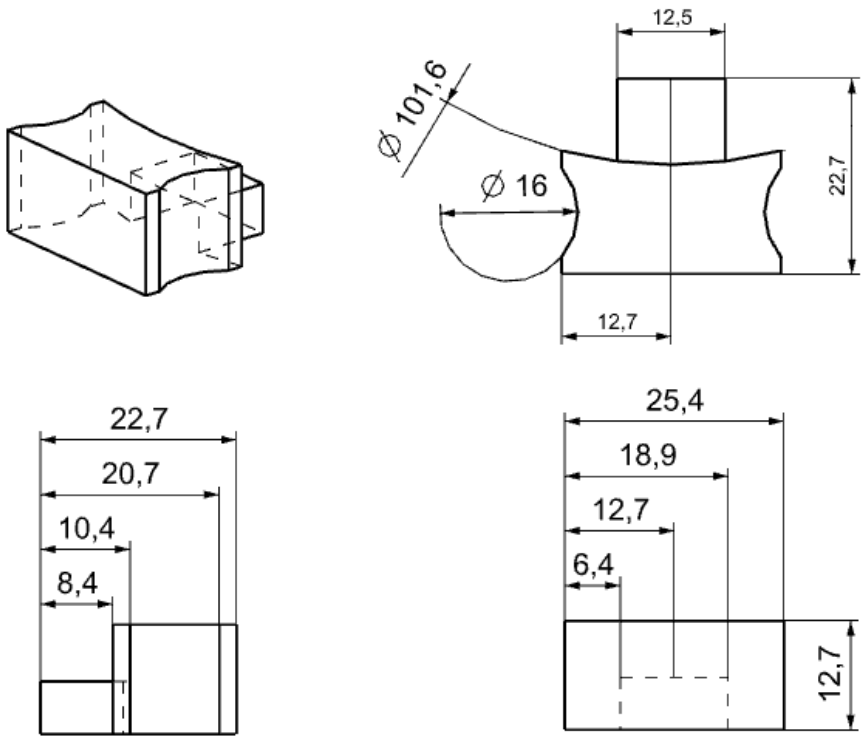

Figure B4. Schematic drawing of the petri dish locking blocks, all dimensions are shown in mm.

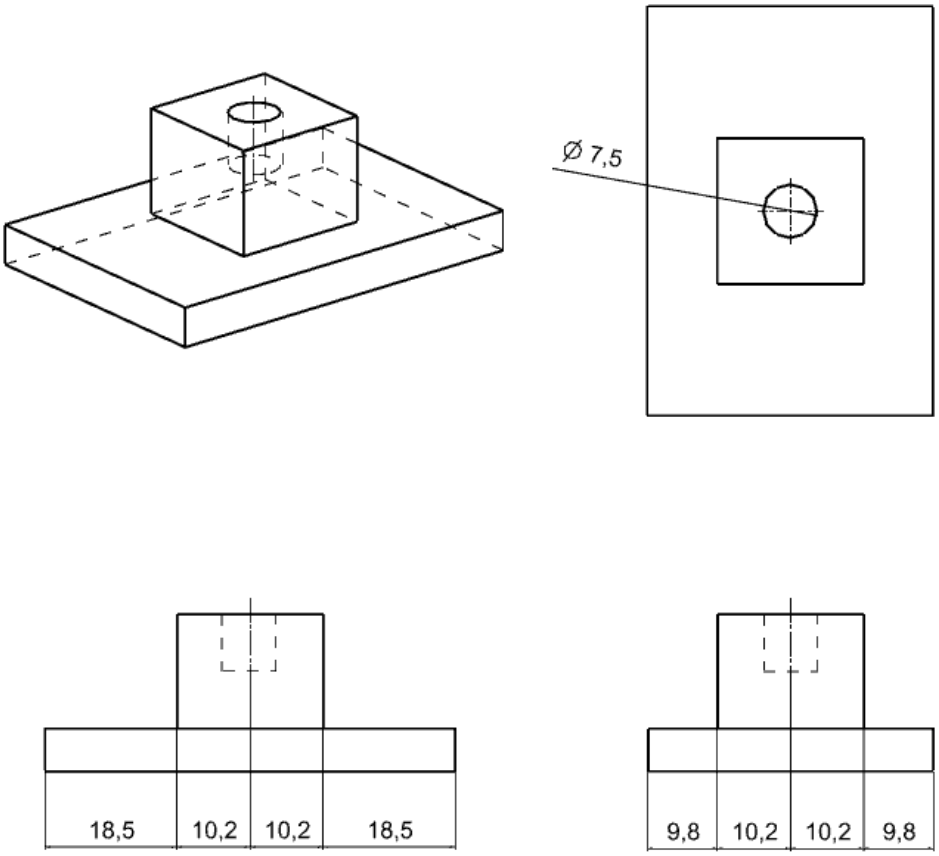

Figure B**5.** Schematic drawing of the build platform, all dimensions are shown in mm.

Appendix C - Characterization Data and Curves

The following Tables and Figures show the original data acquired from the experimental procedure outlined in Section 4.3. Objet VeroClear 810 was characterized using the PSL machine devolved throughout this thesis. The incident light intensity was 0.23 mW/cm^2 and time of exposure was varied to vary the total light exposure (mJ/cm^2).

Table C1. Characterization data for Objet VeroClear 810.

Time	Exposure (mJ/cm2)	Sample 1 Thickness (um)	Sample 2 Thickness (um)	Sample 3 Thickness (um)	Mean (um)	STD DEV
6.5	1.495	483	492	489	488	4.58
6	1.38	415	410	428	417.7	9.29
5.5	1.265	353	352	378	361	14.73
5	1.15	293	289	306	296	8.89
4.5	1.035	248	254	265	255.7	8.62
4	0.92	177	187	183	182.3	5.03
3.5	0.805	148	147	151	148.7	2.08

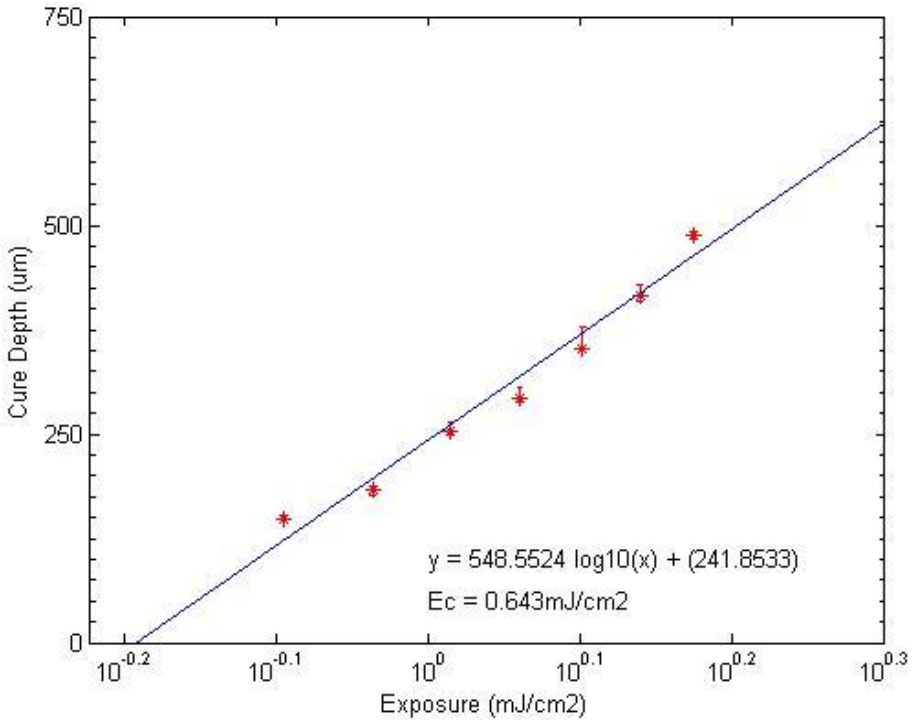

Figure C1. Characterization curve of Objet VeroClear 810.

Table C2. Characterization data for Objet VeroClear 810 with 0.1% MWCNT by weight.

Time	Exposure (mJ/cm2)	Sample 1 Thickness (um)	Sample 2 Thickness (um)	Sample 3 Thickness (um)	Mean (um)	STD DEV
15	3.45	545	506	494	515	26.66
12.5	2.875	458	457	448	454.3	5.51
10	2.3	388	381	386	385	3.61
7.5	1.725	307	312	317	312	5.00
6.66	1.5318	256	256	242	251.3	8.08
5.83	1.3409	195	208	206	203	7.00
5	1.15	149	156	143	149.3	6.51

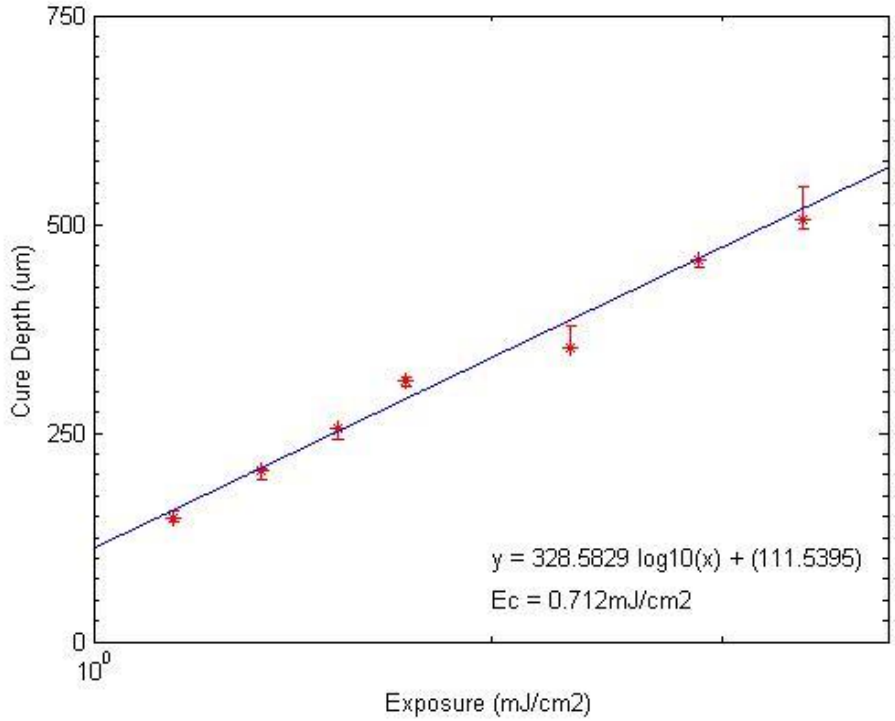

Figure C2. Characterization curve for Objet VeroClear 810 with 0.1% MWCNT by weight.

Table C3. Characterization data for Objet VeroClear 810 with 0.2% MWCNT by weight.

Time	Exposure (mJ/cm2)	Sample 1 Thickness (um)	Sample 2 Thickness (um)	Sample 3 Thickness (um)	Mean (um)	STD DEV
30	6.9	404	406	413	407.7	4.73
25	5.75	384	377	381	380.7	3.51
20	4.6	336	344	335	338.3	4.93
17.5	4.025	296	301	298	298.3	2.52
15	3.45	277	280	269	275.3	5.69
12.5	2.875	230	223	229	227.3	3.79
10	2.3	196	205	208	203	6.24
7.5	1.725	149	161	157	155.7	6.11

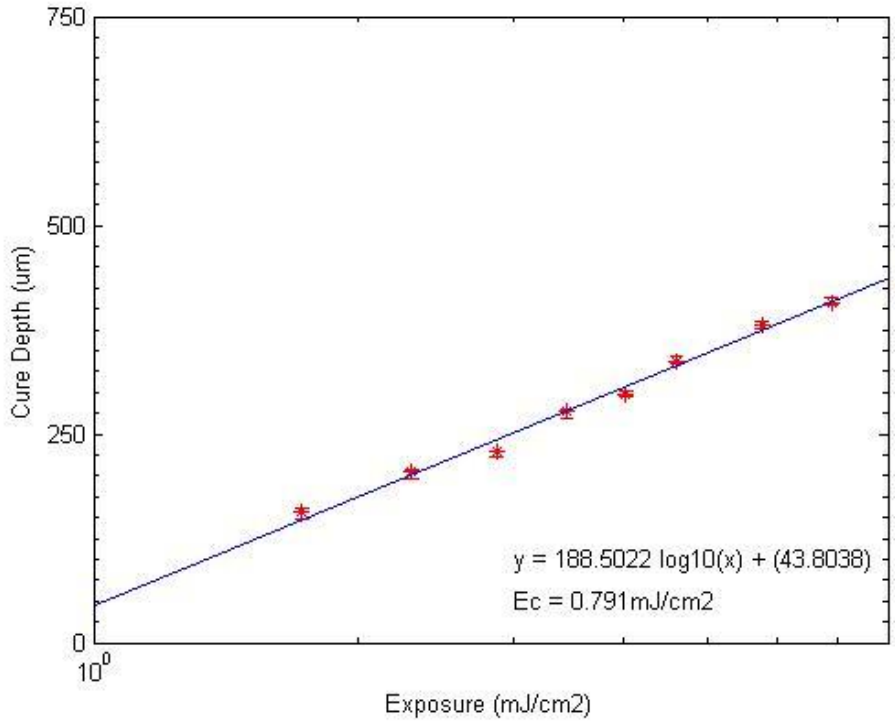

Figure C3. Characterization curve for Objet VeroClear 810 with 0.2% MWCNT by weight.

Table C4. Characterization data for Objet VeroClear 810 with 0.5% MWCNT by weight.

Time	Exposure (mJ/cm2)	Sample 1 Thickness (um)	Sample 2 Thickness (um)	Sample 3 Thickness (um)	Mean (um)	STD DEV
140	32.2	391	376	383	383.3	7.51
120	27.6	357	350	346	351	5.57
100	23	322	325	327	324.7	2.52
80	18.4	282	296	302	293.3	10.26
60	13.8	268	264	271	267.7	3.51
40	9.2	239	235	223	232.33	8.33
30	6.9	207	211	199	205.7	6.11

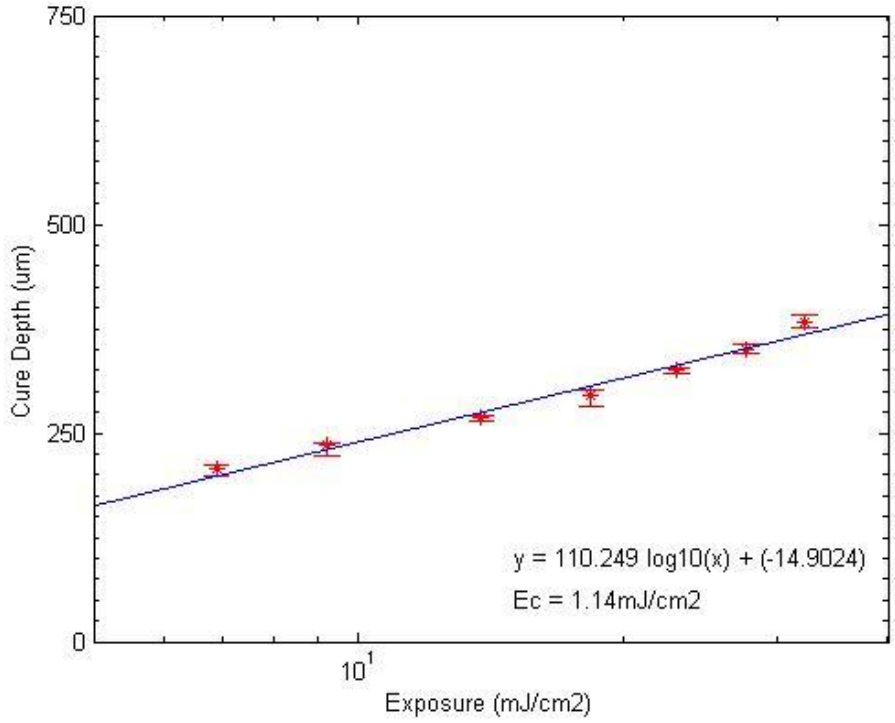

Figure C4. Characterization curve for Objet VeroClear 810 with 0.5% MWCNT by weight.

Appendix D – System Validation Data

Table D1. Measured data regarding the base width and height of the three sample test parts.

Sample	Width (mm)	Height (mm)
1	31.32	23.47
1	32.00	23.54
1	32.07	23.50
2	30.50	22.41
2	31.10	22.60
2	31.32	22.13
3	30.59	22.54
3	31.20	22.97
3	31.63	22.64

Table D2. Measured data regarding the base thickness for the three sample test parts.

Sample	Thickness Left (mm)	Thickness Right (mm)	Thickness Top (mm)	Thickness Bottom (mm)
1	1.69	1.06	1.30	1.59
1	1.90	1.28	1.06	1.39
2	1.95	1.68	1.71	1.77
2	2.27	1.67	1.46	1.87
3	1.76	1.25	1.25	1.52
3	1.62	1.32	1.07	1.52

Table D3. Measured data regarding the sizes of the square features for the three sample test parts.

	Left Square		Center Square		Right Square	
Sample	Width (mm)	Height(mm)	Width (mm)	Height(mm)	Width (mm)	Height(mm)
1	4.65	4.37	4.57	4.56	4.53	4.45
1	4.71	4.43	4.56	4.63	4.68	4.53
1	4.85	4.34	4.55	4.50	4.45	4.35
2	4.52	4.08	4.35	4.19	4.28	4.16
2	4.60	4.18	4.40	4.30	4.35	4.28
2	4.65	4.30	4.40	4.34	4.48	4.27
3	4.46	4.54	4.33	4.33	4.33	4.25
3	4.65	4.60	4.38	4.37	4.36	4.37
3	4.66	4.68	4.59	4.61	4.39	4.35

Table D4. Measured data regarding the locations of the square features for the three sample test parts.

Sample	Horizontal 1 (mm)	Horizontal 2 (mm)	Horizontal 3 (mm)	Vertical 1 (mm)	Vertical 2 (mm)	Vertical 3 (mm)
1	7.11	18.46	28.82	6.28	13.43	20.95
1	7.33	18.63	29.43	6.00	13.59	20.81
1	7.04	18.51	29.20	5.81	13.17	20.34
2	6.87	17.74	27.79	6.57	12.80	19.95
2	6.91	18.04	28.58	6.25	13.23	20.03
2	6.98	18.22	28.78	5.76	12.72	19.54
3	6.82	17.82	28.36	5.98	12.92	20.00
3	6.95	18.26	28.82	5.91	12.83	19.96
3	6.90	18.54	28.90	5.51	12.23	19.61

Appendix E – Tensile Test Data

Table E1. Tensile strength data for Objet VeroClear FullCure 810.

Sample	Maximum Load (N)	Tensile Stress at Break (MPa)	Tensile Strain at Break (%)	Elastic Modulus (MPa)
1	220.68	58.69	7.84	1427.00
2	182.16	53.69	11.74	1035.77
3	178.86	53.80	8.18	955.95
4	164.53	46.37	8.19	1144.36
5	177.41	48.92	8.01	1130.24
Mean:	184.73	52.29	8.79	1138.66
STD Deviation:	21.18	4.79	1.65	178.34
stdev/mean:	11.47	9.15	18.81	15.66

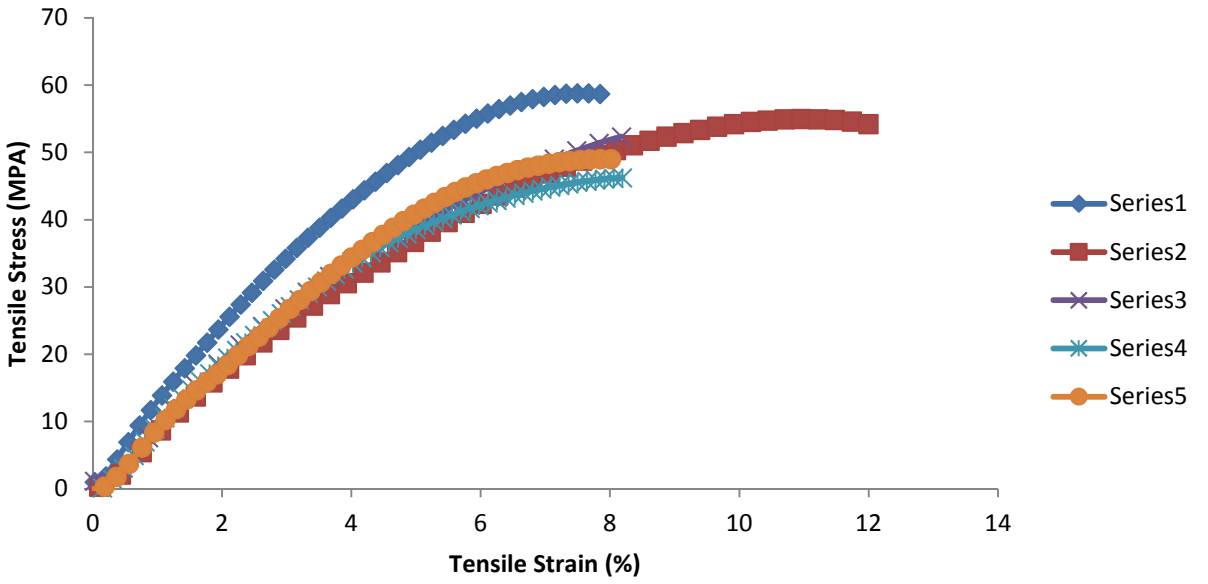

Figure E1. Tensile strength data for Objet VeroClear FullCure 810.

Table E2. Tensile strength data for Objet VeroClear FullCure 810 with 0.1 weight percent WCNT.

Sample	Maximum Load (N)	Tensile Stress at Break (MPa)	Tensile Strain at Break (%)	Elastic Modulus (MPa)
1	94.57	18.49	5.13	694.05845
2	73.72	20.55	4.4	504.89831
3	80.45	17.41	4.11	743.91561
4	53.61	14.26	4.2	415.11392
Mean:	75.588	17.678	4.460	589.497
STD Deviation:	14.752	2.273	0.401	134.485
stdev/mean:	19.516	12.857	8.987	22.813

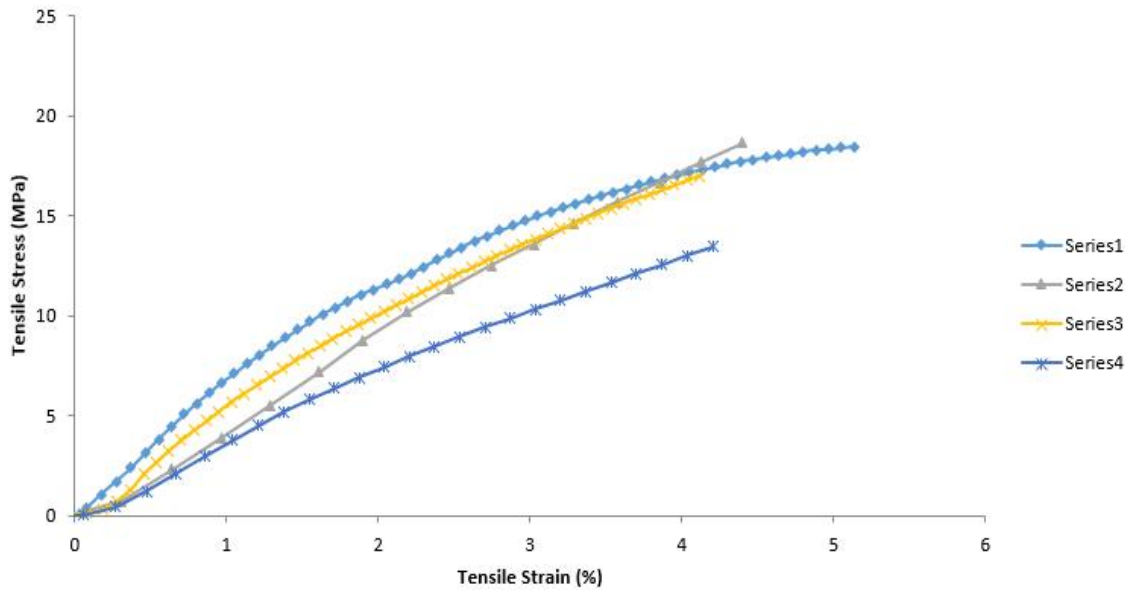

Figure E2. Tensile strength data for Objet VeroClear FullCure 810 with 0.1 weight percent WCNT.

Table E3. Tensile strength data for Objet VeroClear FullCure 810 with 0.2 weight percent WCNT.

Sample	Maximum Load (N)	Tensile Stress at Break (MPa)	Tensile Strain at Break (%)	Elastic Modulus (MPa)
1	94.320	30.990	5.280	884.730
2	117.520	31.700	6.010	854.042
3	107.100	24.700	5.320	841.037
4	112.010	25.830	6.840	698.758
Mean:	107.738	28.305	5.863	819.642
STD Deviation:	9.906	3.552	0.733	82.645
stdev/mean:	9.195	12.550	12.499	10.083

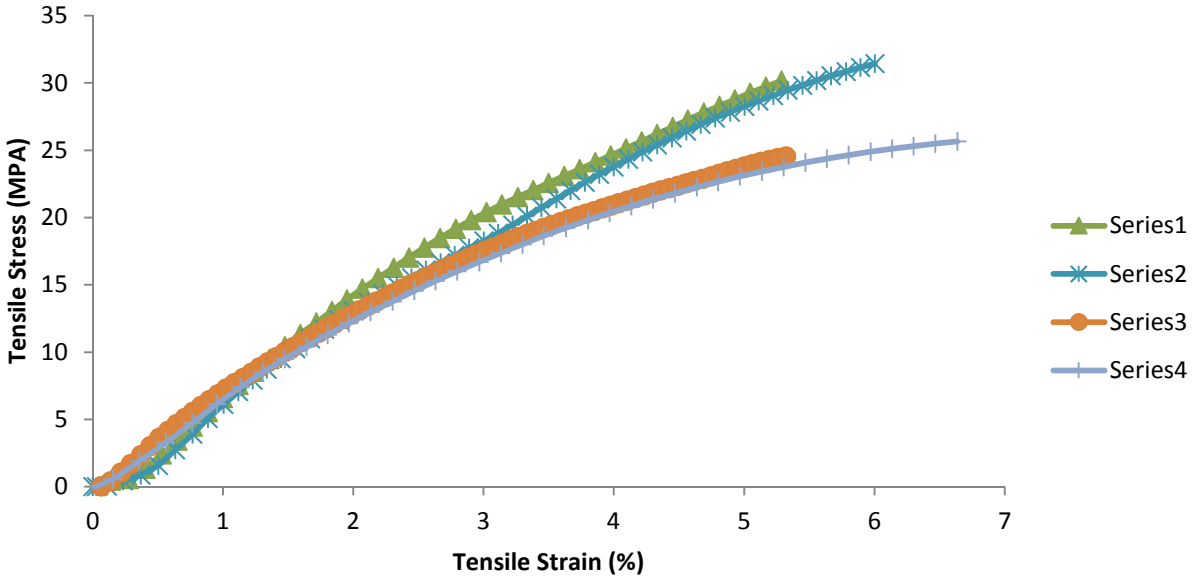

Figure E3. Tensile strength data for Objet VeroClear FullCure 810 with 0.2 weight percent WCNT.

Table E4. Tensile strength data for Objet VeroClear FullCure 810 with 0.5 weight percent WCNT.

Sample	Maximum Load (N)	Tensile Stress at Break (MPa)	Tensile Strain at Break (%)	Elastic Modulus (MPa)
1	25.030	4.210	1.670	310.939
5	25.410	4.320	1.850	290.781
8	30.360	4.830	1.630	393.288
9	36.280	4.870	2.160	342.212
Mean:	29.270	4.558	1.828	334.305
STD Deviation:	5.266	0.341	0.241	44.653
stdev/mean:	17.993	7.485	13.211	13.357

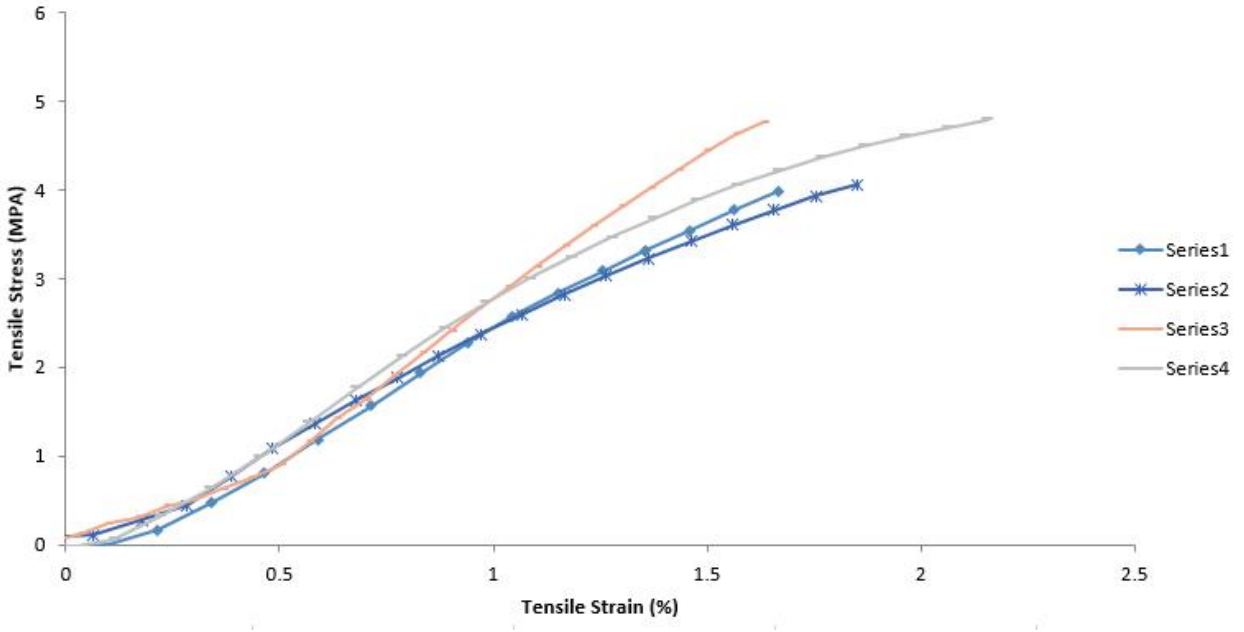

Figure E4. Tensile strength data for Objet VeroClear FullCure 810 with 0.5 weight percent WCNT.